Dipeptide-Based Hydrogelators and 3D Printed Gels

Master's Thesis
University of Jyväskylä
Department of Chemistry
13th of December 2022
Milka Poimala

Tiivistelmä

Tämän pro gradu -tutkielman teoriaosa esittelee lyhyesti supramolekulaarisen kemian, supramolekulaaristen geelien, aminohappojen sekä peptidien konseptit. Kolmea aminohappoa - fenyylialaniinia, lysiiniä ja arginiinia - tarkastellaan lähemmin, koska niitä käytetään tämän tutkielman kokeellisessa osassa. Lisäksi tarkastellaan 3D-tulostusta teorian perusteista lähtien aina aminohappopohjaisten supramolekulaaristen geelien eri tulostustekniikoihin. Lisäksi käydään läpi niiden käyttömahdollisuuksia lääketieteessä. Lopuksi sivutaan joitakin kiinteitä 3D-tulosteita sekä 3D-tulostettuja syötäviä geelejä.

Tutkielman kokeellinen osa suoritettiin Jaume I -yliopistossa, Castellón de La Planassa, Espanjassa. Työn tavoitteena oli löytää sopiva guanylointireaktio dipeptidipohjaiselle hydrogelaattorille. Lisäksi aloitusreagenssina käytettyä dipeptidipohjaista hydrogelaattoria valmistettiin lisää nelivaiheisen synteesin kautta. Tuotteet karakterisoitiin käyttämällä NMR-spektroskopiaa ja massaspektrometriaa. Guanyloidulla gelaattorimolekyylillä suoritettiin geeliytymiskokeita ja valmistetulle hydrogeelille tehtiin 3D-tulostuskoe. Lisäksi geeliä tutkittiin reologisin menetelmin. Guanylointireaktio onnistui, mutta gelaattorimolekyyli ei muodostanut vahvaa geeliä, eikä se siten ollut sopiva käytettäväksi tulostamisessa.

Abstract

The theory part of this Master's thesis introduces shortly the concepts of supramolecular chemistry, supramolecular gels, amino acids, and peptides. The emphasis is on three amino acids; phenylalanine, lysine, and arginine, which are used in the experimental part of this thesis. Furthermore, 3D printing is viewed from the general basics to amino acid based supramolecular gel printing techniques with their applications in the medical field. Also, some solid prints and 3D printed edible gels in food science are introduced.

The experimental part was conducted in the University of Jaume I in Castellón de la Plana, Spain. The aim of the experimental part was to find a suitable guanylation reaction for a dipeptide based hydrogelator. Also, more of the starting reagent, dipeptide based hydrogelator, was synthesized through four step synthesis. The products were characterized by NMR spectroscopy and mass spectrometry. Gelation tests were conducted with the guanylated gelator, in addition to which a 3D printing experiment was performed and rheological studies executed. The guanylation reaction was successful, but the gelator molecule did not form a strong gel. Thus, it unfortunately was not suitable for printing.

Preface

The theory part of this thesis was written during spring 2022, and the experimental part was conducted in the University of Jaume I in Castellón de la Plana, Spain during summer 2022. The supervisor from the University of Jyväskylä was docent Elina Sievänen. PhD student Nagihan Özbek was the supervisor of the experimental work, under the guidance of professor Beatriu Escuder.

This thesis was conducted at an early stage of my Master's studies. The topic is a continuum for my Bachelor's thesis "Supramolecular gels derived from biomolecules", which was conducted in spring 2021 in the University of Jyväskylä.

The topic of 3D printed gels was given by professor Beatriu Escuder, and I had a luck of receiving such a fascinating topic. I really enjoyed researching this area, which was formerly unknown to myself. Encountering studies about 3D printed edible gels, as well as the extensive use of same gelation additives both in food and chemical industry, allowed me to incorporate two of my interests together; food is a passion for me from being a cook by my first occupation, and chemistry amazes me more, the more I study it.

I am grateful to the Universities of Jaume I and Jyväskylä for this thesis writing possibility, and the Erasmus+ for this internship opportunity. Acknowledgements for Elina Sievänen for thorough inspection of the thesis and helping me every time I had questions, and Beatriu Escuder for taking me into the BIOSUPRAMAT group. I want to thank every member of the BIOSUPRAMAT group for making me feel welcomed. I am grateful to Nagihan Özbek for the patience and guidance through the project. I also want to express my gratitude for Janne Frimodig from the University of Jyväskylä for explaining and showing 3D printing to me.

In Jyväskylä, September 2022

Milka Poimala

Contents

Abbreviations

Ace B	Acetate Buffer
API	Active Pharmaceutical Ingredient
Arg	Arginine
BM2	Bone Morphogenic protein-2 peptide
CH	Composite soft Hydrogel
COSY	Correlation spectroscopy
DIPEA	*N*,*N*-Diisopropylethylamine
DLP	Digital Light Processing
DME	Ethylene glycol dimethyl ether
DMSO	Dimethylsulfoxide
F	Phenylalanine
FDA	The Food and Drug Administration
FDM	Fused Deposition Model
Fmoc-FF	Fluorenylmethoxycarbonyl-diphenylalanine
G'	The elastic storage modulus
G"	The elastic loss modulus
GG	Gellan Gum
GO	Graphene Oxide
HME	Hot-Melt Extrusion
IJP	Inkjet Printing
K	Lysine
LMWG	Low-molecular-weight-gelator
Lys	Lysine
m/*z*	Mass-to-charge ratio
ML	Machine Learning
MN	Micro Needle
MRI	Magnetic Resonance Imaging
NP	Nano Particles
OGP	Osteogenic Growth Peptide

PεK	Poly-ε-Lysine
PBF	Powder Bed Fusion
PBS	Phosphate-Buffered Saline
Phe	Phenylalanine
PLL	Poly-L-lysine
PVA	Polyvinyl Alcohol
PVC-DIDA	Polyvinyl Chloride and Diisodecyl adipate
R	Arginine
R-type	"Right-handed"
RIJ	Reactive Inkjet Printing
RGD	Arginine-Glycine-Aspartic acid
S-type	"Left-handed"
SERS	Surface Enhanced Raman Spectroscopy
SLA/SL	Stereolithography/Stereolithography apparatus
SLM	Selective Laser Melting
SLS	Selective Laser Sintering
SP	Soy Protein
SPP	Soy Peptide Powder
SSE	Semi-Solid Extrusion
STL	Stereolithography
$ZFKC_3$	Molecule containing: protecting group – phenylalanine – lysine - carbon tail

Theory part

1. Introduction

Three-dimensional (3D) printing has been invented in the early 1980's but in recent years it has developed rapidly and is being used widely for different purposes.[1] 3D printing is a manufacturing method that transforms a digital design into a physical 3D object, for example, by adding selected material layer by layer.[2] 3D printing has been utilized in various fields, including biomedicine, polymer science, food industry, and in flow chemistry.[3,4,5,6] Artificial reefs, titanium horseshoes, jewellery, guns, smart dynamic objects, and even houses have been printed due to the possibility of using different materials as ink for printing.[2]

Food 3D printing can be used for the need for special consumer categories, and it can enhance the nutritional value of the material. Though typical edible gels are conventional chemical gels, the knowledge obtained from printing them can be expanded into supramolecular gel printing; designing complex geometries, optimising printing parameters, and the possibility for printing *via* hot or cold extrusion.

3D printing of gels can be characterized to be an empirical science, due to printable gels being usually found by trial and error. Preliminary studies are conducted to improve the level of understanding which gel morphologies are printable.[7] Usually research groups use commercial fused deposition model (FDM) 3D printers, which are modified to the specific occasion. Various printing obstacles, including air bubbles in the nozzle of the printer, must be overcome.[8] Different printing methods can be exploited, including wet spinning, bath supported printing, and inkjet printing. In addition, the consistency of the gel used as the ink can be improved by using different additives or blended inks.

3D printing has a huge potential for applications in the biomedical field and the pharmaceutical industry. The first 3D printed tablet has been available for consumers from 2015. Hydrogels have many suitable features for being used as biomaterials including structural stability, exceptional nutrition and oxygen permeability, biocompatibility, and low toxicity. Hence, they are used as standard extracellular matrix substituents. However, not all hydrogels fit the criteria to be used in 3D printing, for example, due to their unstable structure. In addition, supramolecular gels possess unique features, which are beneficial in tissue engineering *via* 3D printing. For example, they are responsive and capable of self-healing, meaning that they can return to their original shape after distortion. Due to the responsiveness, it is possible to create applications, such as functional artificial muscles, from them.

Soft hydrogels have an amazing resemblance to soft human tissues. When printing with cell-containing gels as bio-inks, the softness of the ink-hydrogel is a key feature. Otherwise, the cells might fracture and die. By 3D printing of hydrogel with neural cells can brain-like structures for *in vitro* applications be manufactured. The printed structure can form a working neural network post-printing. Furthermore, with rapid 3D printing of hydrogels could custom made organs, such as aortic valves, be created in only from 14 to 45 minutes.[9]

Amino acid and protein-based hydrogels as biomaterials are desired for their many suitable features, including their anti-microbial nature and anti-inflammatory activity.[10] In addition, studying of the hydrogelation of amino acids phenylalanine, lysine, and arginine is important for many reasons, including that their aggregation plays a role in Alzheimer's disease. Peptide-based hydrogels together with 3D printing technology open new opportunities for biomimicking applications in the pharmaceutical industry. With proper additives, amino acids such as lysine, can be used as hydrogel inks. Furthermore, lysine is the most investigated amino acid as a gelator for supramolecular gels.[11] Amino acid phenylalanine derived gels can be used as drug carriers, as well as in 3D printed scaffolds. Compared to casting techniques, 3D printed peptide gels as tissue models can exhibit complex *in vivo* organizations, such as complex skin structures.[12]

2. Amino acids and peptides

All ever occurred proteins are constructed from the same set of 20 amino acids, which are covalently linked together to form a protein. Each amino acid has a unique, chemically distinctive side chain, or R group. It varies in structure, size, and solubility in water, which is caused by the difference in the electric charge of the side chain. Each amino acid has a three-letter abbreviation and a one letter symbol of their own. All the common 20 amino acids have a carboxyl group and an amino group bonded to the same carbon; thus, they are α-amino acids. For the exception of glycine, amino acids are chiral molecules and therefore have two possible enantiomers (D, L system). Virtually all the protein-constructing amino acids are L stereoisomers. Like other chiral molecules, amino acids are also optically active and rotate plane-polarized light.[13] In biological context, usually the L enantiomer is effective, whereas the D enantiomer can be invalid or even toxic.[14]

The phenylalanine and lysine, among 7 other amino acids, are called essential since the human body cannot produce them. Arginine is classified as a semi essential amino acid, and it is one of the most metabolically versatile amino acids.[15] The natural properties of amino acids, such as biocompatibility and biodegradability, is the reason behind their wide use in biomedical domains and pharmaceutical field.[16] The amphiphilic amino acids possess an ability to hydrogelate, due to the opportunities for hydrogen bonding with hydrophilic parts and the stabilization effect towards water molecules. The hydrophobic parts may prompt aggregation.[17] Amino acids can be used as precursors for creating functional molecules with wide range of gelation properties.[18]

Phenylalanine has an aromatic side chain, and therefore is relatively nonpolar. At neutral pH of 7.0, the side chains of lysine and arginine are positively charged. These basic amino acids are hydrophilic.[13] Although the similar R-group of these amino acids, they interact with the environment rather differently. Lysine is more likely to be deprotonated inside a membrane than arginine, and arginine is more efficient in stabilizing membrane pores.[19] The L-structures of phenylalanine (Phe, F), lysine (Lys, K), and arginine (Arg, R) are illustrated in Figure 1. Lysine and arginine play a key role, for example, in many biological recognition processes, gene regulation, and vesicle transport.[20] Studying hydrogelation of Phe, Lys, and Arg is important in respect of Alzheimer's disease, due to the protein aggregates in the brain containing these amino acids.[20,21]

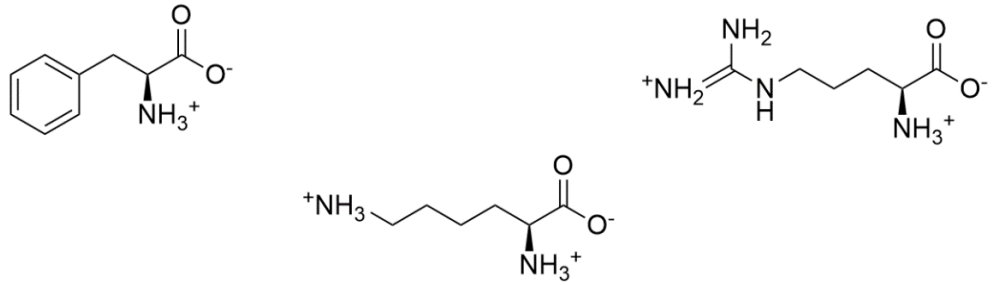

Figure 1. From left to right; L-structures of Phe, Lys, and Arg in neutral pH.

The covalent bond between two amino acids is a substituted amide linkage, which is formed by dehydration. The removed water molecule is from the α-carboxyl group of one amino acid and the α-amino group of another. The formation of a peptide bond is illustrated in Figure 2. The equilibrium of the reaction favours the free amino acids over a peptide. The formed peptide bond in proteins is stable, possessing a half-life of 7 years, by average, in most intracellular conditions. The peptide bond is rigid, and the atoms of the carboxyl group and amino group are

co-planar toward each other. The C—N bond of a peptide is shorter than the C—N bond of a simple free amine, indicating a resonance or partial sharing of two pairs of electrons between the carbonyl oxygen and the amide nitrogen. The oxygen and the nitrogen have partial charges, negative and positive, respectively.[13]

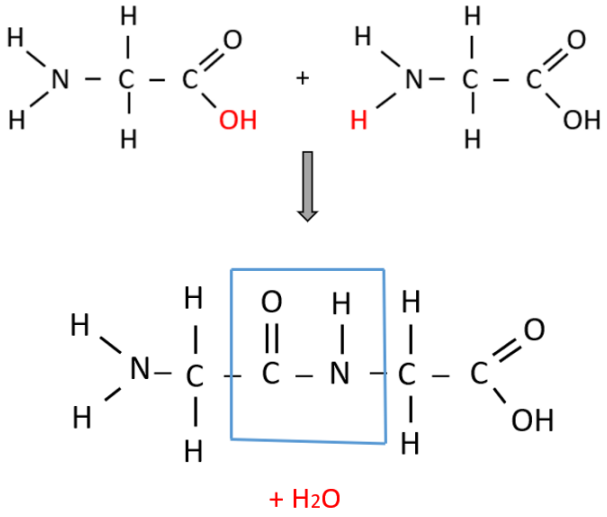

Figure 2. Two glycine amino acids form a dipeptide with separation of a water molecule. The peptide bond is highlighted with blue color.

The sequence of amino acids forms a peptide, called the primary structure of the protein. Every protein has its own unique three-dimensional structure, which stems from its secondary, tertiary, or quaternary structure. Size of the protein can vary from just a few amino acids to colossal polymers. The most prominent secondary structures, formed with weak interactions including hydrogen bonding, are the α-helix and β-conformations. The tertiary structure covers longer-range aspects of amino acid sequence and is the completely folded form of a protein. The quaternary structure is the spatial arrangement of a complex containing two or more polypeptide subunits.[13]

The (R) and (S) system is used with molecules containing several chiral centres for specifying the configuration around the centres. The α-helices can be either *R*-type, meaning "right-handed", or *S*-type ("left-handed").[13] It is widely regarded that the chirality of constituent amino acids of peptides or of amino acid derivatives is a key factor of controlling the handedness of supramolecular organizations constructed with them.[22]

3. Supramolecular Gels

Supramolecular chemistry has attracted the attention of numerous researchers over the past five decades and can be defined as 'chemistry of molecular assemblies and of the intermolecular bond'. Supramolecular chemistry can also be referred to host-guest-analogy, which implies the weak interactions between a 'host' and a 'guest' molecule.[23] The formation of a host-guest complex is shown in Figure 3. The supramolecular systems are made from molecular building blocks by non-covalent interactions, and they can show stimuli-responsive behaviour. Furthermore, chemical architectures, such as rotaxanes, catenates, and knots, can easily be prepared through templated synthesis. These complexes are difficult to manufacture from more traditional covalent chemistry. Supramolecular chemistry has been widely explored in various areas, such as molecular machines, gas absorption, and nanoreactors.[24]

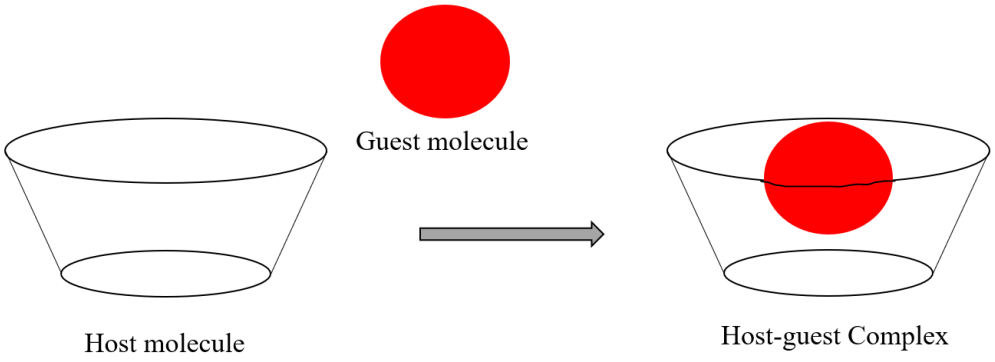

Figure 3. The supramolecular self-assembly *via* weak interactions between a host molecule and a guest molecule.

Gels are topological and familiar from everyday life, for example, in the form of toothpaste, contact lenses, hair products, and food substances. The physical nature of gels can be studied through rheology, which examines the flow and the deformation of matter under applied stress.[25] By one definition, the conventional gels differ from supramolecular gels in the way that they do not express hierarchical self-assembly nor thermoreversible sol-gel transition.[26] The conventional chemical gels are composed of permanent covalently bonded polymer 3D-network imbibed a vast quantity of liquid.[27] The physical supramolecular gels, which can be created with low-molecular-weight-gelators (LMWGs), are built *via* non-covalent interactions, such as hydrogen bonding and van der Waals forces. Typically, an LMWG-molecule consists of a strong hydrogen bond donor or acceptor.[28] The representation of the formation of a supramolecular gel is shown in Figure 4. Supramolecular gels, built with appropriate LMWGs,

are responsive to external stimuli. Thus they can perform transition between gel and solution states under the influences including changes in pH, heat, ultrasound, and mechanical force.[29] The reversibility of interactions between LMWG-molecules results in a dynamic behaviour, which leads to opportunities, such as self-healing and slow release of drugs.[28]

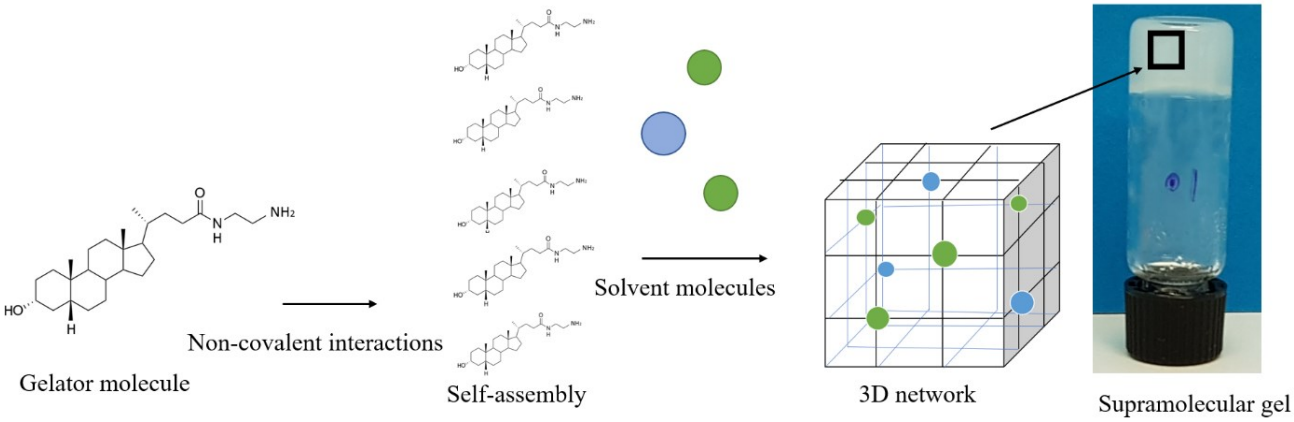

Figure 4. Schematic illustration of the formation of a supramolecular gel.

Supramolecular gels, also known simply as molecular gels, can be named according to the liquid component of the gel. In hydrogels the component is water, in organogels it is organic solvent, and in aerogels the component is in gas phase.[28,30,31] The network of metallogels is held together with metal-metal or metal-ligand interactions.[32] The high amount of water in hydrogels attributes a liquid-like behaviour to these solid-like rheological materials. This feature gives them a remarkable resemblance to the human tissue.[33] Applications of supramolecular gels vary from targeted drug delivery systems to waste management, and even to optoelectronic devices.[34,35,36]

Some molecular gels exhibit a phenomenon called *thixotropy*, which can be defined as an increase of viscosity when resting and a decrease of viscosity when applied to a constant shearing stress. Thus, by shaking the gel liquifies, and returns to solid state at rest. This feature is beneficial in some cases, for example when molten hydrogels are injected by a syringe, and returning to solid form after injection.[37] It is not well understood, why some molecular gels are thixotropic and some are not.[7]

3.1 Phenylalanine, lysine, and arginine-based hydrogels

Peptide-based molecular gels have been widely studied for over the last decade due to their potential in biomaterial science and in areas of nanoscience, due to the many beneficial features of peptides including low toxicity, biodegradability, and biocompatibility.[38] In addition, peptide-based gelators have been used to develop stimuli-responsive and self-assembling structures.[10] Furthermore, peptide-based hydrogels have attracted a lot of attention recently due to their self-assembly of fibrous structures *via* π-π stacking of β-sheets resulting to a biocompatible, nanofibrous mimic of an extracellular matrix.[39] These gels have potential applications in tissue engineering, antibacterial and anticancer agents, wound healing, bioimaging, and 3D printing to name a few.[10]

L-phenylalanine is the smallest molecule to form supramolecular hydrogels, reported in 2002[40] (and still reported in 2017)[41]. Phe forms intermolecular weak interactions, including π-π -stacking, in aqueous media.[42] Phe-based hydrogels are potential as drug delivery matrices. The network of hybrid hydrogel, including peptide-based gelator and Phe-derived polyelectrolyte, is constructed by longer and unidirectional fibrils, compared to the helically twisted fibrils for the pure peptide. Thus, by supramolecular gel design can synergistic properties arise.[43]

The LMW hydrogelator helices formed by Phe derivatives can be left- or right-handed, even though the same *R*-type chiral center of the amino acid is used. This with the covalent bonding of achiral substituents to each terminus of the gelator structure influences the handedness of the helix, but also exhibits unexpected chirality inversion. Desired handedness for smart materials can be controlled with probing the supramolecular chirality.[22]

A supramolecular gel formed by two lysine-derived gelator molecules in dimethylsulfoxide(DMSO)/water mixtures might be resulted from jammed suspensions of mainly linear clusters. These mesoscopic clusters resemble those at the origin of crystallization. A presence of a chlorine atom together with an aromatic ring of the other lysine-derivative induced a decreased performance of rheological properties and an increased gelation time scale.[11] The lysine-derivatives are shown in Figure 5.

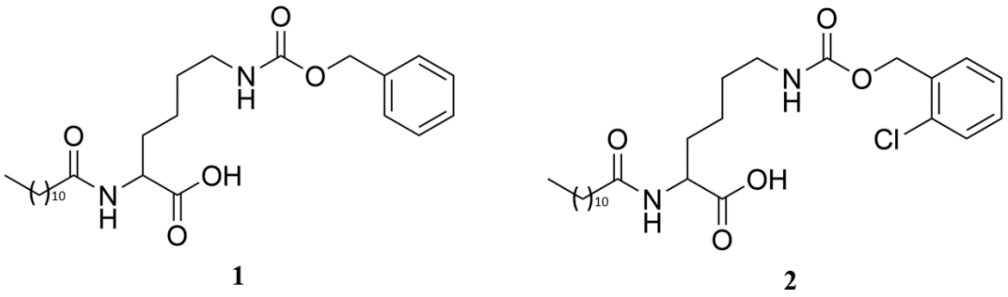

Figure 5. Two lysine-derived LMWGs

The water-soluble poly(α-L-lysine) (PLL)-based biopolymers can be used as antibacterial agents, drug delivery systems, in bio-sensing, bio-imaging, and tissue engineering. These applications are derived primarily from the cationic charge properties of PPL. However, the same positive feature also correlates with cytotoxicity. The cytotoxicity increases with increasing size of the polymer.[16]

Addition of L-arginine to a gel can improve its water holding capacity, hardness, springiness, and cohesiveness. Due to the water holding capacity feature of L-arginine, it can be utilized in the food industry for improving the texture of meat products.[44]

4. 3D printing

The conventional printers print text and images with ink usually on a paper in a flat, two-dimensional space. By adding a third dimension, depth, with length and width, workable objects which can be used and held, can be printed. The 3D printed objects of this additive manufacturing technique can take almost any form depending on the size of the printer. Furthermore, after printing it is possible to link or fuse different parts together to form larger objects for creating objects with a variety of shapes. 3D printers were first utilized for industrial needs for rapid prototyping. The 3D printer is an ideal solution for anything that required moulds in the past. Nowadays by advancements in technology the costs of the 3D printers have decreased, opening the consumer markets with reasonable prices. In addition, the sizes of the printers have decreased while the types of starting materials, and filaments, have greatly increased.[2] In Figure 6 is a 3D printed object, which is printed with fused deposition modelling (FDM) printer using a thermoplastic filament.

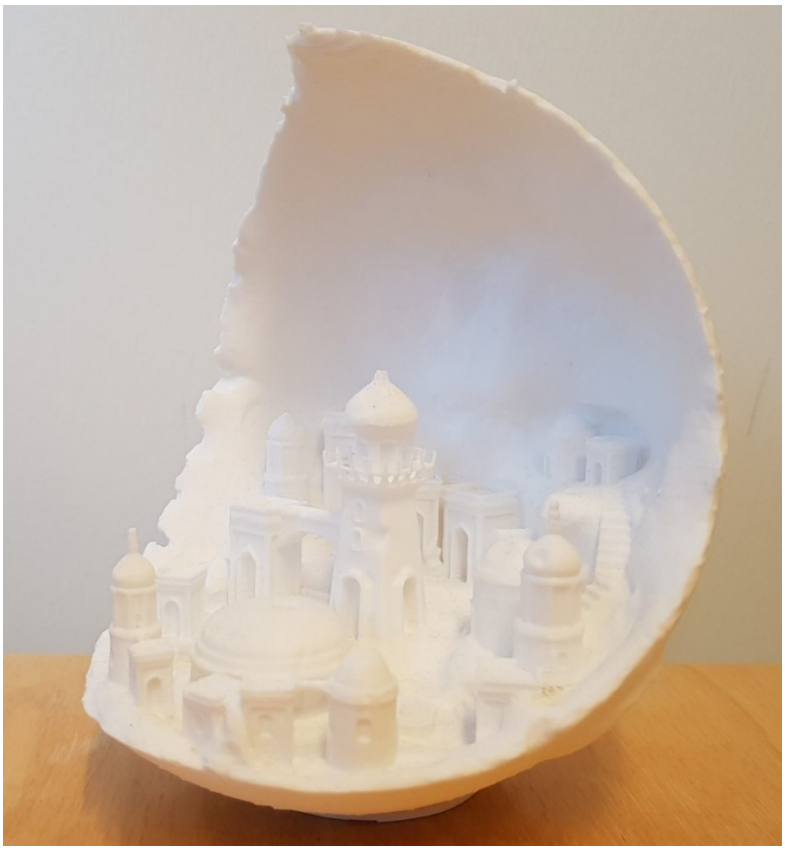

Figure 6. FDM 3D printed thermoplastic object.

The 3D printing process starts with obtaining a model or a digital design by using computer programs, scanners and camera, parametric mathematical equations, or downloading a premade model from an online library. The 3D digital model of the desired solid object consists of triangles. Information of the triangles' surfaces is converted to the computer to describe and define the geometry of the design. In Figure 7 is a computer aided design of a desired printable object and the triangle-model of the design. The design information is transferred to the computer by selecting a proper file format, most commonly the Stereolithography (STL) format. Before printing the model must be sliced with slicing software for obtaining printable layers of the desired object. By slicing, all the information is converted into a blueprint, or G-code, which the printer follows when printing layer by layer. The code includes all the instructions that the printer needs, such as temperature, paths of each layer, and fan start and stop time. Some objects may need support and rafts while printing. The printing time varies greatly depending on the size and material of the printed object; a print can take several hours at longest. Finally, the printed object may be refined by methods of finishing, including smoothing the layers by sanding and painting.[2]

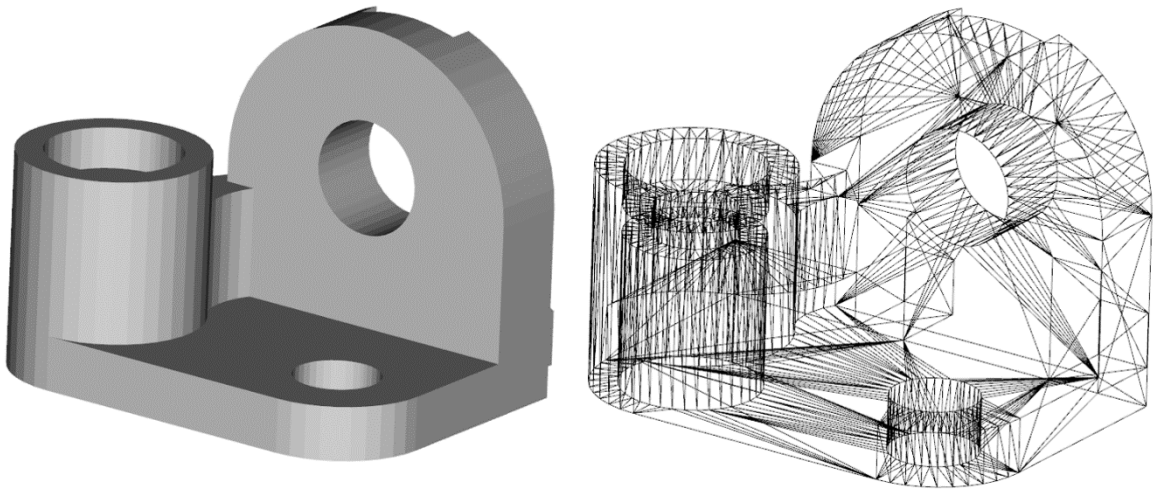

Figure 7. A computer model of a desired printable object, and its ‘triangle’-design.

A variety of materials, including plastic, metal, and food, can be used as the starting material, also called as the ink, depending on the type of the printer. One of the most popular desktop and industry model 3D printer, FDM printer, usually uses spooled thermoplastics (called the filament) for printing. A great selection of plastic filaments is available with differing features, such as melting temperature and flexibility. The name FDM has many aliases depending on the manufacturer. The printing temperature of FDM can be as high as 255 ℃.[2]

An FDM printer consists of several common components. Bed is the surface area where the object is printed on. Extruder is a motorized device that includes the cold and the hot end. The cold end pulls the filament from the spool and the hot end heats and melts the filament into the desired temperature. Nozzle is a small metal device with a fixed hole for the extrusion to happen onto the build area, which is the bed with dimension of height. Linear rod or rails help either the extruder, the bed or both to move during printing. Local controller is a device which allows giving commands directly to the printer.[2] Figure 8 shows the main components of the FDM printer. In Figure 9 an image of an FDM printer is presented.

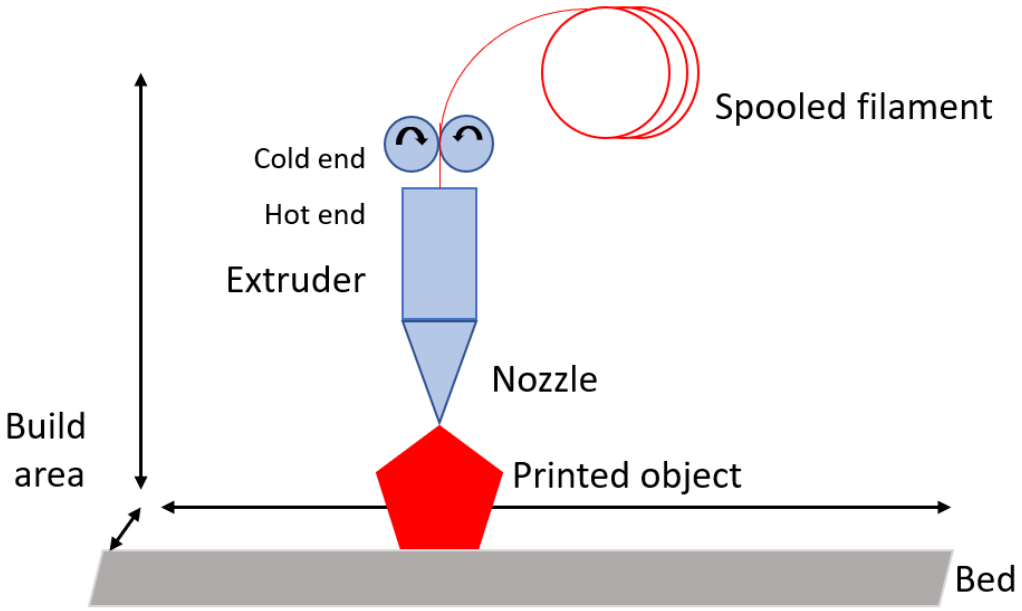

Figure 8. A simplified scheme of the FDM technology.

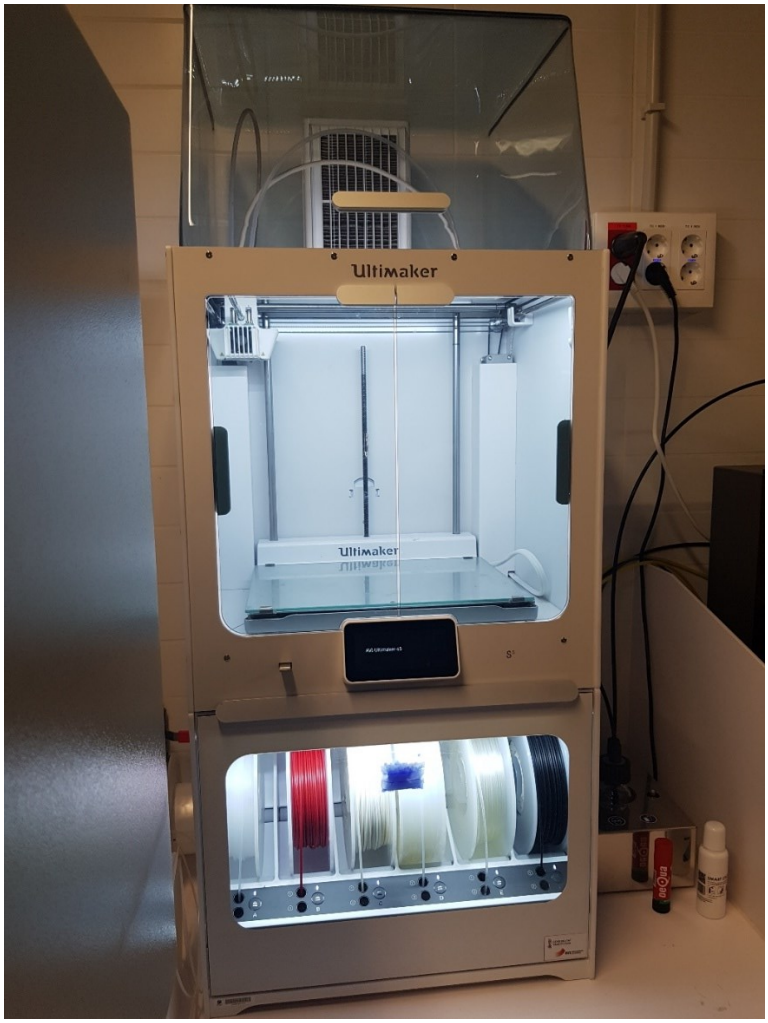

Figure 9. An image of an FDM printer, which uses thermoplastic filament as ink.

Material extrusion-based method of FDM can use liquid monomers, particle colloids, polymer solutions, gels, plastic powders, and continuous thin filaments as the ink for printing.[4] A method of FDM, hot-melt extrusion (HME), can be utilized among various techniques, in hydrogel printing for pharmaceutical and food industry purposes.[1,45] The technology of coupled HME together with FDM can be exploited in the pharmaceutical industry.[46]

Other 3D printing methods include powder bed fusion (PBF), and vat photopolymerization. The PBF uses powder materials which are fused together. A thin layer of material is spread to the print chamber area and the outline of the print object is melted. This process is repeated layer by layer, and at the end the un-melted material is blown away revealing the new object. PBF methods, selective laser melting (SLM) and selective laser sintering (SLS), use a laser to melt the powder. The vat photopolymerization method uses liquid photopolymer resins in different deployment methods that use light instead of heat to fuse or to cure the resins in layers to form the desired object. A vat photopolymerization method, stereolithography (SL), also known as stereolithography apparatus (SLA), uses an ultraviolet light to cure the added layers of the object. For example, SL is utilized in the dental industry for manufacturing customized crowns and braces.[2]

Regardless of the printing method, the printed materials can be bought ready-to-use, or they can be self-made to a limit. Also, the printed material can be tuned pre- or post-printing. The features of the printed object can be enhanced by incorporating additives into the suitable easily printed matrix. In addition, by the same manner can substances, which are not suitable for printing, be printed. For example, chemical functionality can be improved by adding another polymer, resin, oxide, crystallized materials, salt or molecular compound into the printable matrix, such as Nylon-12.[47]

4.1 3D printed labware

3D printing has been utilized in organic chemistry, for example, by manufacturing customized labware and reactionware since many chemical processes require a unique labware. In addition, the struggle with cleaning, reusing, and storing glassware and laboratory equipment can be avoided in some cases with 3D printing. Some downsides with 3D printed thermoplastic labware should be noted, including the non-transparency of the ware and the possible reactions between the ware and the chemical substances.[48]

The possibility of 3D printed reactionware has attracted attention in the field of continuous-flow organic chemistry. Organic compound synthesis through flow systems, instead of traditional batch production, has been frequently reported. Dragone *et al*.[6] demonstrated an in-house designed reactionware for the synthesis of imines from the reaction of a range of aldehydes and primary amines. One of these reactionwares is schematically represented in Figure 10. These inexpensive and chemically inert polypropylene reactors are suitable for use in single-step or multistep reactions in flow.

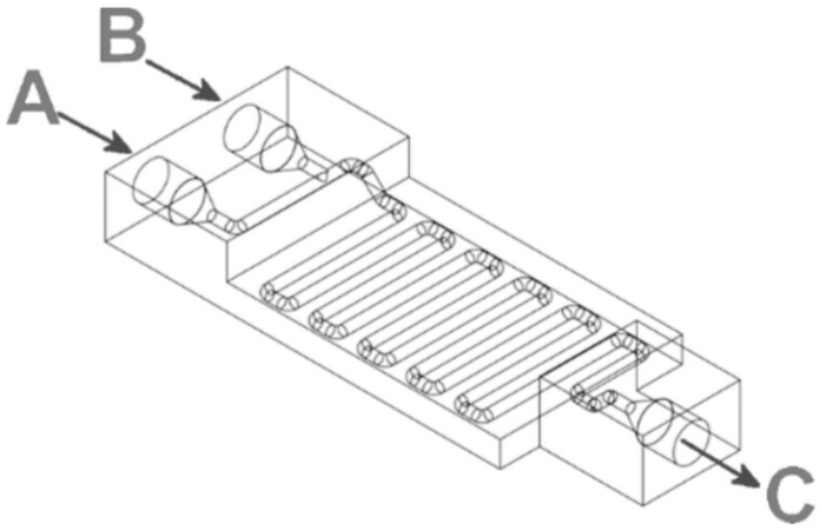

Figure 10. The schematic representation of flow chemistry reactionware for imine synthesis with display of internal channels. A and B are input channels and C is an output channel. Figure adapted and partially reproduced from ref. 6 with permission of Beilstein Journal of Organic Chemistry.

4.2 3D printing in food science and printed edible gels

Food printing combines the 3D printing and digital gastronomy to create food with customized shape, colour, flavour, texture, and even enhanced nutrition value. Even though current printers are too slow and cannot meet consumer requirements, they offer an engineering solution for personalized nutrition control along customized food design. In the sector of personal gift market logos painted onto food, letters carved into cookies and frosted patterns on chocolate are available.[49] Ideally in restaurants by identically printing complex shapes the chef is freed to work on other tasks. Also, the amount of food waste can be reduced, for example, by using all parts of the vegetable when printing.[2]

3D printed food is one solution for the demand of special consumer categories, such as elderly and athletes. This is achieved by processing of additives, flavours, and vitamins. Also, the self-life of food products can be improved with printing.[5] The difference of physical structure between 3D printed and cast gels can lead to better nutritional value. The printed gels are more prone to swelling than cast gels. Study by Kamlow *et al*.[50] demonstrated a higher fraction of released thiamine at a higher rate with a 3D printed edible gel when compared to a cast gel.

Portion of the printed foods, such as chocolates and gels, are in edible form immediately after printing, but majority of traditional foods need to be post-cooked after printing.[49] Maintaining the 3D shape throughout cooking process is a significant challenge with 3D printed foods, because these processes involve heat penetration and result in non-homogeneous mixture. This challenge regarding baking, steaming, and deep-frying can be overcome by recipe control or using additives.[51] Lipton *et al*.[52] printed and cooked foods including meat-pure and cookie dough successfully with maintaining their structures during the cooking process.

Typical edible gels, such as gelatine-based desserts and custards thickened with potato starch, can be categorized as conventional chemical gels. Thus, they cannot be re-heated without destroying its structure. Gelatine is usually derived from pork skin. Some gels are formed using agar, which is extracted from different types of red algae. Agar is a polysaccharide, whose main component is agarose that consists of D- and L-galactose units.[53] Due to its thermoreversible nature among other features differing from gelatine-based gels it has been exploited in the field of molecular gastronomy.[54,55] Also, due to agar's plant-based origin it is suitable for people with restricted diets, including Muslims, vegetarians, and vegans.

Edible 3D printed gels are studied for the possible opportunities, including designing complex geometries without moulds, and producing softer foods mimicking normal food appearance for people with conditions such as dysphagia. Hydrogels can be printed with cold extrusion when the gel is set in advance, or with hot extrusion method when the component is printed at sol state and the sol-gel transition occurs on the printing bed rapidly after printing.[50]

Yang *et al*. [1] and Wang *et al*.[56] have studied optimizing 3D printing parameters to conventional chemical gels, which were lemon juice gel thickened with potato starch and fish surimi gel strengthened with NaCl. The gels were set before printing. The printing parameters of nozzle diameter, nozzle height, nozzle moving speed, and extrusion rate all play an important role in printing 3D constructs with a desired design with fine resolution, smoother surface texture, fewer defects, and no compressed deformation. Results of different extrusion rates on lemon juice gel are shown in Figure 11. In a previous study by Wang and Shaw[57] an equation for the

critical nozzle height estimation was proposed, but in both of the studies of Yang and Wang the equation failed to have an optimal outcome. The study with lemon gel proposed a new equation for explaining the relationship between the nozzle diameter, and the nozzle moving speed and the extrusion rate. Equation (1) can be applied for other 3D printed gels for estimation of the optimal extrusion speed based on the known nozzle moving speed and nozzle diameter.

$$V_d = \frac{\pi}{4} V_n D_n^2 = \frac{4}{\pi} V_n h_c^2 \quad (1)$$

In the equation V_d is volume of the extruded rate in mm^3/s, V_n is the nozzle moving speed in mm/s, D_n is the nozzle diameter in mm, and h_c is the nozzle height, which is equal to the nozzle diameter.

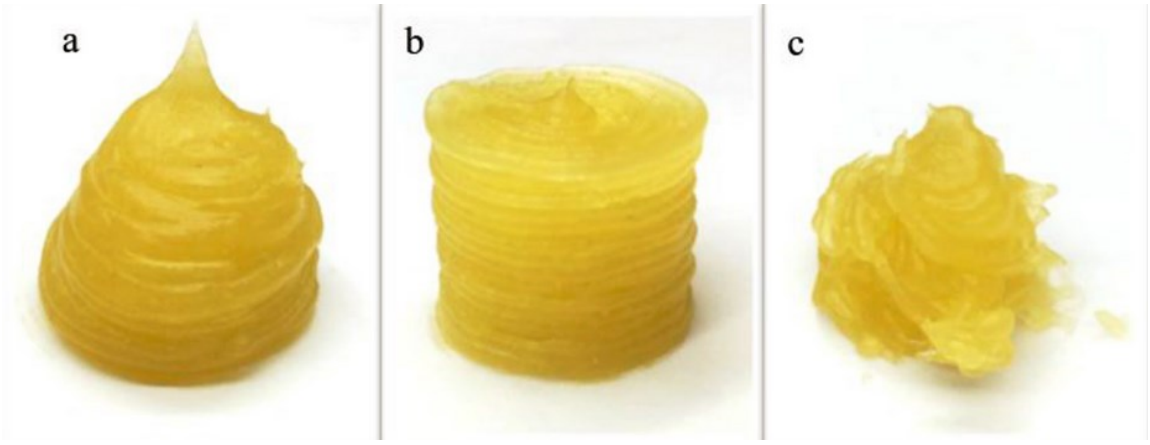

Figure 11. Printed lemon juice gel with increasing extrusion rates. Figure adapted and partially reproduced from ref. 1 with the permission of Elsevier.

Studies regarding 3D printing of emulsion gels for creating reduced-fat meat analogues has led to a discovery of thixotropic inks by biosurfactants promising for printing. The demand for low-fat meat replicas is increasing these days, due to the environmental-aspect of plant-based food and the nutritional downsides of high-fat containing food products. Soy-based emulsion with fat-replacing hydrophobically modified biosurfactants forms a dynamic and recoverable ink. In addition to better texture and mouthfeel, fat replacement with surface-active biopolymers offer supramolecular functional properties to the ink dispersion, which might adjust its flow behaviour and reinforce the mechanical strength of the printed structures. The study of the emulsion ink with a monomodal particle size distribution, shear-thinning behaviour, thixotropic properties, and viscoelastic properties adds understanding of printability and extrudability of biomaterials.[58]

4.3 Gel 3D printing

3D printing offers a new field for self-healable, supramolecular soft materials with up-sides such as fast processing and freely designable shapes. Printability of supramolecular gels can be based on reversible thermal- and shear-induced dissociation of a gelator polymer network, which generates stable and self-supported structures after printing. These structures can be stable at room temperature and below.[59]

While a vast number of different hydrogels are known, only a few of them have been discovered to form stable structures *via* printing. Swelling is a common phenomenon in hydrophilic gels,[60] which can sacrifice mechanical properties as well as printing resolution. However, for biological applications the high permeability of swelling gels is beneficial.[61] Using the reversible intermolecular/supramolecular weak bonds, hydrogels have been exploited vastly, since they can create stable structures after printing while enabling flow during the printing process.[62] The stability of a 3D printed chemical hydrogel after seven days is shown in Figure 12.

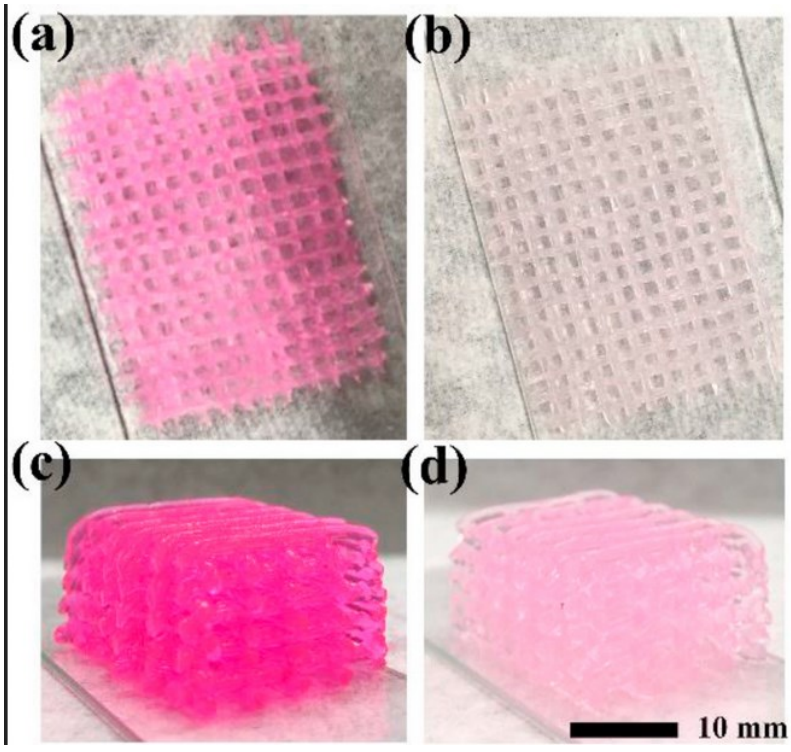

Figure 12. The stability of a multilayerd 3D printed structure of a conventional hydrogel. Figures a) and c): the gel immediately after printing. Figures b) and d): the printed gel after 7 days of soaking in deionised water. Figure adapted and partially reproduced from ref. 60 with permission of Elsevier.

Similar to conventional gels, optimizing the printing parameters, including extrusion volume and speed, printing height and printer movement speed, will lead to better resolution with LMWG-based gels.[7] A 98 % recovery from mechanical damages has been reported with a 3D printed self-healing supramolecular gel, with dynamic imine bond formation.[8] In Figure 13 the recovery process of a printed supramolecular gel is shown. The speed of the deforming and the recovery of the printed gel can be improved, for example, with using gel fibres with small diameters.[63]

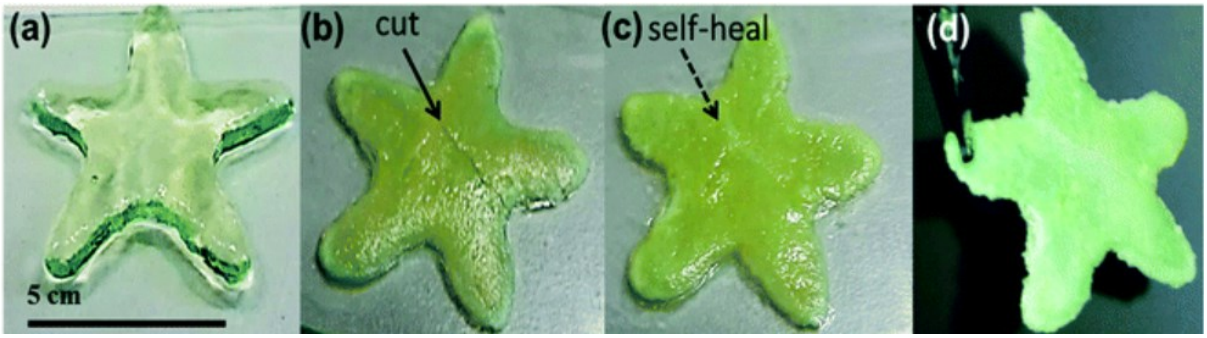

Figure 13. The self-healing process of a printed gel-star. a) The star immediately after printing. b) The star with a deep cut made with scalpel. c) The self-healed star 30 minutes after the induced cut. d) The star after one hour of recovery while drying in ambient conditions. The star is lifted as a single unit managing self-support against gravity without falling apart. Figure adapted and partially reproduced from ref. 8 with the permission of Royal Society of Chemistry.

A 3D printable window demonstrates the optimal area of circumstances when printing molecular gels. A schematic representation of the 3D printable window is illustrated in Figure 14. By creating gels with rapid formation and full maturation of the gel before printing can an extended printing window be achieved and the limitations of the time-dependent printing be overcome.[8]

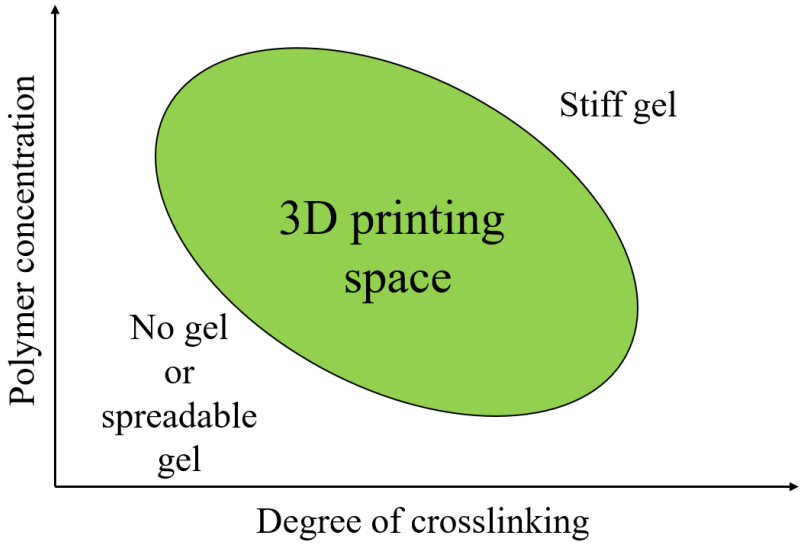

Figure 14. Schematic presentation of the 3D printable window.

3D printed gels are often cured post printing typically in air or in ultraviolet light.[64,65] They can be incubated, for example, in ferric solution, for producing tough molecular gels.[63] In addition, the printed samples can be immersed into different substances, such as deionized water, to allow swelling or to achieve equilibrium state.[63,65]

Molecular gels can be created using 1D inorganic nanowires as the host molecule to manufacture 3D printed flexible electronics, such as flexible UV-sensors. These gels can be self-supporting while printing (Figure 15). The thixotropicity of the gel combined with the high viscosity of the gel facilitates the extrusion-based printing of the functional nanowire gels. Water soluble and single-layered 2D nanosheets of the gel function as physical crosslinkers. In aqueous suspensions, the nanosheets can knot-tie and stabilize the nanowire junctions. These 3D printed silver nanowire-based gels exhibit a remarkable electrical conductivity.[66]

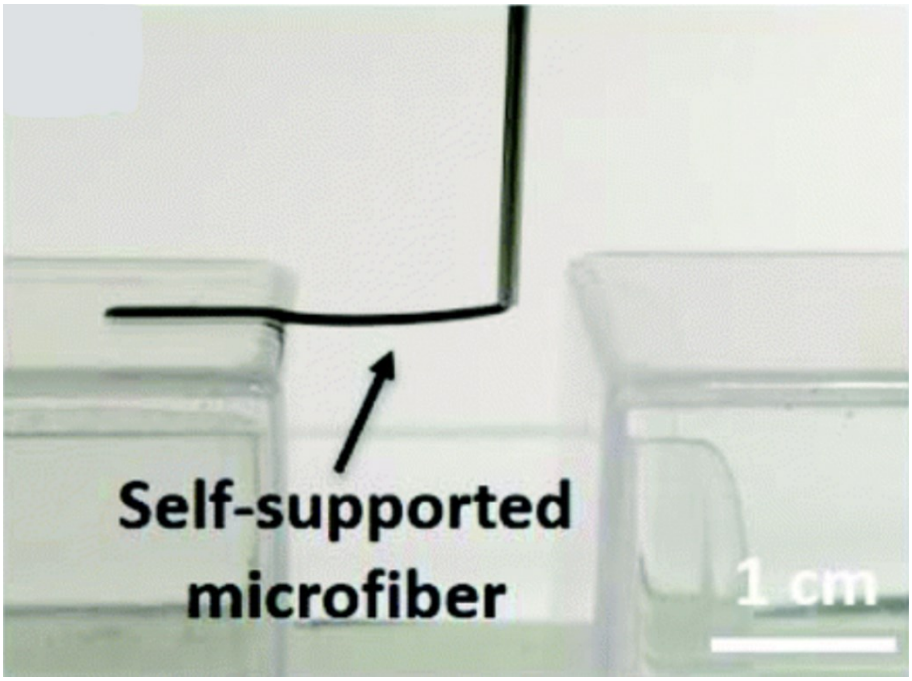

Figure 15. A molecular nanowire gel supporting itself on air while printing from a nozzle. Figure adapted and partially reproduced from ref. 66 with the permission of Royal Society of Chemistry.

Wet spinning is a method used widely with polymers but can also be suitable for LMWGs. The solid gelator is dissolved in a good solvent followed by extrusion into a coagulant (solvent-non solvent mixture) solution, in which the gelator self-assembles when in contact.[67] Figure 16 illustrates the process of wet spinning to fabricate gel filaments.

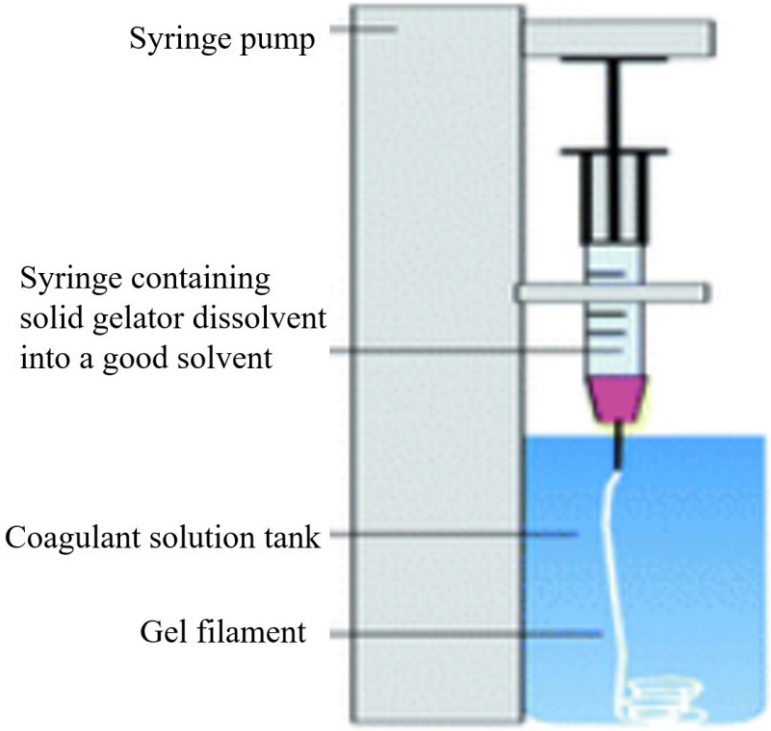

Figure 16. Wet spinning process. The gel filament is created by the reaction between the extruded solution and the coagulant non-solvent. The non-solvent used can be water. Figure adapted and partially reproduced from ref. 67 with permission of Royal Society of Chemistry.

Study by Piras *et al*.[67] showed that LMWG-based gel prepared by wet spinning can be extended into 3D printing. The gel showed excellent stability for at least a week in water and maintained its ability for *in situ* precious metal reduction, yielding Au nanoparticles. The AuNP loaded gel is biocompatible and enhances stem cell metabolism. These results show potential for 3D gel printing for tissue engineering applications.

4.3.1 3D form from 2D printed gels

Inkjet printing (IJP) is a type of non-contact 2D printing method. It is characterized by the droplet formation by a sudden pressure pulse in the nozzle chamber. Inkjet inks typically have low viscosity and rather low solid concentration in order to leave the nozzle and to allow fast droplet generation. The pressure pulse, which is an electric voltage pulse by nature, can be created for example with heat or with a piezoelectric element. The shape of the pulse will effect on the printing parameters including the droplet size.[68]

Some 3D shapes, such as pyramids, helices, and even blooming flowers, can be created onto the surface of strong hydrogel sheets with commercially available 2D inkjet printer and an aqueous ferric solution as the ink for patterning. Figure 17 illustrates 3D gel objects created by using this method. The shape deformation, including twisting and bending, is driven by nonuniform internal stresses caused by the uneven swelling or deswelling of the different parts of the printed gel. In its convenience and diversity of designing complicated patterns, this method is superior to most existing methods. On the other hand, size of the printed object remains a challenge. With 2D printed hydrogels can soft machines be fabricated, and optical devices, drug delivery systems, and artificial muscles ultimately be created.[69]

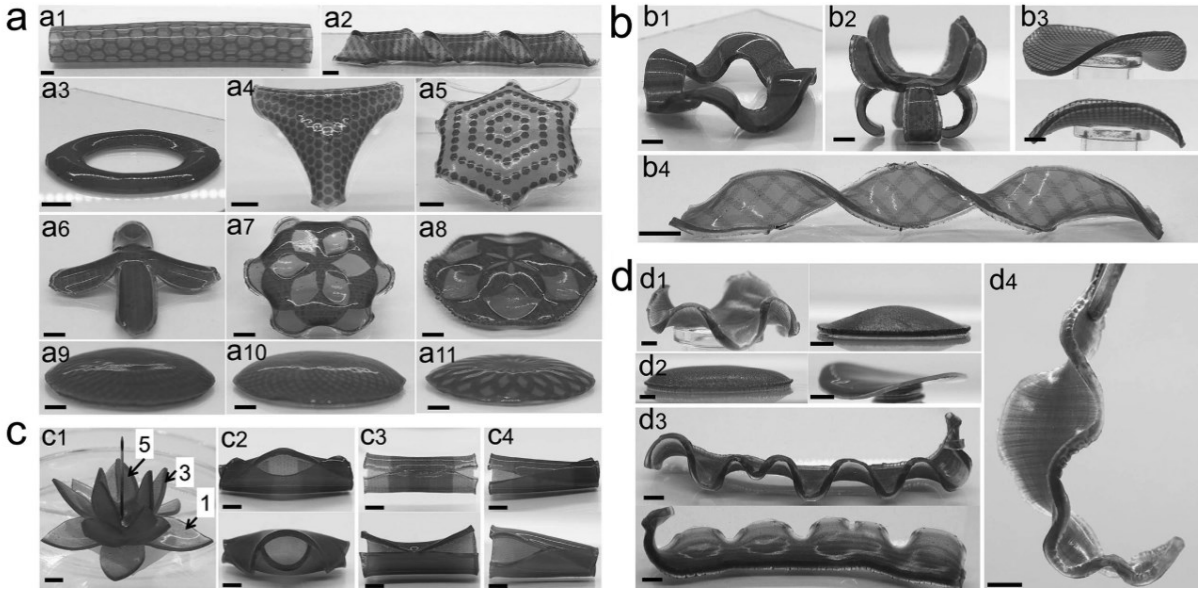

Figure 17. 2D printed patterned hydrogels. a) Patterns printed on only one surface of the gel. b) Both sides are patterned. c) Hydrogels with different or gradient patterns on one surface. d) Different or gradient patterns on both sides. Reproduced from ref. 69 with the permission of Wiley and Sons.

4.3.2 4D printing

Four-dimensional (4D) printing is the integration of active material technologies to 3D printing.[70] Conventional 3D printed materials, including gels, can be seen as static objects. The fourth dimension is the self-evolving aspect, that transforms the structure into a predetermined shape, changing property and function after printing.[71] Environmental stimulus, such as heat or

moisture, can switch the printed components between multiple configurations. Two main active polymers used in 4D printing these days (2017) are hydrogels and shape memory polymers.[70] The used hydrogels are integrated with a non-swelling polymer or filament for creating the mismatch strains between the two materials, leading to overall shape change.[71] The integration of the heterogeneous gels can be executed by printing with multiple nozzles.[63]

Designing and manufacturing biomimetic structures, such as lily flowers with ruffled-edged petals, can be achieved with 3D printed composite hydrogels, which exhibit shape-morphing after printing. The morphosis by immersion of water of the 4D structure from the 3D structure can develop under 5 minutes. Figure 18 shows the progression into a 4D object and the range of morphologies of printed flowers.[65]

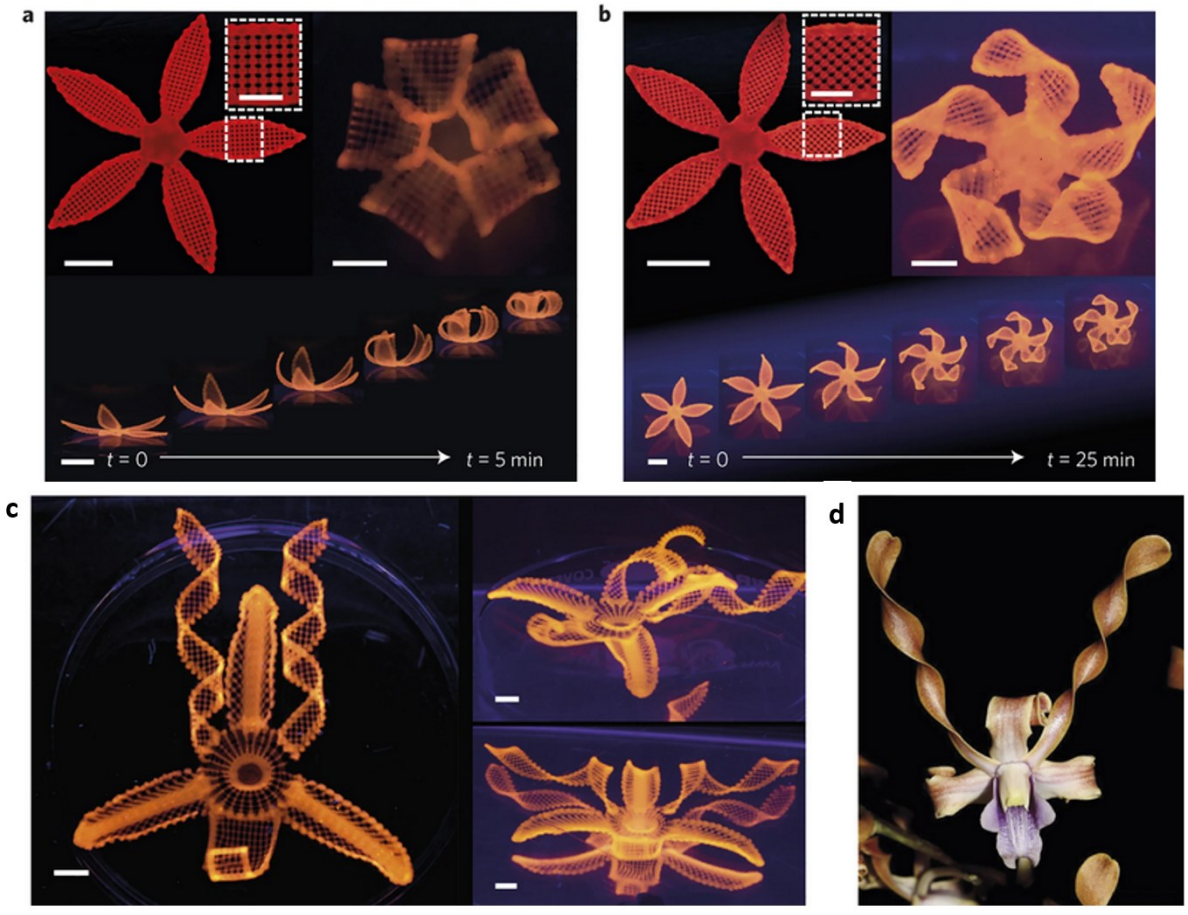

Figure 18. a) and b) time-lapse sequences of the simple flowers during swelling process. Scale bar 5 mm (inset = 2.5 mm). c) A flower demonstrating a range of morphologies inspired by a native orchid. d) Based on the printing path, the structure of the orchid exhibits different kind of configurations: bending, twisting, and ruffling. Scale bars 5 mm. Figure adapted and partially reproduced from ref. 65 with the permission of Nature Materials.

Zheng *et al*.[63] created a 3D printed tough hydrogel four-armed gripper, which is able to deform and recover with a high speed. The grip is able to clamp a plastic ball with a high holding force, as large as 115 times the weight of the grip itself. Two highly viscoelastic hydrogel solutions and their mixtures were printed into 3D structures with multiple nozzles. The polymers were printed in air and incubated in ferrine solution for crosslinking the gel. After preparation the sample was transferred into pure water to achieve equilibrium state. The fibres of only the other gel contract considerably in concentrated saline (NaCl) solution, and this mismatch of responsiveness creates the 3D construct. The formation of the grip took 60 seconds, whereas the recovery in water took 90 seconds. The holding force was measured by pulling the ball out of the closed grip on a tensile tester. This printing strategy can be applicable to other tough hydrogels for creating programmed deformations. Figure 19 shows the actuation of the printed hydrogel grip clamping the plastic ball.

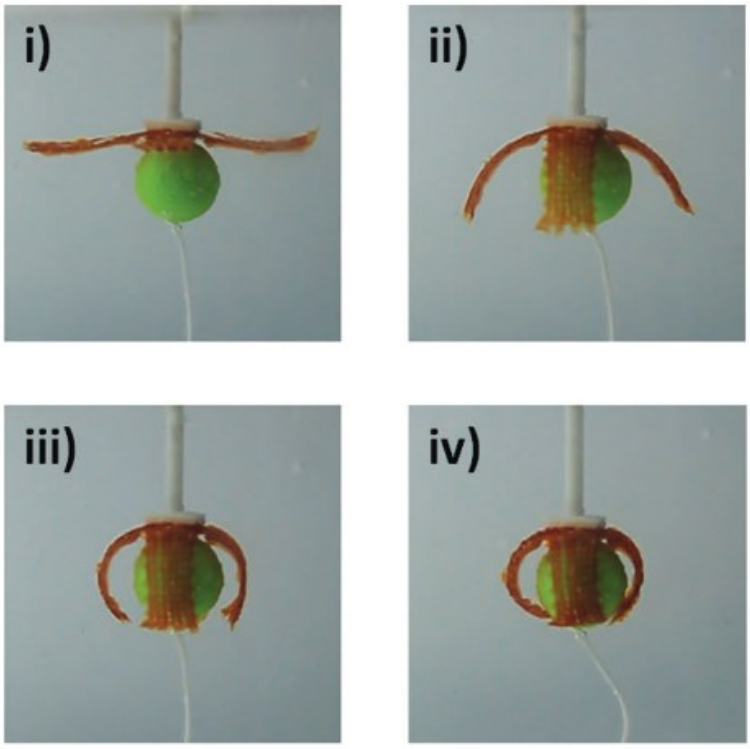

Figure 19. Actuation of the 3D printed hydrogel grip in saline solution to gripe a plastic ball, with a diameter of 10 mm and weight of 13 mN. Figure adapted and partially reproduced from ref. 63 with the permission of John Wiley and Sons.

Another example of creating four dimensions with 3D printing is thermally induced transformation, which can be created by composing the printed object with thermally responsive swelling gel with a passive thermally non-responsive gel. Poly-*N*-

isopropylacrylamide can be used as the responsive gel with polyacrylamide as the non-responsive gel. A variety of shape changes can be created using this method, thus exhibiting a high level of tunability and customization, which can be exploited in robotics and in biomedical engineering.[72] Figure 20 shows bending and gripping of 3D printed dual-gel objects.

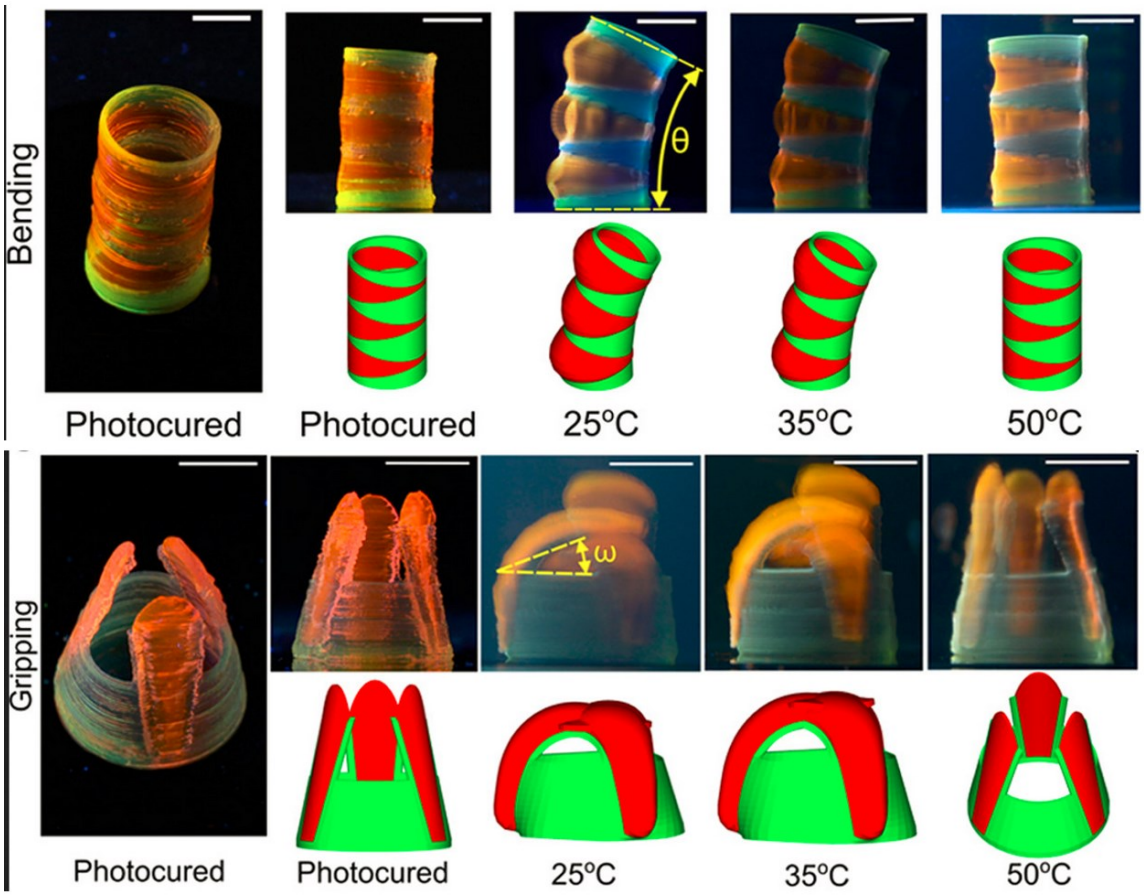

Figure 20. The bending and gripping motions of a 3D printed dual-gel at different temperatures. The θ-angle varies between 0° and 25° and the ω-angle between 35° and 80°. Scale bars are 1 cm. Figure adapted and partially reproduced and from ref. 72 with permission of American Chemical Society.

4.3.3 Bath-supported 3D printing

In bath-supported 3D printing, also known as embedded printing, the nozzle of the printer is inside the supporting gel. Molecular thixotropic gels can be used as support baths. The solid gel converts to fluid at the tip of the moving nozzle allowing the printed polymer solution to be dispensed, followed by quick transformation back to solid-state. The gel-bath maintains the

shape of the printed polymer during printing and a possible subsequent cross-linking. When printing with polymers the printing and cross-linking in the same bath is beneficial when the desired outcome is ceramics without no-interlayer interfaces.[73]

Gels can also be printed into the gel-bath if the yield stress of the bath is higher than of the ink material. In addition to the physical support of the ejected ink, the bath provides an aqueous environment. Furthermore, the bath itself can be used, for example as vessel networks, after removing the fugitive ink.[74] A schematic of bath-supported 3D printing with hydrogel is shown in Figure 21.

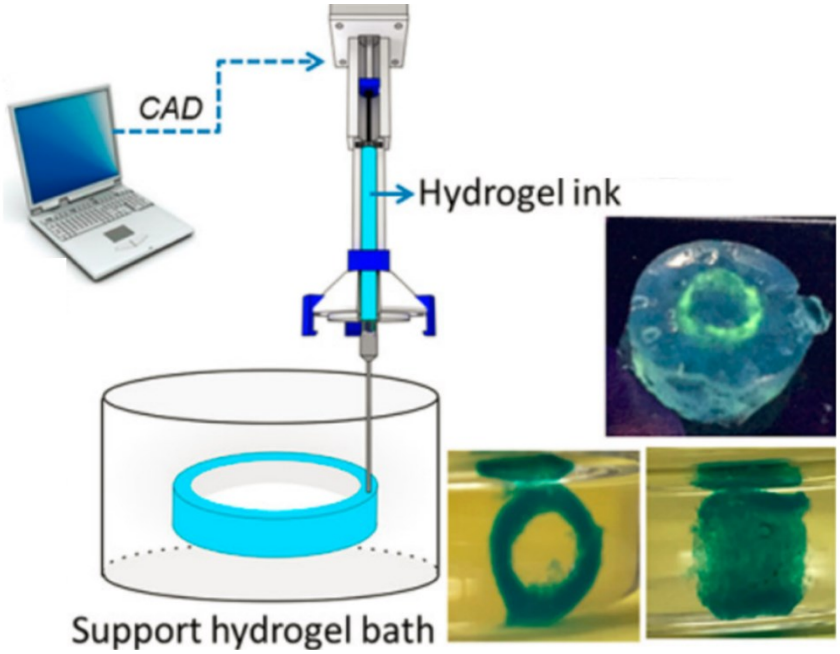

Figure 21.[75] Illustration of a bath-supported 3D printing system. (CAD = computer aided design.) Figure adapted and partially reproduced from ref. 75 with permission of American Chemical Society 2022.

4.3.4 Cryogenic 3D printing

With cryogenic 3D printing, very soft materials, such as soft hydrogels, can be printed with retaining their shape after printing. Extremely soft materials are unable to withstand their own weight, which is why the printed structure is usually too soft for further additional layers. Cryogenic printing can be one solution for overcoming this challenge.[76] Furthermore, the relatively low temperature (−32 °C) allows the incorporation of biomolecules or drugs into scaffolds at large quantities with maintaining a high level of biological activity.[77] The printed

ink is rapidly cooled down below its freezing point to create a gel with stabile structure.[76] The cooling down can be achieved, for example, by printing the ink onto a stainless steel bed with a bath containing solid carbon dioxide (dry ice) and isopropanol underneath it, or by printing the ink directly into a liquid coolant (liquid nitrogen). With the latter, monitoring that the upper surface of the liquid is on the same level as the highest deposited layer of the object is important to ensure the freezing is controlled precisely.[76,78] Figure 22 shows a printed porous polycaprolactone scaffold for tissue engineering printed in different temperatures by cooling the printing bed.

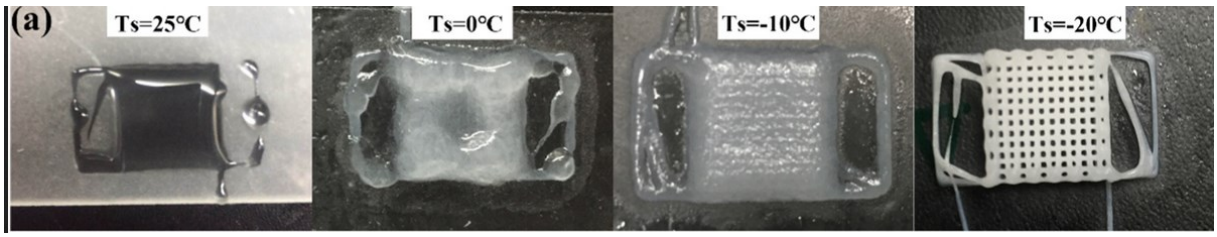

Figure 22.[79] A 3D printed scaffold, with low melting point of 60 ℃, using different cryoprinting temperatures. Reproduced from ref 79 with permission of Elsevier.

4.4 3D printing in biomedicine and in pharmaceutical industry

The algae derived agar, used in the culinary industry, has excellent rheological properties and therefore many applications also in the biomedical industry.[80] Agar has a relatively high melting point compared to other solidifying agents, which makes it suitable for scientific applications that requires incubation at body temperature.[81] Addition of agar to 3D printable ink greatly improves the viscosity of the ink and guarantees high printing precision, due to agar's high viscosity at low temperatures.[60]

In the medical field 3D printing can be utilized in unique ways, including implants, tools, prosthetics, organs, and hearing aids. More and more ideas and breakthroughs are being made every day for helping both humans and animals.[2] Hydrogels are suitable ink candidates for 3D printing in biomedical field due to their features, including low cytotoxicity.[60] Furthermore, printed very soft hydrogels can mimic the mechanical properties of the softest tissue in the human body, including brain and lungs, resulting in possible applications in tissue engineering purposes.[76]

The FDM method is the most investigated 3D printing technology for manufacturing personalized medicines, while the high temperature of the process limits its wider application. This becomes an issue, for example, when using a filament created with heating and extruding a drug loaded polymer strand. Many active pharmaceutical ingredients (APIs) are thermosensitive, but few exceptions are found. In some cases, lowering the temperature to 90 ℃ instead of the usual 150-230 ℃ of the process results in the desired outcome.[82] FDM is also considered to be the best method for bioprinting[83], however, low resolution is a challenge. One solution to obtain better resolution is to use combined ink, for example agar with alginate.[60]

Another less studied extrusion-based 3D printing method, semi-solid extrusion (SSE), is designed for printing gels and pastes. Its advantages are rapid printing possibility at low temperatures.[84] Using SSE can applications such as solid lipid tablets from emulsion gels be created. Poorly water-soluble drugs can be transformed to more pleasant form to pediatric and geriatric patients.[85]

With 3D printing can scaffolds with customized shape, tailored pore sizes, porosity, as well as other desired features be manufactured. In addition, a 3D printed scaffold can have versatile functions.[86] Combining 3D printing of medicines with machine learning (ML) can save costs and streamline the printing process in the near future. The combined technology raises potential for making accurate and rapid predictions of drug release profiles and innovative formulation design. ML also provides the possibility for fully automated printing and final product quality control. Furthermore, development of data-driven omics and the manufacture of personalised medicines would be accelerated.[87]

4.4.1 3D bioprinting and stem cell printing

3D bioprinting combines bioink, meaning biomaterials and living cells, with 3D printing to form biologically active 3D tissue constructs.[88] This vigorous process can be used for fabrication of *in vitro* biological functional tissues. The bio-ink gel must be on the weaker side, otherwise the cells can fracture and die while extruding from the nozzle.[12] Bioprinting can be executed through various methods, including FDM and inkjet printing.[89] Combining stem cells with custom 3D scaffolds for personalized regenerative medicine has attracted a lot of interest. However, several technological issues must be addressed before the regeneration of complex tissues and complex organs can be routinely created with 3D printing.[3] With 3D printed stem

cells can tissues such as cardiovascular, musculoskeletal, neural, hepatic, adipose, and skin be created.[90] These 3D printed human tissues can also be used for drug-screening models.[89]

Alginate is the most explored bioink for extrusion printing though it has limited cell-material interactions. Bioink functionality can be improved by incorporating small amounts of poly amino acids with alginate. The blended ink does not significantly change the viscosity or gelation properties required for printing. The printed alginate-poly amino acid gels can be used as scaffolds for bone engineering.[91]

An unconventional wet spinning process, co-axial wet spinning, combines bioink with the coagulant bath by delivering them simultaneously. The bioink gelates when extruding. In some opinions this method is superior to other 3D bioprinting methods, with advantages of simplicity, versatility, and performance. Hollow fibres of vascular networks can be created with co-axial wet spinning.[92] Figure 23 shows the hollow fibres created with a multilayer co-axial extrusion system to achieve direct 3D printing using biomimicking bioink.

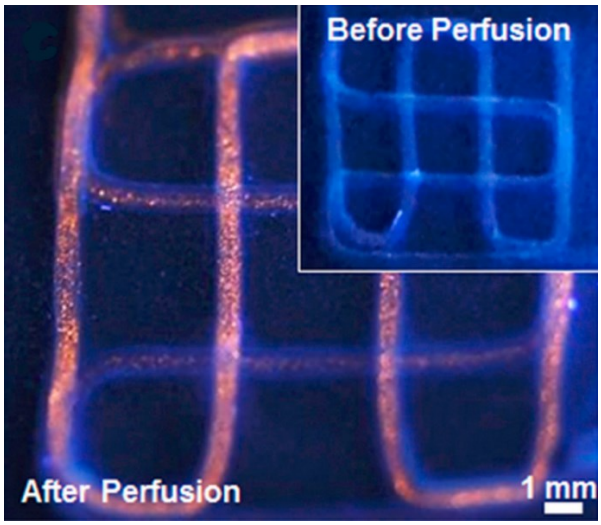

Figure 23.[93] Fluorescence photograph of a continuous bioprinted tube before and after perfusion into the lumen with red fluorescent microbeads. Figure adapted and partially reproduced from ref. 93 with permission of Elsevier.

4.4.2 Applications of solid 3D prints in pharmaceutical industry

3D printing of tablets results in smooth surface and tight texture, therefore exhibiting better extended drug release rates compared to directly compressed tablets.[45] Other benefits of using hot-melt extrusion method includes the use of organic solvents becoming unnecessary, and the

possibility of increasing the release rate of poorly water-soluble active pharmaceutical ingredients (APIs).[94,95] The first approval for 3D printed tablet from The food and Drug administration (FDA) was admitted in the year 2015.[87]

In 2021 Arany *et al*.[96] released an article of a vaginal ring, which had been 3D printed with FMD method using commercially available thermopolymer filament. The ring was filled with agar-gelated medicine. In the same year another research group released an article about vaginal ring developed with drug-fused filament using hot-melt extrusion.[97]

3D printing can also be exploited with modified 3D printed electrodes, which can determine individual enantiomers from a mixture. This method provides a fast, low-cost analytical pathway for the challenging recognition process. The identification and separation of enantiomers from each other is important, due to the difference in biological activity of the chiral compounds. A modified electrode of a magnetic covalent organic framework favors the L-enantiomer of the amino acid tryptophan.[14]

3D printed wristbands can help the utilization of screen-printed electrodes, which detect the phenylalanine levels in saliva and serum. Rapid monitoring of phenylalanine levels is important with patients suffering from phenylketonuria.[98] The electrochemical sensor is created by printing ink, such as silver or carbon, onto a substrate e.g., ceramic.

4.4.3 Applications of 3D printed gels in pharmaceutical industry

Complex organ models including nose with nares and ear auricles can be 3D printed, for example, using a suitable hydrogel derived from bioink. The printed constructs can return their original shape without any deformities after distorting them by pressure, thus demonstrating good flexibility. Digital light processing (DLP), a type of 3D printing polymerization process, can be used.[2,99] By DLP high resolution with rapid printing speed is possible in spite of the complexity of the printed object.[99]

3D printed non-implant skin derived from hydrogel formed with agar and crushed egg shelves can replace bandages on burned wounds. Traditional bandages have the downside of peeling skin when removing it. The printed hydrogel exhibits non-adhesive behaviour, heat transfer, and can be customized by shape for the patient. Furthermore, it is capable of reducing the rehabilitation time.[80]

Artificial muscles can be 3D printed (or 4D printed, depending on the definition) using thermoplastic electroactive gels, which can be fabricated simply by heating, thus avoiding the previous hazardous and time-consuming solvent-based methods. The PVC-DIDA (polyvinyl chloride and diisodecyl adipate) gel can be melted and reformed, and it is an anodophilic smart material, which implies the movement to the direction of anode, for increasing the surface area contacting the anode. The contraction of the gel is shown in Figure 24. The PVC-DIDA gel, with contraction up to 17.75 %, is currently suitable for low-force artificial muscle applications. It requires improving its near-instantaneous response times and low-activation voltages before using as a functioning biological muscle.[100]

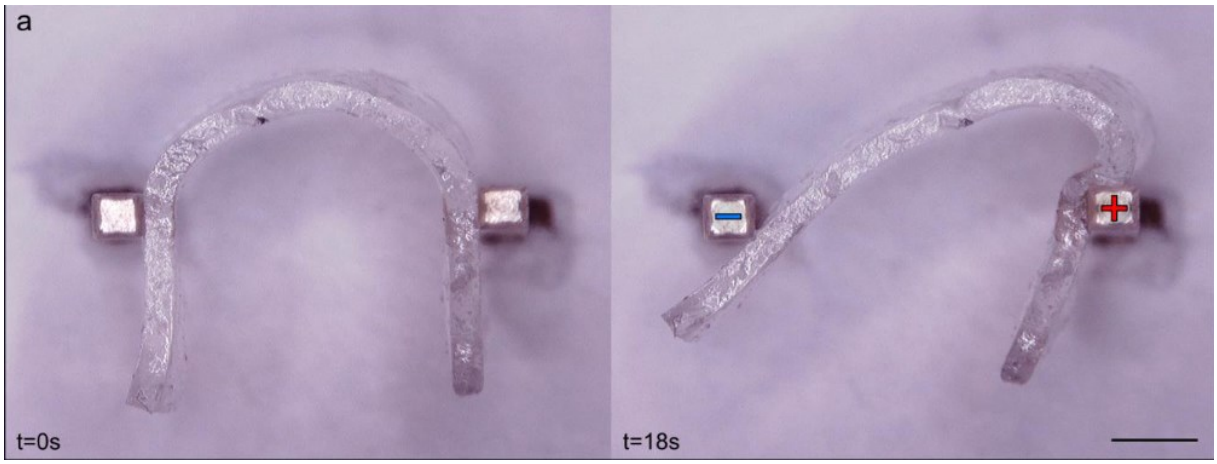

Figure 24. The behaviour of an electroactive 3D printed gel when electrodes are charged. Scale bar = 1 mm. Figure adapted and partially reproduced from ref. 100 with the permission of IOP Publishing.

Another example of 3D printed gels is the study conducted by Mirdamadi *et al.*[101] concentrating on alginate-based full-sized model of the human heart using a supporting bath of hydrogel. The model of the organ was obtained from patient-derived magnetic resonance imaging (MRI) data sets. The alginate derived model mimics the elastic modulus of cardiac tissue. When printing softer material without supporting baths in air, they easily deform by the effect of gravity. Figure 25 shows the print path, the printed heart model, and a functioning coronary artery segment of the heart.

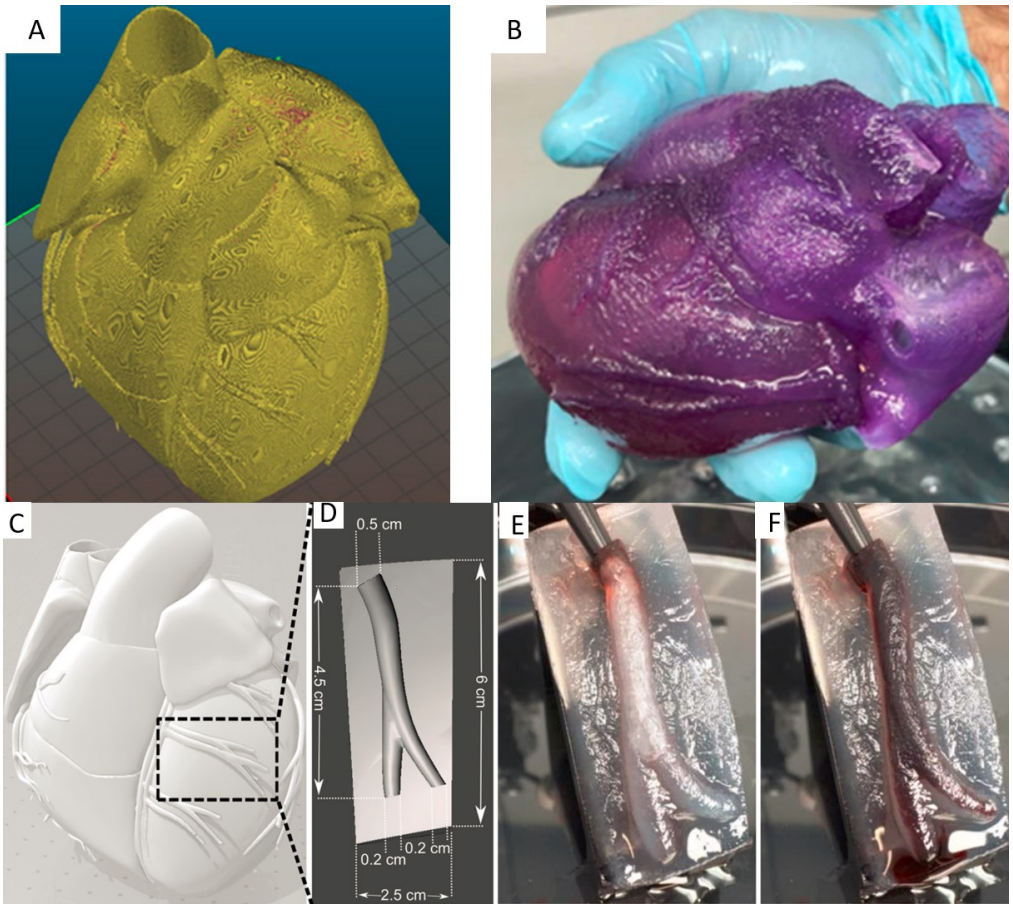

Figure 25. A) The print path of the heart; B) the full-sized stained bioprinted heart model; C) and D) a desired coronary artery segment for embedded 3D printing. E) and F) The printed segment before and after perfusion with red glycerol, demonstrating patency through the bifurcation. Figure adapted and partially reproduced from ref. 101 with permission of American Chemical Society 2022.

A composite soft hydrogel (CH) of poly(vinyl) alcohol (PVA) and Phytagel used as the ink shows potential for use as tissue phantoms or in surgical training. With 3D cryo-printed CH can hollow structures be produced - a feature lacking from cast gels. Furthermore, by coating the printed gel structure with collagen gel, poly-L-lysine or gelatine, can living cells be attached onto the surface and survive for 72 hours with significant percentages.[76]

A fragile hydrogel made with *N*-heptyl-D-galactonamide as the LMWG is biocompatible and allows the growth and differentiation of human neural stem cells into neurons and glial cells. Therefore, it can be used as a scaffold or as sacrificial ink in bath-supported printing. The hydrogel is manufactured by wet spinning, the gelator molecule is dissolved into dimethylsulfoxide (DMSO) and the solution is extruded into water.[102]

4.4.4 3D printed peptide-based hydrogels

Brain-like structures for *in vitro* -applications, including cell behaviour studies, understanding of brain injuries, and neurodegenerative diseases for drug testing, can be fabricated with 3D printed hydrogels. A study of Lozano *et al*.[103] encapsulated cortical cells into a hydrogel for representing a cortical tissue, and the hydrogel ink was printed into discrete layers. Some layers had cells distributed throughout them, while others had no cells in them. The used bio-ink for printing was a novel peptide-modified biopolymer, gellan gum-RGD (RGD-GG) combined with primary cortical neurons.

RGD is a tripeptide Arg-Gly-Asp, which is the most common peptide motif responsible for cell adhesion to the extracellular matrix, found in many species.[104] The used polysaccharide GG, among other natural gum polymers, has attracted attention recently due to its features such as gelling temperature, texture, gel strength, and ability to dissolve in water. These unique properties have led to applications in the tissue engineering area of the gum, which was originally introduced to food industry as alternative to gelatin and agar.[103]

The peptide modification of gellan gum hydrogel showed profound positive effect on network formation and cell proliferation. In addition, crosslinking the GG gel with $CaCl_2$ produced crosslinked gels that retained their printed shape and supported cell viability. A 3D neuronal network was created less than in five days after printing, and axons begun to penetrate an acellular layer, shown in Figure 26. The axonal development demonstrated that internal porosity of the printed gel allowed nutrition flow. Furthermore, there were no difference in viability or cell morphology when comparing to non-printed (cast) controls, proving that cortical cells were not damaged by the printing procedure.[103]

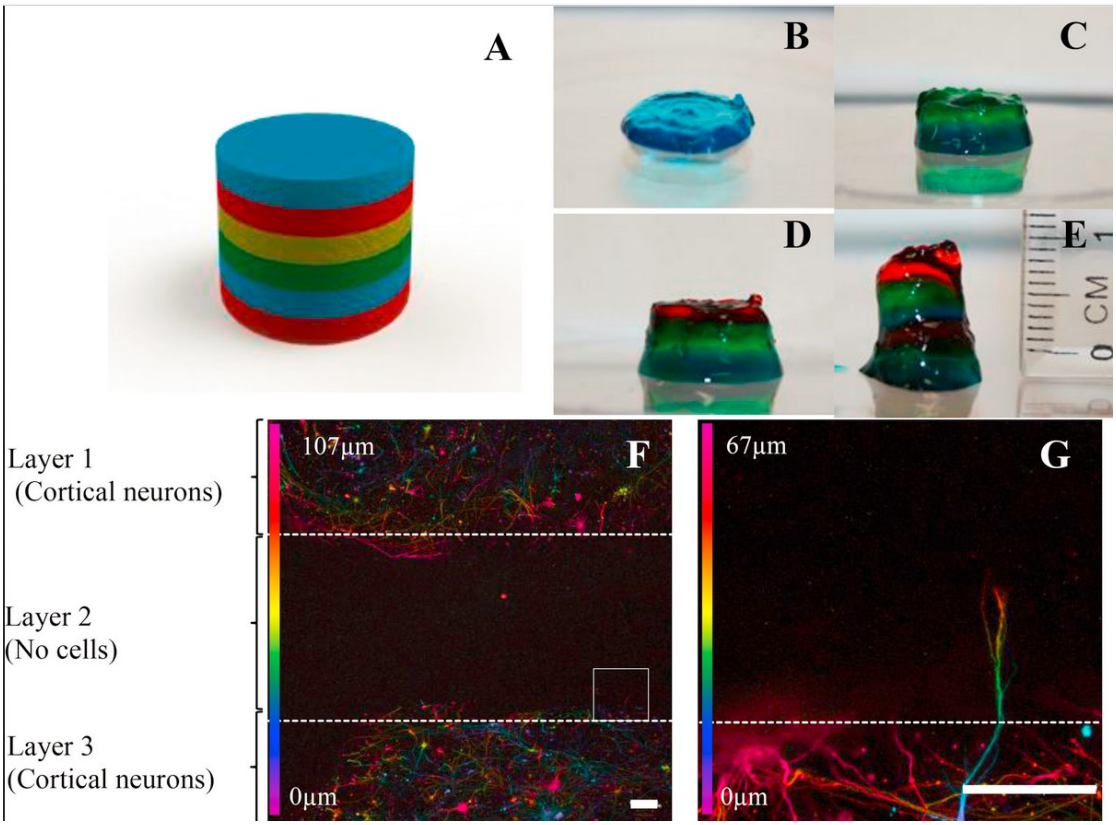

Figure 26. 3D printed brain-like layered structure. A) Representation of proposed structure. B- E) The printing process, each colour represents a different layer. F) Confocal microscope picture of neurons in different layers 5 days after printing. G) Zoomed area from picture F demonstrating an axon penetrating into the adjacent layer. Scale bars 100 µm. Reproduced from ref. 103 with permission of Elsevier.

Another example of 3D printed peptide-based hydrogels is lysine-derived hydrogels, which can be used to manufacture organs which demand a high resolution, such as corneas. Currently damaged corneas are treated by using transplants from donors. Printed poly-ε-lysine/gellan gum (pεK/GG) objects demonstrate an 80% transparency and a honeycomb topography, which makes the dual gel a suitable candidate for being used as a cornea replacement.[105]

The pεK/GG constructs were printed using reactive inkjet printing (RIJ) technology, which has a few advantages compared to other 3D printing methods, including solution processability and fine resolution at a micron range. In addition, the RIJ offers a versatility to tailor the printed objects with various dimensions and thickness. In RIJ, the inkjet prints two separate deposits, which solidifies through a chemical reaction when the deposits are in contact. The printing process is demonstrated in Figure 27 A. This process usually requires two separate printers. The ink droplets are precisely dispersed onto a substrate, which are built to form a 3D shape.

For RIJ to be used with hydrogels, the gelation must happen immediately after printing and ink droplets must maintain the 3D structure. RIJ is a great 3D printing option for bioprinting due to its high resolution.[105]

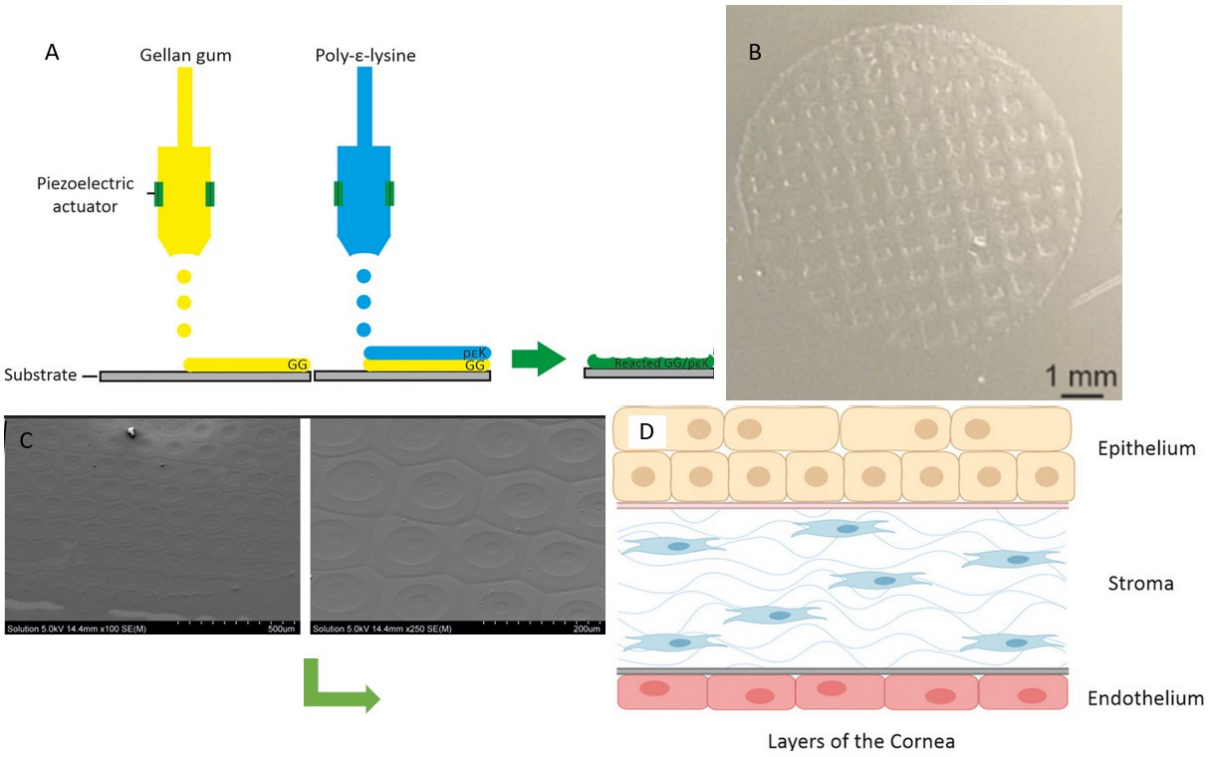

Figure 27. A) The RIJ printing process where the two separately printed gels react and form the outcome. B) A picture of the printed cornea. C) SEM (scanning electron microscope) images of the cornea with 100x and 250x zooms. D) The structure of a cornea. Figure adapted and reproduced from ref. 105 with permission of Elsevier.

The naturally occurring, unusual cationic polymer, pεK is made of L-lysine. Due to its biodegradability and non-toxic nature, it has been utilized, for example, in food industry and in biomedicine.[106] The positive charges in the amino groups at the pεK backbone can form ionic bonds with negatively charged polymers such as GG. This makes the gels suitable for RIJ.

Printed pεK/GG-hydrogels show cyto-compatibility with both corneal epithelial and endothelial cells. After 10 days of culture a significant cell attachment was shown. When the printed hydrogel was compared with a casted control, they exhibited a comparable transparency, both approaching the transparency of a human cornea. Furthermore, the hydrogel can be tuned for printing outcome with or without pores, the latter being a desired outcome with cornea replacement. The structure of a cornea, the printed cornea, and a SEM-image of the printed cornea is shown in Figure 27 B-D.[105]

In a different study conducted by Liu *et al*.[107] 3D printed porous scaffolds were constructed of gelatin/sodium alginate hydrogel with soy protein or soy peptide powder for self-promoted angiogenesis. With tissue engineering *via* 3D printing there is a challenge of reconstructing a vascular network in addition to issues regarding finding a proper ink. The vascular network has an important function of providing nutrition and oxygen, while removing waste from the cells. The formation of blood vessels in adults is called angiogenesis, which predominantly occurs from pre-existing blood vessels. Soy protein (SP) and soy peptide powder (SPP) are widely used in tissue engineering, but their role in angiogenesis was not studied before. Soy protein includes lysine and arginine among other amino acids.

After printing, $CaCl_2$ was used for crosslinking the scaffolds, and the resulting structure was washed and freeze-dried for achieving a porous structure. The angiogenesis effect of the printed scaffold was tested with chicken embryos and with living rats. The results showed that both SP and SSP had good cytocompatibility, and both were suited for cell adhesion and were able to promote cell proliferation. SP had greater mechanical properties, whereas SSP had a better biocompatibility. Both were able to promote cell migration, whereas SPP had a better effect on it. Furthermore, the promotion of angiogenesis and the integration of the scaffold of SPP was observed to be clearly better. The results show that 3D printed gelatin/sodium alginate gels with soy protein or with soy peptide powder have both a great potential for use in tissue and in organ engineering.[107]

4.4.4.1 Peptides incorporated with 3D printing

One of the most notable peptide-based hydrogel is fluorenylmethoxycarbonyl-diphenylalanine (Fmoc-FF). Incorporation of nanoparticles (NPs) to hydrogels enables a variety of biomedical applications. These peptide-metal nanocomposites have been used for drug delivery and biomolecular sensing. A 3D printed template filled post printing with Fmoc-FF hydrogel loaded with gold or silver NPs has been used successfully in surface-enhanced Raman spectroscopy (SERS) allowing detection of molecules at very low concentrates.[39]

A small peptide, acetyl-hexapeptide 3 (AHP-3), has great anti-wrinkle properties and furthermore, low toxicity compared to Botox. The downside of this Botox-mimicking peptide is poor permeability of skin due to its large molecular weight and hydrophobicity. Personalized microneedles (MNs) for patients' faces created with digital light processing (DLP) 3D printers

can be a solution for the delivery of this drug. Commercially available photocurable resins for 3D printing are not suitable for fabrication of drug loaded delivery systems these days. Seng *et al*.[108] however, created a suitable polymer resin, formed by two liquid monomers, for producing an MN with 3D DLP-printing. This study shows that with an optimised resin together with the 3D printing process may other peptides of therapeutic effects be used.

The photochemical processability or thermal nature of synthetic polymers is the reason why they are widely used as 3D printed degradable scaffolds. Post printing surface modification with bioactive molecules of scaffolds can result in better cell attachment, proliferation, and differentiation, leading to tissue generation, while saving the bioactive molecules from the harsh printing conditions. The printed scaffolds can be made from L-phenylalanine derived poly-ester ureas, and the used surface coating material can be naturally occurring linear tetradecapeptide osteogenic growth peptide (OGP) or bone morphogenic protein-2 peptide (BM2), which is composed of 20 amino acids. The scaffold immobilized with OGP or BM2 has shown a significant enhancement of osteogenic differentiation of human (adult) stem cells compared to unfunctionalized scaffolds.[109]

Amino acid-derived gels can also be used as an ingredient with small amounts in printing inks. For tumour resection-induced bone defection treatment, Wang *et al*.[110] created a water-in-oil emulsion inks containing multiple functional agents for cryo-printing into hierarchically porous and mechanically strong nanocomposite scaffolds. The ink contained β-tricalcium phosphate and high dose osteogenic peptide for osteogenic cell differentiation and bone regeneration, in addition of 2D black phosphorus nanosheets for photothermotherapy purposes and local release of cytotoxic antibiotics to repress tumour recurrence. Zhang *et al*.[111] created a similar multifunctional cryo-printed scaffold with incorporation of graphene oxide (GO) for improving the wettability and mechanical strength of the scaffold. The addition of GO also improved the sustainability of osteogenic peptide release. Figure 28 shows *in vivo* -implantation of the scaffold with a rat, micro-computational tomography images of the scaffold and the bone regeneration of control and with scaffold after 4 and 12 weeks.

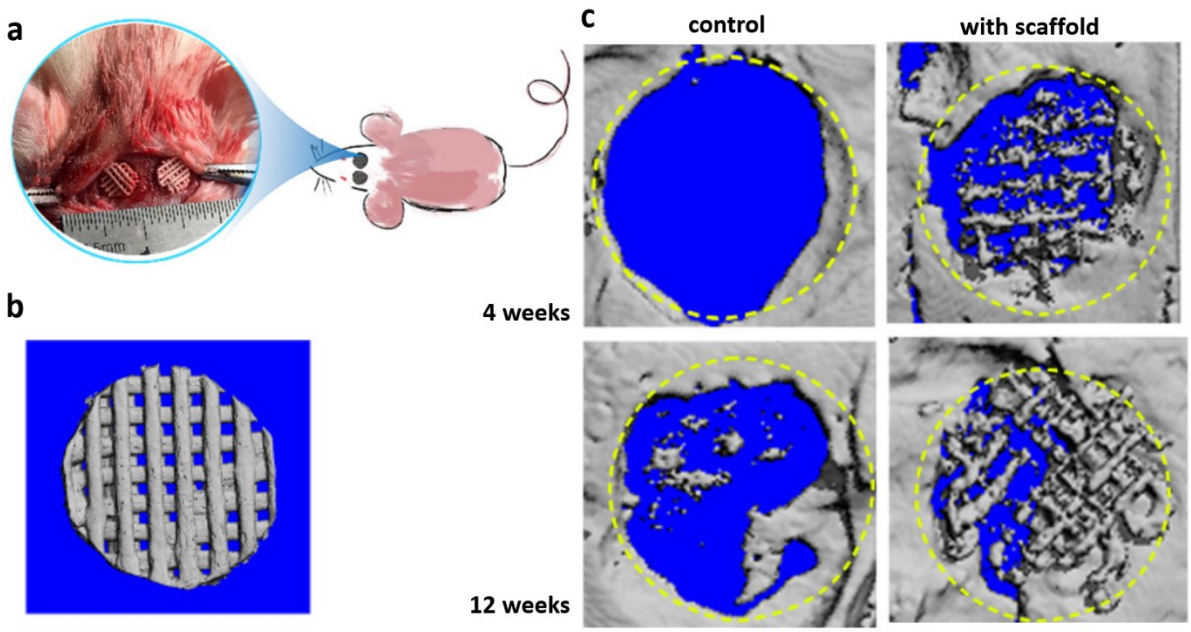

Figure 28. a) Implantation procedure; b) Micro-CT image of the printed scaffold; c) Reconstructed 3D images of the bone regeneration of the control and with scaffold after 4 and 12 weeks after the implantation. Figure adapted and partially reproduced from ref. 111 with permission of Molecules.

5. Summary

This relatively new area of research of 3D printed gels possesses a promising future. While the FDM-method is the most investigated, the other various 3D printing techniques are noteworthy for more research. Naturally the method should be chosen based on the chosen ink and the desired outcome. Modifying the ink and trying different methods might also be beneficial. When printing gels it is useful to consider the possible added value. Sometimes better features emerge but sometimes the features of the printed structure are as good as the control cast version. In these cases, no printing is needed.

While the printed food architectures appear flashy, the use of 3D printers in the food industry seems vain. Some printed gels exhibit a better release of nutrients compared to cast gels; however, the same result can be obtained by simply extruding the gel through a syringe. The same applies for some printed medical gels. The upsides of 3D printed foods include the possibility of exploiting the achieved results in medical field in some cases. In addition, the possible future of serving customized food for people with medical conditions. Furthermore, it

enables the distribution of exact contents of nutrients needed to consume for people who are busy or who only eat to stay alive. In my opinion, this takes away the pleasures associated with cooking and eating. The possibility of creating muscles by 3D cell printing for the medical industry could also have a place in the food industry. Creating printed muscles for consumption is more facile than creating them with functionalities, such as the ability to contract. If in the future the printed meat would have a lower carbon footprint value compared to farmed meat, it would also serve better ethics.

Even though amino acid-based hydrogels are weak, they can be strengthened for printing with the use of proper additives. The research of printed amino acid hydrogels is profitable, due to the great features of the gels themselves combined with the features of 3D printing, leading to synergistic features. The printed gel structures, such as the nose, could be used as prosthetics already these days. The opportunity for custom manufacturing in the biomedical field offers an endless set of applications. Including replacing the need of organ donors when organs such as hearts and corneas are required. In addition to the use of printed gels in the biomedical field, opportunities in the electric field have been raised. This may result in many useful applications, such as self-healing cell phone screens.

Experimental part

6. Introduction to the experimental work

As previously mentioned, the self-assembling peptides have possible applications in various interdisciplinary areas. For example, the peptide-based supramolecular hydrogels are versatile biomaterials for sustained release of encapsulated drug molecules, both *in vitro* and *in vivo*.[10] Furthermore, they can be used as scaffolds for 3D cell culture or for tissue repair.[112]

When designing self-assembling LMWGs from peptides, the choice of amino acid sequences is the key parameter. In an ideal self-assembling peptide, a suitable balance of hydrophobicity/hydrophilicity is essential, in which molecular self-assembly forces are greater than the precipitation forces of the peptides.[10]

Aromatic amino acids, such as phenylalanine, have been extensively used when designing functional LMWGs from self-assembling peptides. The hydrophobicity, the aromatic interactions, and the synergetic effects can be increased by incorporation of *N*-terminal aromatic protection. The *N*-terminal protecting group is used to facilitate the unidirectional peptide synthesis for achieving the desired outcome with minimum side products and with excellent yields.[10] The rational design possibilities make aromatic dipeptide hydrogels promising materials for bioinks in 3D printing and in cell cultures.[113]

Amines and their derivatives are important in many areas of chemistry. Especially, guanidine derivatives are useful pharmacophores in medical chemistry due to their ability to interact through hydrogen bonds and electrostatic interactions with functional groups in enzymes or receptors.[114] Due to heavily polar nature of guanidines, working with them can be difficult. 1H-pyrazole-carboxamidine hydrochloride is commonly used in guanylation reactions with primary amines as electrophile.[115]

Loudet[116] *et al*. reported a synthesized guanidine group being used as a cell penetrating warhead unit in non-covalent drug carrier molecules in intracellular delivery, which are inspired from a protein of HI-virus. Pep-1 (Chariot^{TM}) molecule mimics this protein. Pep-1 is a synthetic cell penetrating peptide (CCP) that has successfully been used for delivering proteins and other pharmaceutical macromolecules into cells. Pep-1 consists of a hydrophobic domain and a lysine-rich hydrophilic domain.[117] The structure from the Loudet *et al*. research of the positively charged cell-penetrating warhead is illustrated in Figure 29.

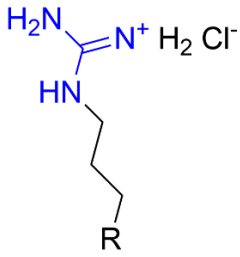

Figure 29. The positively charged cell-penetrating warhead of a non-covalent drug carrier molecule. The guanidine part is highlighted with blue, and R stands for side chain.

Homo-arginine (hArg, hR) is the methylene homologue of L-arginine. hArg seems to have beneficial effects on human health but the biological processes are largely unknown, and the potential use of hArg as a therapeutic drug or as a nutritional supplement needs more research.[118] The L-homo-arginine, as well as arginine, contains a guanidine group. The analogy of structures between L-homo-arginine and guanidine is illustrated in Figure 30.

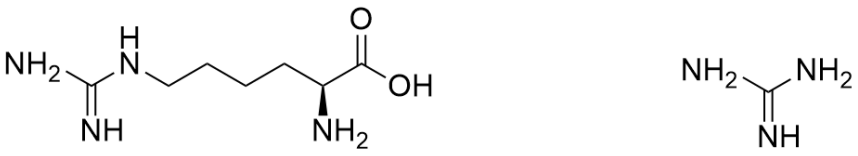

Figure 30. The structures of L-homo-arginine and guanidine.

Nuclear magnetic resonance (NMR) spectroscopy is a great option to investigate the structures and dynamics of supramolecular gels, since it can provide information about the regions of aggregates which are participating in the weak interactions, which are the key element of the stability of the dynamic networks of the gel.[26] When conducting a measurement, the sample is placed into a homogeneous magnetic field. ^{1}H and ^{13}C nuclei have spin and are magnetically active and thus magnetic signal is detected when their spins undergo transitions between allowed spin states. Proton NMR spectra reveal chemical shifts of atoms in different chemical environments. In addition, it can reveal the relative populations of spins in each environment. With phase-sensitive correlation spectroscopy (COSY) experiment, it is possible to obtain a 2D spectrum, which reveals the existence of couplings between protons.[119]

Mass spectrometry (MS) is an analytical technique that reveals the mass-to-charge (*m/z*) ratio of the molecules in the sample with very high sensitivity. The spectrum shows a plot of ion abundance against *m/z*. In the analysis the sample is converted to gas phase and ionised,

followed by acceleration into an electric or magnetic field. Depending on the type of the detector, ions with different *m/z* values land on a different place of the detector or have different flight times. The exact molecular weight of the examined molecule can often be calculated from the results.[120] With metal-containing gels MS can be used for obtaining snapshots of large aggregates, which provides evidence of the formation of the gel.[26]

Oscillatory rheometer is used for characterizing the toughness and viscoelastic properties of self-assembling hydrogels. All of the information concerning the mechanical properties of hydrogels can be obtained through rheological studies.[10] Concerning supramolecular gels, rheology is probably the most important defining feature. Rheology describes the resistance of flow, the viscosity, of solutions and melts. When measuring, the sample is placed between two plates or cylinders and stress is applied to one of the plates. This induced movement of the other plate is decomposed into an in- and out-of-phase components resulting in measuring the elastic storage modulus, *G'*, and the elastic loss modulus, *G''* as a function of applied stress or oscillation frequency.[26]

7. Aim of the experimental work

The aim of this project was to synthesize a homo-arginine derivative gelator molecule and to study its hydrogelating properties. The simplified reaction scheme is presented in Figure 31.

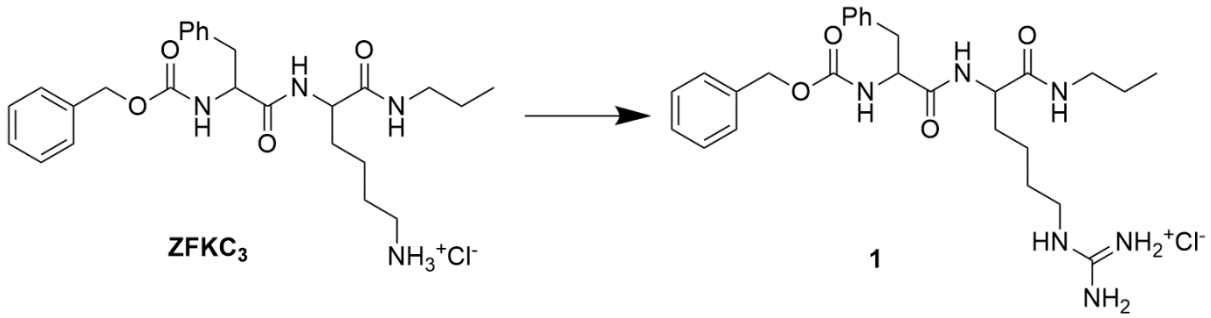

Figure 31. A reaction scheme for synthesizing the target gelator molecule (**1**) from the starting reagent $ZFKC_3$.

The synthesis of the target gelator molecule (**1**) includes a guanylation reaction, which converts amines to guanidines. The first batch to prepare the molecule was performed on a small scale, by letting $ZFKC_3$ and 1H-pyrazole carboxamidine hydrochloride react with DIPEA in

acetonitrile. The starting reagent $ZFKC_3$ used in the first batch had been prepared earlier. The more described structures of $ZFKC_3$(the racemic configuration is unknown) and **1** are shown in Figures 32 and 33. $ZFKC_3$ is a dipeptide based gelator molecule containing amino acids phenylalanine and lysine, which contains a primary amine group. The molecule also contains an *N*-terminal protecting group. The molecule **1** contains the same elements as $ZFKC_3$, with a difference of the amine group of lysine is replaced with a guanidine group, hence lysine is converted into homoarginine. After a successful guanylation reaction was found, more $ZFKC_3$ reagent was synthesized through a four-step reaction, and a second batch of **1** was prepared using larger scale.

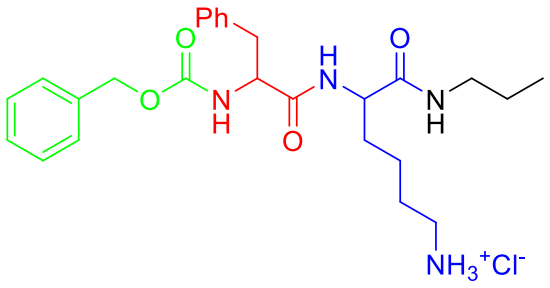

Figure 32. Structure of $ZFKC_3$. Protecting group Z in green, amino acid phenylalanine F in red, and lysine K in blue.

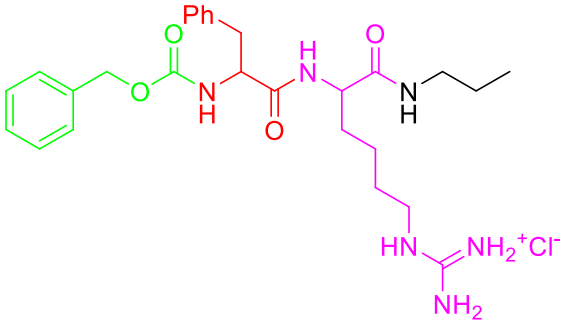

Figure 33. Structure of **1**. Protecting group in green, phenylalanine in red, and homo-arginine in magenta.

The four-step reaction for synthesizing $ZFKC_3$ was designed and it was tested earlier by Nagihan Özbek using chapter 3, and references cited therein, of Marta Tena-Solsona's[121] doctoral thesis as a reference. Figure 34 shows a simplified reaction scheme for synthesizing $ZFKC_3$ with used reagents and products numbered. The synthesis for $ZFKC_3$ includes reaction

between compound **2** and propylamine in DME for obtaining compound **4**, followed by hydrogenation of this intermediate product. The hydrogenated compound **5** is coupled with compound **6** in DME for creating compound **7**. At last, compound **7** is reacted with hydrogen chloride in dioxane for obtaining $ZFKC_3$.

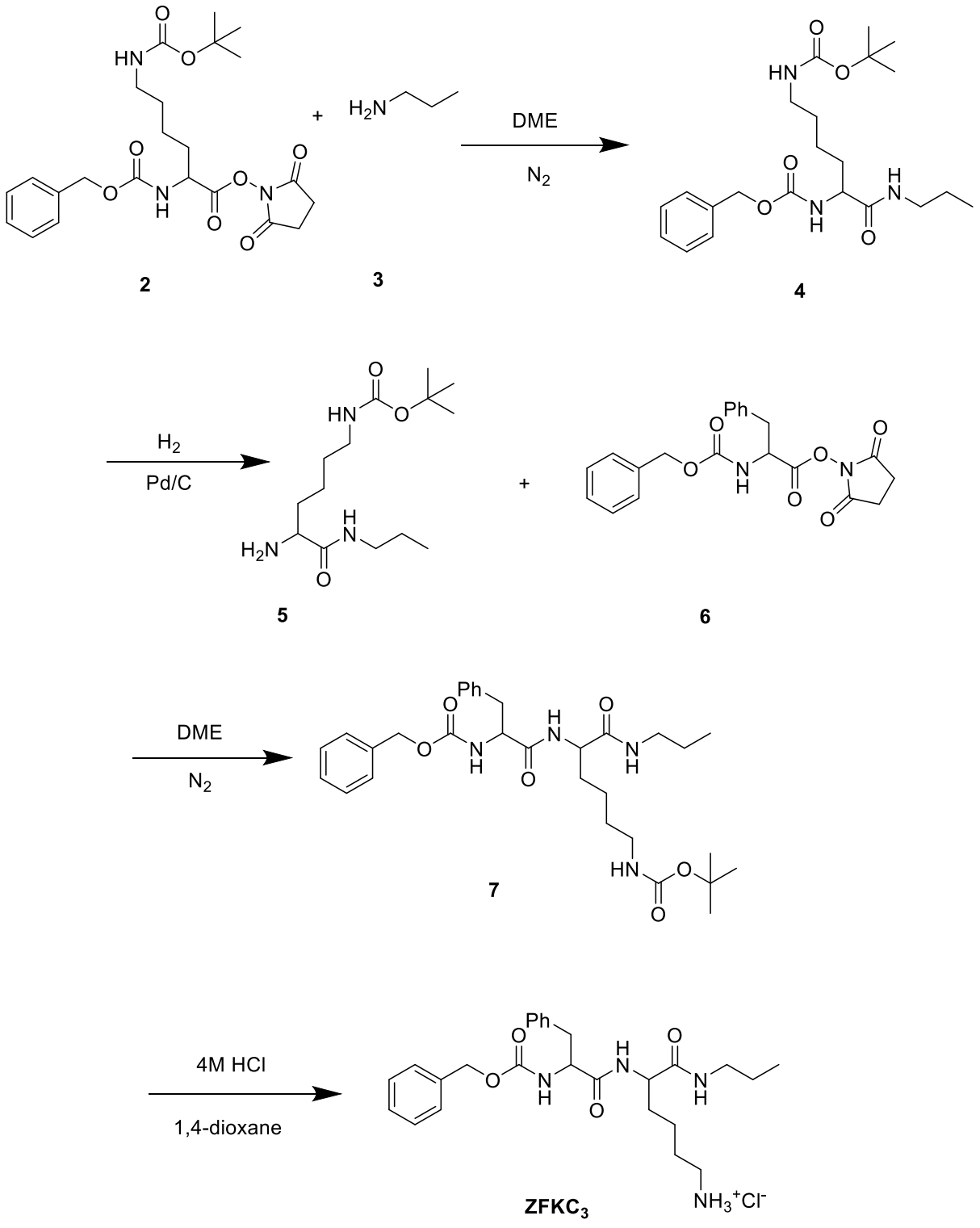

Figure 34. The reaction scheme for synthesizing $ZFKC_3$ with reagents and products numbered.

A lot of guanylation reactions, that use water or DMF (dimethylformamide) as solvent, are available. $ZFKC_3$ is not water soluble, thus some non-polar solvent is needed. The use of DMF is tried to be avoided due to the difficult removal of it after the synthesis. The current reaction is thus modified from Bakka and Gautun's[115] study, which uses acetonitrile as solvent. In order to release $ZFKC_3$ and 1H-pyrazole-1-carboxamidine hydrochloride from its salt, a slight excess of DIPEA acting as an amine was used. Also, the amount of acetonitrile was increased compared to the original reaction.

The structures of the synthesized molecules were confirmed by NMR spectroscopy. Some compounds underwent mass spectrometry as well. For molecule **1**, some gelation tests were performed, and the prepared hydrogel was studied with rheology. Also, a printing trial was conducted with the hydrogel.

8. Materials and methods

The used reagents in the reactions with information of the supplier and purity are listed in Table 1.

Table 1. Used reagents with their information

Reagent	**Producer**	**Purity**
1,4-dioxane	Scharlau	extrapure
1H-pyrazole-1-carboxamidine hydrochloride	Aldrich	99 %
4M HCl in 1,4-dioxane	SIGMA ALDRICH	-
Acetonitrile (MeCN)	Scharlau	HPLC grade
Dichloromethane	Scharlau	HPLC grade
Ethylene glycol dimethyl ether (DME)	Acros organics	99+%
Methanol	Scharlau	HPLC grade
N,*N*-Diisopropylethylamine (DIPEA)	Fisher	-
Propylamine	Acros organics	99+%
ZFOSu	Prepared earlier	-
Z-Lys(Boc)-Osu	BACHEM	-

The scale used for weighing was Mettler Toledo XA105, and the ultrasound bath in use was Elmasonic S 60 H. The TLC tests were conducted with Macherey-Nagel aluminium/silica G/UV_{254} sheets. The used rotary evaporator model was Hei-VAP Expert from Heidolph, centrifuge Orto Alresa Digicen 21 and vacuum oven Binder. The NMR spectra were measured by Bruker Ascend^{TM} 400 or Bruker-300 Ultrashield NMR spectrometers, and Merck's NMR Chemical Shifts of Impurities Charts[122] were used when assigning impurities from the spectrum. The mass spectra were measured with a triple-quadrupole mass spectrometer with an electrospray source (Waters). The used 3D printer was Nordson EFD PROPlus4 equipped with DispenseMotion software, and the rheometer was Discovery HR-1 hybrid rheometer.

9. Synthesis of $ZFKC_3$

The first step of the synthesis of $ZFKC_3$ is illustrated in Figure 35.

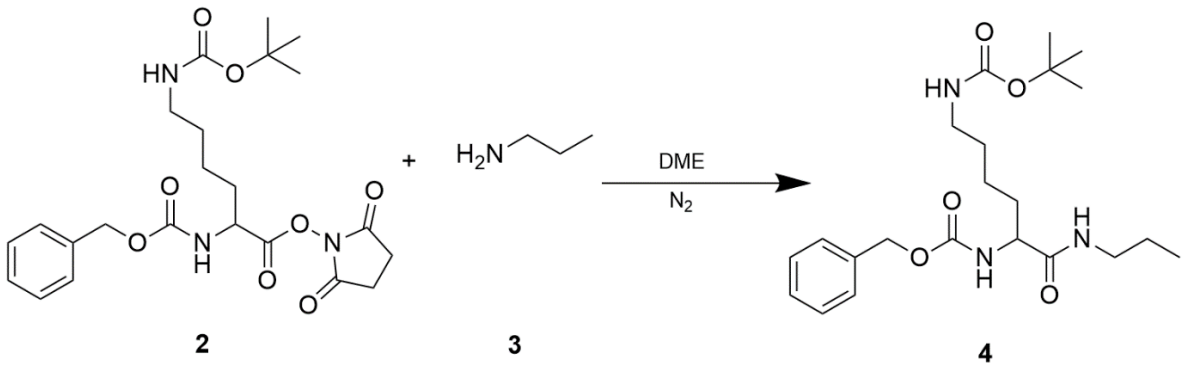

Figure 35. Reaction between Z-Lys-(Boc)OSu (**2**) and propylamine (**3**).

5 g (10.5 mmol, 1 eq.) of Z-Lys-(Boc)OSu (**2**) was dissolved into 30 ml of DME in a double-necked flask. 1035 µl (12.6 mmol, 1.2 eq.) of propylamine (**3**) was mixed with 10 ml of DME, and the mixture was added dropwise into the flask under nitrogen atmosphere. The clear colourless mixture was left stirring overnight. The success of the reaction was followed using TLC after 23 and 28 hours of reaction. Even after 28 hours **2** was present in the reaction mixture, but the reaction was stopped anyway.

The solvent was evaporated from the mixture, and the remains were dissolved into 30 ml of dichloromethane. Then the mixture was washed with (~15 ml) of 0.1 M Na_2CO_3, 0.1 M HCl,

and water, respectively. The organic layer was dried with anhydrous magnesium sulphate followed by evaporation of the solvent. The product was dried under vacuum at room temperature. The yield of white solid **4** after washing and drying twice was 3.44 g (8.2 mmol, 77.9 %).

Interpretation of ^{1}H NMR spectrum with assigned protons of the re-washed **4** is shown in Figure 36. ^{1}H, ^{1}H COSY NMR spectrum of **4** is presented in Appendix 1.

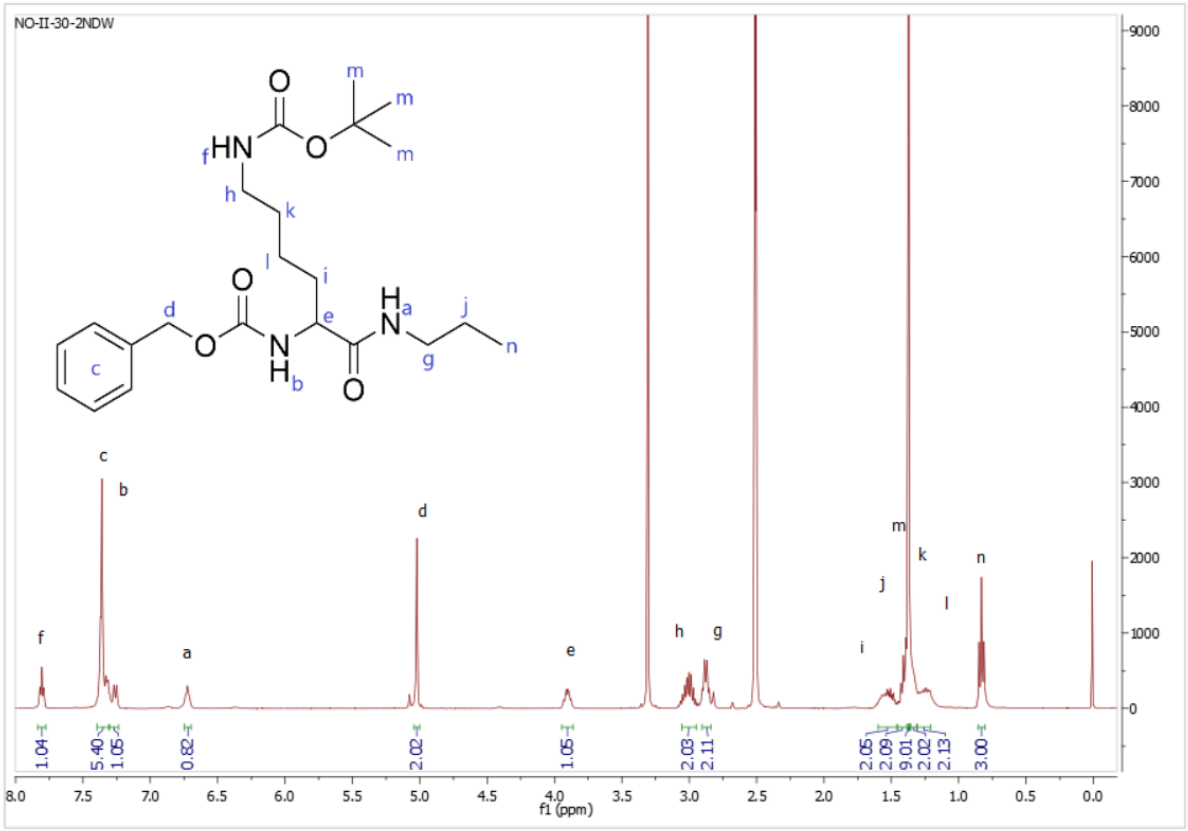

Figure 36. ^{1}H NMR spectrum with assigned protons of **4**.

4, ^{1}H NMR (DMSO, 400 MHz): δ 0.83 (t, 3H), δ 1.25 (m, 2 H), δ 1.33 (m, 2 H), δ 1.37 (s, 9 H), δ 1.41 (m, 2 H), δ 1.51 (m, 2 H), δ 2.86 (dd, 2H), δ 3.00 (m, 2 H), δ 3.90 (dd, 1H), δ 5.01 (s, 2H), δ 6.72 (s, 1H), δ 7.25 (d, 1H), δ 7.35 (m, 5H), δ 7.80 (t, 1H). Residual DMSO δ 2.50, and its internal water δ 3.30.

The second step of the synthesis of $ZFKC_3$ is illustrated in Figure 37.

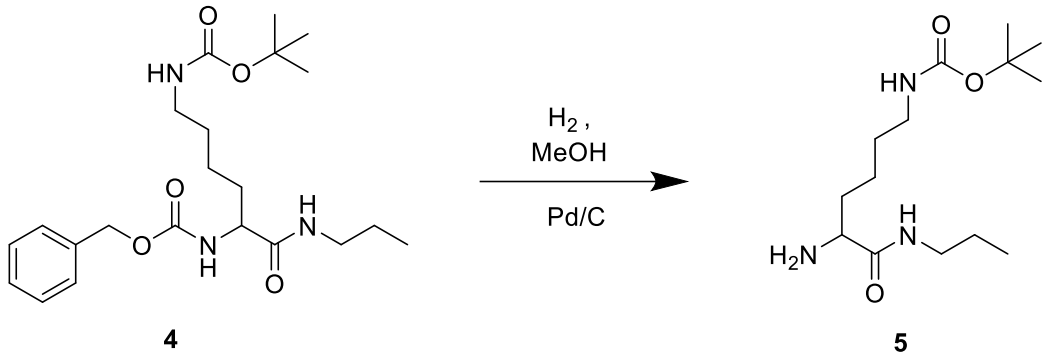

Figure 37. Hydrogenation of **4**.

3.44 g (8.2 mmol) of **4** was dissolved into 40 ml of MeOH. 346 mg (10 m-%) of Pd/C was added to the mixture. Reaction was left stirring under a hydrogen atmosphere at room temperature overnight. TLC was conducted the following day, and it proved that reaction had succeeded. The reaction mixture was filtered through celite into a flask. The colour of the reaction mixture after filtration was yellowish. The solvent was evaporated, and the product was dried under vacuum at room temperature overnight. The yield for the oily product **5** was 2.25 g (7.8 mmol, 96.0 %).

Figure 38 shows the ^1H NMR spectrum of **5** with assigned protons. ^1H, ^1H COSY NMR spectrum of **5** is presented in Appendix 2.

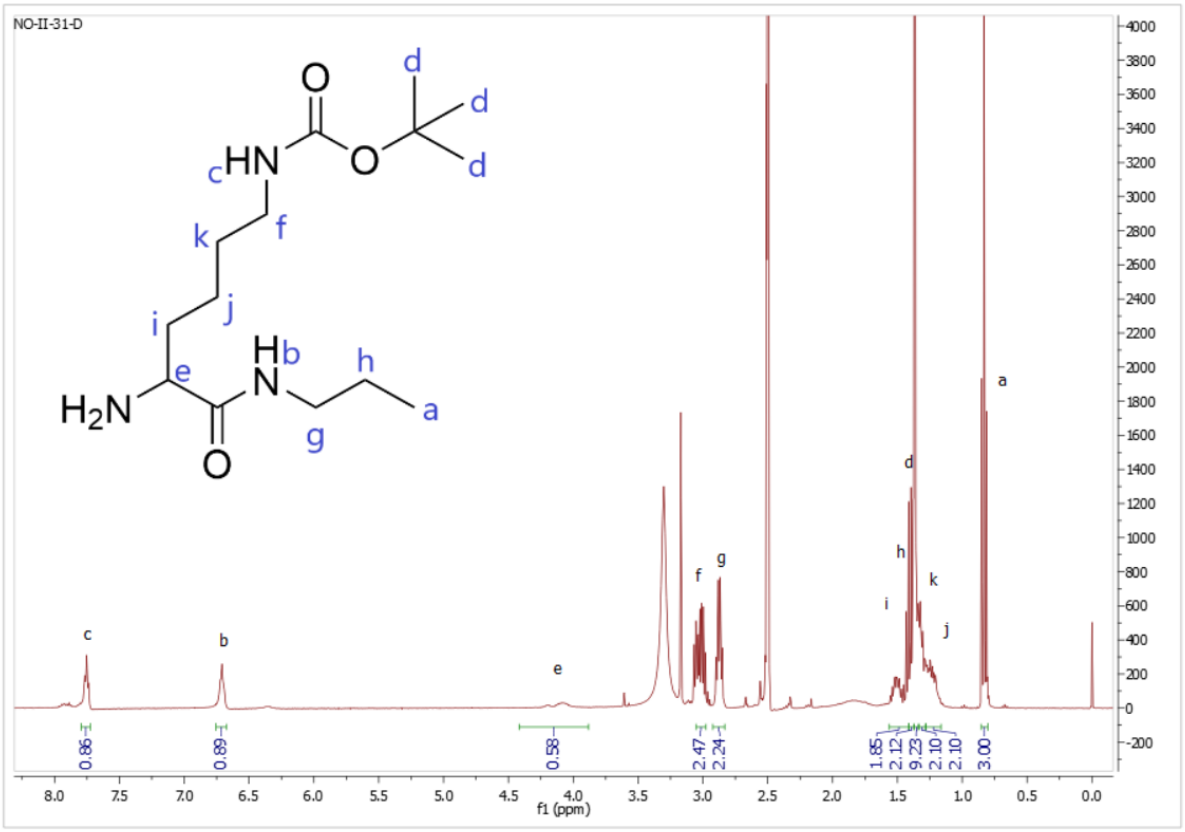

Figure 38. ^{1}H NMR spectrum of **5** with assigned protons.

5, ^{1}H NMR (DMSO, 400 MHz): δ 0.83 (td, 3H), δ 1.23 (m, 2 H), δ 1.31 (m, 2 H), δ 1.37 (s, 9 H), δ 1.39 (m, 2 H), δ 1.52 (m, 2 H), δ 2.87 (dd, 2H), δ 3.01 (m, 2 H), δ 4.14 (d, 1H), δ 6.71 (s, 1H), δ 7.75 (t, 1H). Residual DMSO δ 2.50, its internal water δ 3.30, and MeOH δ 3.17. Protons from -NH_2 group are not seen, due to formation of intramolecular and intermolecular hydrogen bonds with water.

The third step of the synthesis of $ZFKC_3$ is illustrated in Figure 39.

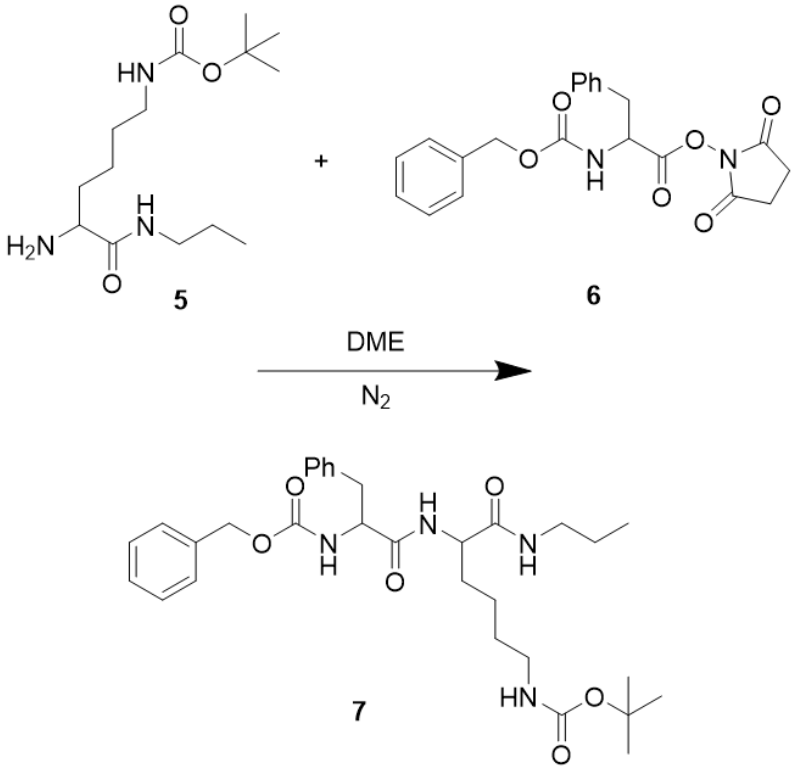

Figure 39. Coupling of **5** and ZFOSu (**6**).

3.39 g (8.6 mmol) of ZFOSu (**6**) (1.1 eq.) (prepared earlier by Nagihan Özbek) was dissolved into 20 ml of DME in a double necked flask. 2.24 g (7.8 mmol, 1 eq.) of **5** was dissolved into 15 ml of DME and added dropwise into the mixture under nitrogen atmosphere. Appearance of the mixture was clear with a brownish colour. 10 ml of THF and 15 ml of DME were added for achieving a better solubility. Reaction was left stirring overnight at room temperature. The following day the appearance of the reaction mixture had changed to white and cream-like. The mixture was filtered through a sinter and the filtrate was washed with (~15 ml) of 0.1 M Na_2CO_3, 0.1 M HCl, and water, respectively. Product was dried overnight under vacuum at 50 ℃ resulting in white powder. The yield for **7** was 2.72 g (4.8 mmol, 61.4 %).

^{1}H NMR spectrum of **7** with assigned protons is shown in Figure 40. ^{1}H, ^{1}H COSY NMR spectrum of **7** is presented in Appendix 3.

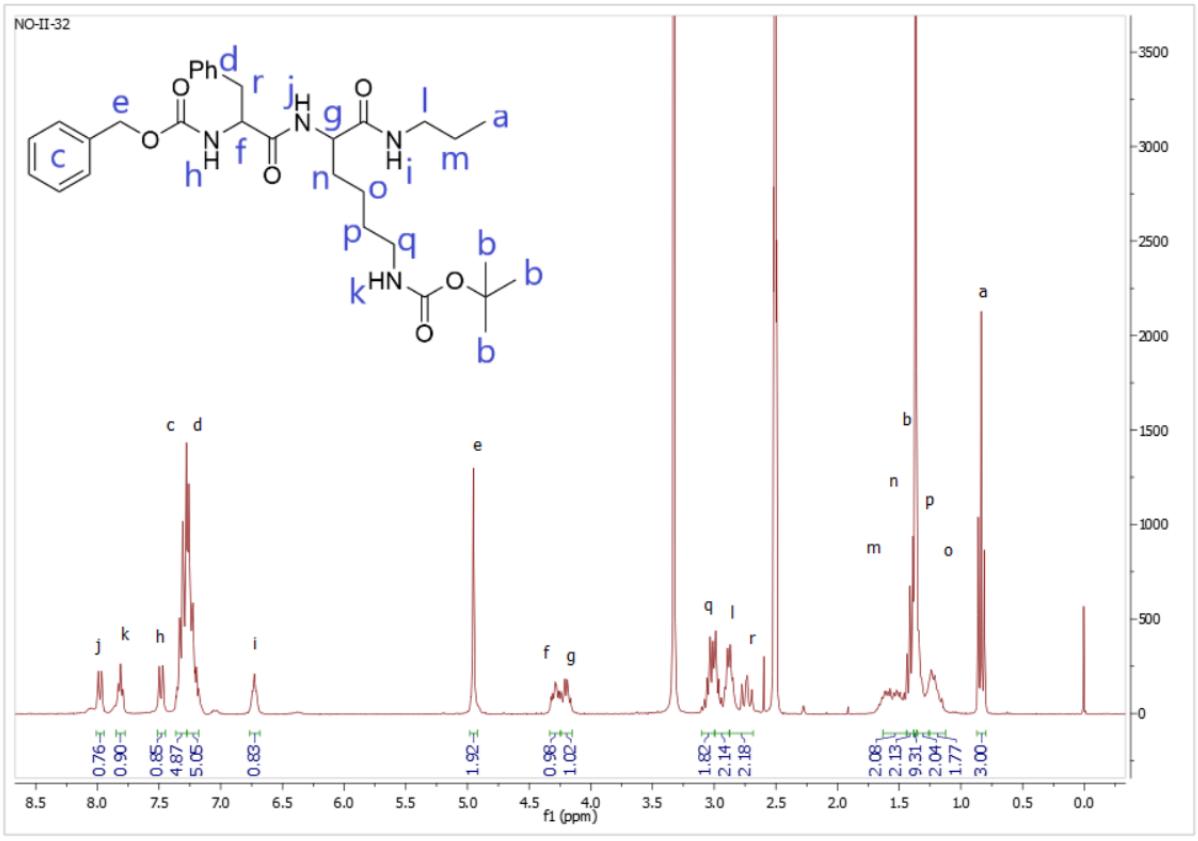

Figure 40. ^{1}H NMR spectrum of **7** with assigned protons.

7, ^{1}H NMR (DMSO, 300 MHz): δ 0.84 (t, 3H), δ 1.20 (m, 2H), δ 1.29 (m, 2H), δ 1.37 (s, 9H), δ 1.39 (m, 2H), δ 1.53 (m, 2H), δ 2.78 (m, 2H), δ 2.93 (m, 2H), δ 3.04 (m, 2H), δ 4.19 (m, 1H), δ 4.2 (m, 1H), δ 4.95 (s, 2H), δ 6.73 (s, 1H), δ 7.22 (m, 5H), δ 7.32 (m, 5H), δ 7.48 (d, 1H), δ 7.81 (t, 1H), δ 7.98 (d, 1H). Residual DMSO δ 2.50, and its internal water δ 3.30.

The fourth and final step of the synthesis of ZFKC$_3$ is illustrated in Figure 41.

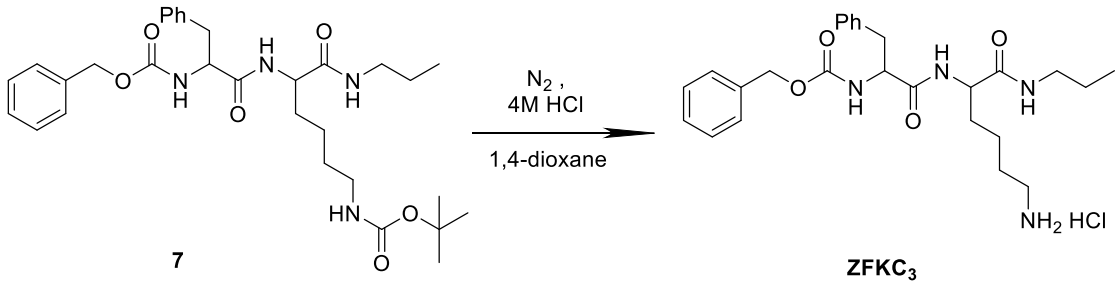

Figure 41. Reaction scheme leading to ZFKC$_3$.

2.72 g (4.8 mmol) of **7** was dissolved into 15 ml of dioxane. 20 ml of 4M HCl in dioxane was added dropwise under nitrogen atmosphere. The colour of the reaction mixture changed from white to clear. The mixture was left stirring overnight at room temperature.

On the following day the reaction mixture was white and gel-like. The gel was dissolved into a small quantity (~5 ml) of dioxane. The product was filtered through a sinter and dried in a vacuum oven at 40 ℃ overnight resulting in white powder. The yield for $ZFKC_3$ was 2.26 g (4.5 mmol, 93.9 %).

Mass spectrum was measured from the two day-dried $ZFKC_3$ (Appendix 4). It showed the highest peak at m/z value of 469.6 corresponding to ion $[M\text{-}HCl+H]^+$, which confirms that the desired product was formed. The calculated molecular mass (with stable isotope masses) for the corresponding ion of compound $ZFKC_3$ is 469.

^1H NMR spectrum of $ZFKC_3$ with assigned protons is shown in Figure 42. ^1H, ^1H COSY NMR spectrum is presented in Appendix 5.

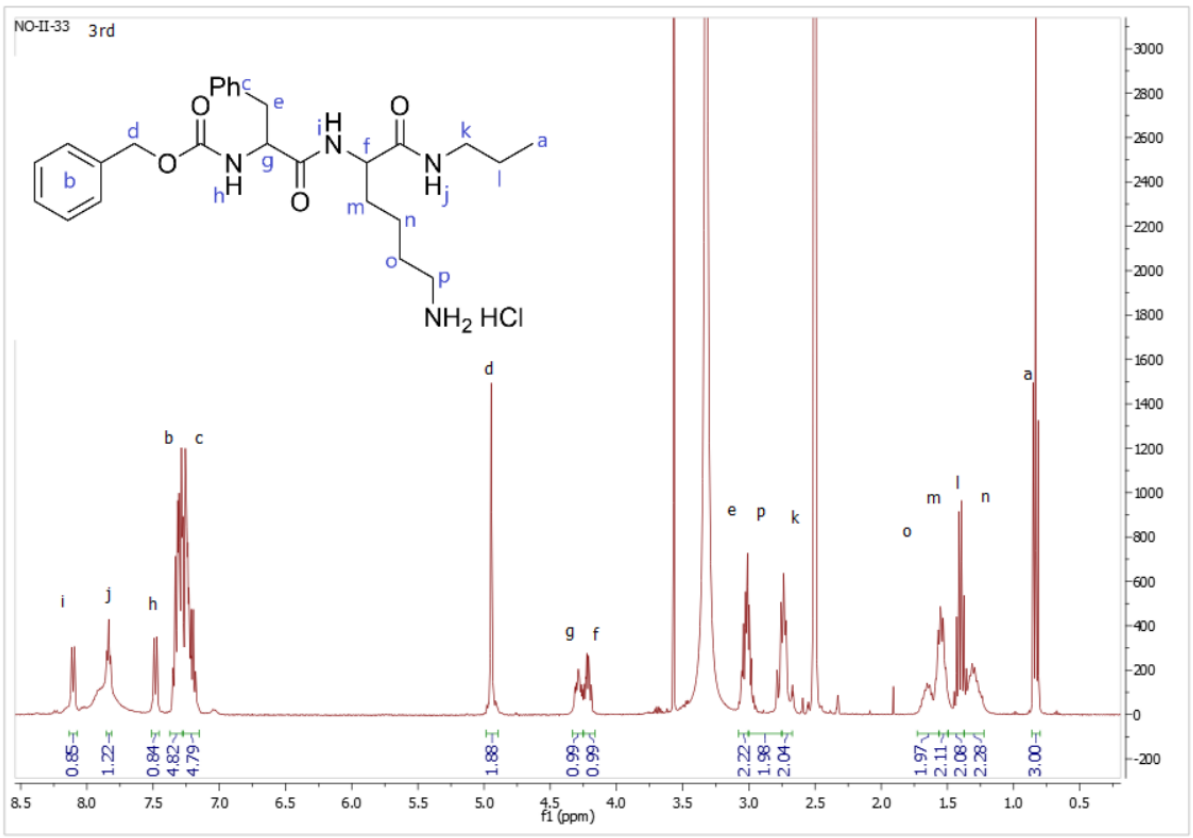

Figure 42. ^1H NMR spectra of $ZFKC_3$with assigned protons.

$ZFKC_3$, ^1H NMR (DMSO, 400 MHz): δ 0.83 (t, 3H), δ 1.32 (s, 2H), δ 1.41 (m, 2H), δ 1.54 (s, 2H), δ 1.61 (m, 2H), δ 2.71 (m, 2H), δ 2.90 (m, 2H), δ 3.41 (m, 2H), δ 4.21 (m, 1H), δ 4.29

(m, 1H), δ 4.95 (s, 2H), δ 7.22 (m, 5H), δ 7.32 (m, 5H), δ 7.48 (d, 1H), δ 7.84 (m, 3H), δ 7.84 (m, 1H), δ 8.10 (d, 1H). Residual DMSO δ 2.50, its internal water δ 3.21, and dioxane δ 3.57.

9.1 Guanylation of $ZFKC_3$ – First batch

The guanylation of $ZFKC_3$ is illustrated in Figure 43.

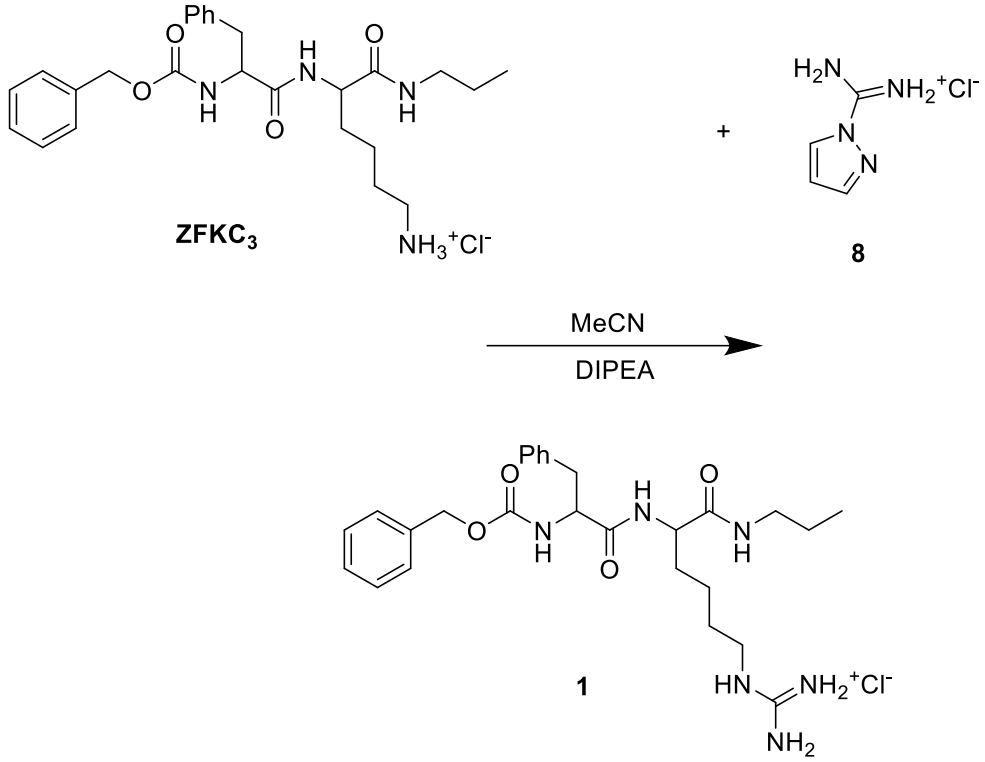

Figure 43. Reaction scheme of guanylation of $ZFKC_3$.

300 mg (0.6 mmol, 1 eq.) of $ZFKC_3$ (prepared earlier by Nagihan Özbek) was dissolved into MeCN (~35 ml) in a double-necked flask. 310 µl of DIPEA (1.8 mmol, 3 eq.) and 78.4 mg (0.5 mmol, 0.9 eq.) of 1H-pyrazole-1-carboxamidine hydrochloride (**8**) was added into the mixture. The colour of the mixture was cloudy white. The mixture was stirred overnight at room temperature.

The TLC check in the following day showed that no reaction seemed to have occurred. No change was seen on the appearance of the mixture either. The mixture was then stirred at 60 ℃ for 21 hours. After two hours the colour had disappeared and the solution was clear.

No precipitation was observed while the solution was cooled down. The solvent was evaporated to half of the volume of the mixture. The mixture was placed in the fridge over a weekend.

Precipitation was trialled with the mixture with 20 ml of diethyl ether, but it was not successful. The colour of the mixture changed to white. The solvent was decanted off leaving a sticky yellow wax, which was dissolved in acetonitrile (~20 ml), and the acetonitrile was evaporated off. The residue was dried under vacuum at room temperature.

Precipitation of the product was induced by addition of water (~20 ml). White solid was formed. The precipitate was separated by centrifugation and dried in a vacuum oven at 38 ℃. pH of the supernatant was ~6, in other words neutral. The yield for **1** was 0.052 g (0.1 mmol, 16.1 %).

The success of the reaction was ensured with ^{1}H and COSY NMR experiments and by measuring mass spectrum of the product resulting in $[M+H]^{+}$ = 511.30 (calc. 511). ^{1}H, ^{1}H COSY NMR spectrum and mass spectrum of **1** are presented in Appendices 6 and 7.

Figure 44 shows the ^{1}H NMR spectrum of **1** with corresponding protons assigned.

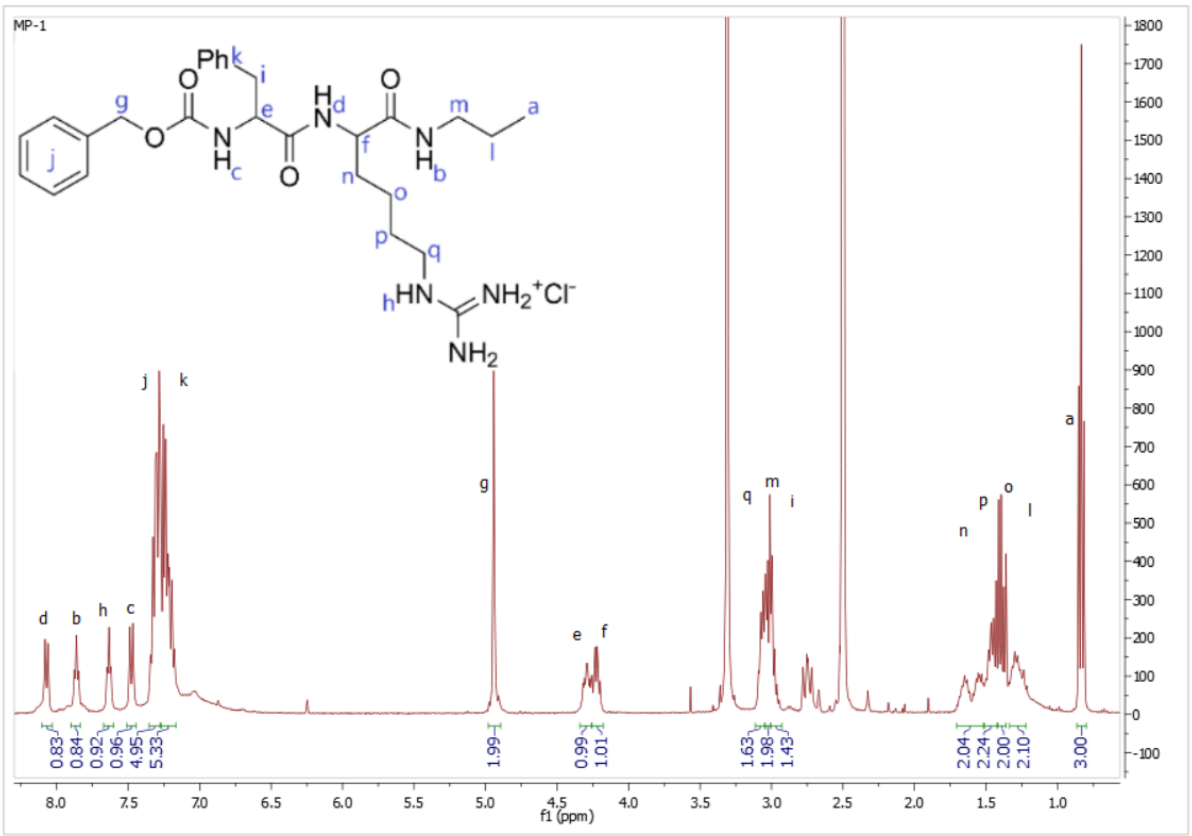

Figure 44. ^{1}H NMR spectrum of **1** with assigned protons.

1, ^{1}H NMR (DMSO, 400 MHz): δ 0.83 (t, 3H), δ 1.26 (m, 2H), δ 1.37 (m, 2H), δ 1.46 (m, 2H), δ 1.59 (m, 2H), δ 2.97 (m, 2H), δ 3.02 (m, 2H), δ 3.07 (m, 2H), δ 4.22 (m, 1H), δ 4.29 (m, 1H),

δ 4.94 (s, 2H), δ 7.21 (m, 5H), δ 7.31 (m, 5H), δ 7.48 (d, 1H), δ 7.63 (t, 1H), δ 7.86 (t, 1H), δ 8.07 (d, 1H). Residual DMSO δ 2.50, its internal water δ 3.31, and impurities δ 2.70. Protons from the amidine group (~δ 7.1) resonate with a broad peak due to interactions with water.

9.2 Guanylation of $ZFKC_3$ – Second batch

2 g (4.0 mmol, 1 eq.) of $ZFKC_3$, 180 ml of acetonitrile and 2070 µl (11.9 mmol, 3 eq.) of DIPEA was introduced into a double-necked flask. Dissolving took almost 3 hours, with heating to 60 ℃ and with using ultrasound bath. 522.25 mg (3.6 mmol, 0.9 eq.) of **8** was added to the mixture. Then the mixture was stirred at 60 ℃. TLC was taken after 23 h of reaction time, with both of the starting reagents still visible. After 26 hours the reaction was stopped, and the solvent was evaporated off leading to a yellow oil. Precipitation was induced by water (~50 ml), after which the colour of the precipitate was white and little brownish. The brown substance at the bottom of the flask did not dissolve. After 30 minutes in an ice bath the texture of the content of the flask changed to gel-like. The flask was transferred into the fridge overnight. The following day the contents of the flask had converted into a gel. It was centrifugated in total of 11 times 10 min 6000 rpm, and the small amounts of separated water was collected. The gel was filtrated (3 hours), and the concentrated gel was dried under vacuum over weekend at 50 ℃. After drying the appearance was like a dried yellow-brown wax. The yield was 0.6 g (1.1 mmol, 31.2 %).

^{1}H and COSY NMR experiments together with mass spectrometry were conducted. The proton NMR showed a peak arising from DIPEA. The product was washed with (~30 ml) water and diethyl ether and dried in a vacuum overnight at 50 ℃. The proton spectrum measured after the additional purification still showed the presence of DIPEA. Figure 45 shows the ^{1}H spectrum of the second batch of **1** with assigned protons. The mass spectrum of the product resulting in $[M+H]^+$ = 511.3042 (calc. 511). ^{1}H, ^{1}H COSY NMR spectrum and mass spectrum of the second batch of **1** are presented in Appendices 8 and 9.

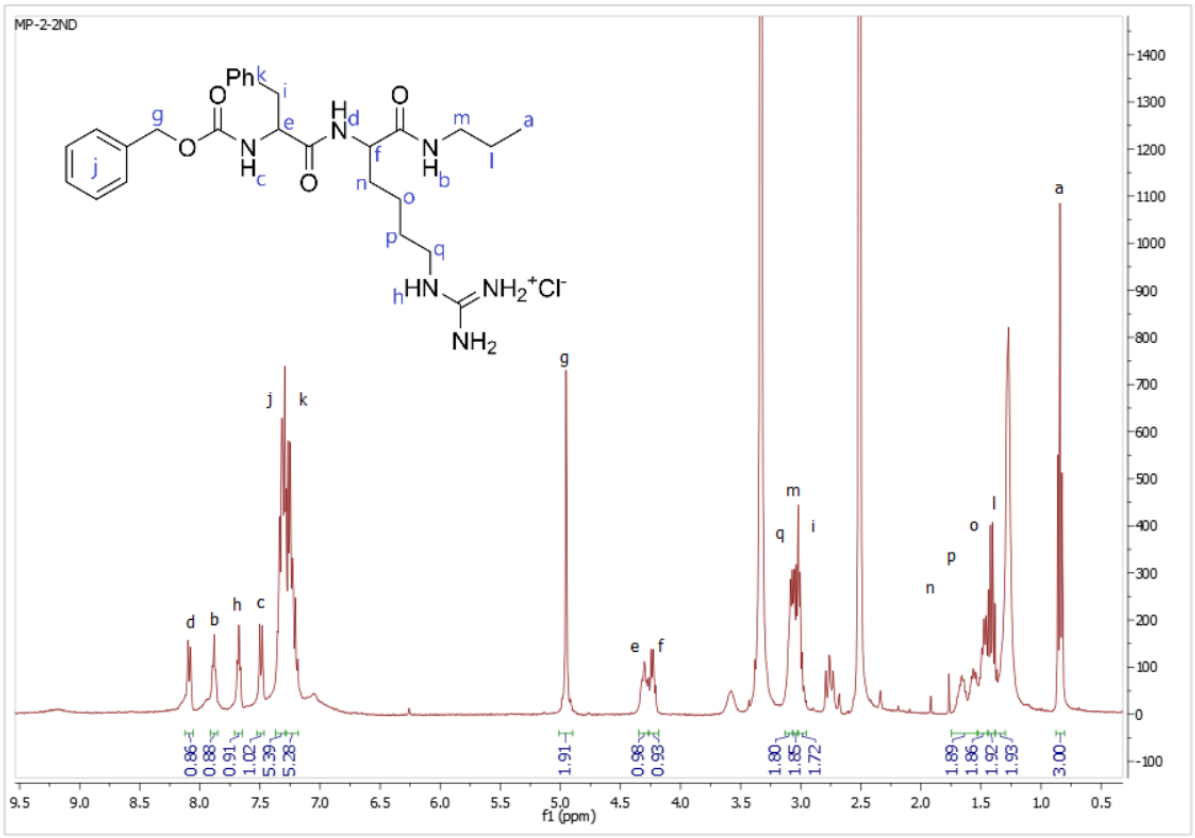

Figure 45. ^{1}H NMR spectrum of second batch of **1** with assigned protons.

Second batch **1**, ^{1}H NMR (DMSO, 400 MHz): δ 0.84 (t, 3H), δ 1.33 (m, 2H), δ 1.40 (m, 2H), δ 1.47 (m, 2H), δ 1.59 (m, 2H), δ 3.00 (m, 2H), δ 3.04 (m, 2H), δ 3.08 (m, 2H), δ 4.23 (m, 1H), δ 4.29 (m, 1H), δ 4.94 (s, 2H), δ 7.23 (m, 5H), δ 7.32 (m, 5H), δ 7.49 (d, 1H), δ 7.67 (t, 1H), δ 7.88 (t, 1H), δ 8.09 (d, 1H). Residual DMSO δ 2.51, its internal water δ 3.33, dioxane δ 3.58, DIPEA δ 1.27, and impurities δ 2.76.

9.3 Gelation tests, 3D printing trial, and rheology

For the gelation tests concentrations of 10 mM or 20 mM of compound **1** from the first batch was tested. The solvents that were used included 0.1 M acetate buffer (Ace B), H_2O, 0.1 M phosphate-buffered saline (PBS), and 0.1 M Na_2CO_3. The used solvent volumes were 1000 µl. The mixtures were treated with ultrasound for 1 minute after mixing, followed by heating until all of **1** was dissolved into the solvent. The gelation was observed with inversion tests 15 minutes after the treatment.

The gel for 3D printing trials was prepared using the second batch of **1**. The concentration of **1** was 20 mM in 5 ml of PBS. Printing details: used nozzle was Nordson 27GA with a diameter of 50 μm, printing speed was 50 mm/s, pressure was between 5 and 6 psi (7-41 kPa), and the chosen printing pattern was a circle. The gel was printed into two plastic and one glass Petri dishes. The other plastic and the glass dishes were treated with high frequency generator for decreasing the surface tension.

Rheology measurements were conducted three times. The concentration of the gel was 20 mM in PBS. The gelator molecule **1** was dissolved into the solvent with heating, and the resulted liquid was placed into the plate of the rheometer for measuring. The measuring time was 30 minutes.

10. Results and Discussion

During the synthesis of **4** traces of dichloromethane caused a small burst when drying in the vacuum. After the first drying the yield was 93.1%, and the ^{1}H NMR spectrum revealed impurities. Thus, the compound was washed and dried again. When inserting the flask into the vacuum for the second drying, an burst happened again, because the product was not completely dry. Because of that some product was lost. The final yield for **4** was 77.9 %.

During the synthesis of **5** the yield after drying was 99.0 %. Because the NMR spectrum revealed residues of water and methanol, **5** was dried for a second time. The yield was 96.0 %, which was still high.

The yield of **7** was 61.4 %, which was on the lower side. The reaction step for synthesizing **7** was performed with the smaller number of troubles, thus the low yield is surprising. It might be a result of low solubility or too short reaction time.

The yield of $ZFKC_3$ was at first over 104 %. NMR revealed some residual dioxane at δ 3.57, which is why the compound was dried again. After two days of drying NMR still showed remains of dioxane, and the yield was high: 97.8 %. The product was dried once more overnight in the vacuum oven at 40 ℃. The final yield was 93.9 %, still containing residual dioxane.

The yield in the first batch of **1** was 16.1 %. One reason for the low yield may be the partial water solubility of the product, meaning that part of the product may have been lost at the centrifugation phase.

The synthetic route leading to the second batch of **1** slightly differed from the previous one, and the reaction was conducted with higher quantities for obtaining more product. It would have been beneficial to centrifugate the mixture right after precipitation before it formed a strong gel. The yield was low, only 31.2 %. First of all, product was lost when it was transferred from container to container. Second, the product was tried to be purified by washing it with water and diethyl ether, but NMR revealed still remains of dioxane at δ 3.58, and DIPEA at δ 1.27 together with an unknown impurity at δ 2.76. The same impurity was present in the spectrum that was measured from **1** of the first batch.

Results from the five gelation tests are summarized in Table 2.

Table 2. Gelation tests of **1** in different solvents.

	1	2	3	4	5
Concentration (mM)	10	10	10	10	20
Solvent	Ace B	H_2O	PBS	Na_2CO_3	PBS
Gelation after 15 min, and after 1 day	liquid suspension	liquid	suspension, weak gel	liquid suspension	suspension, weak gel

Strong gels were not formed. Weak gels were formed in PBS. When the concentration was increased, the formed gel was stronger. Figure 46 shows the inverted vials for the gelation tests 1-4 after 15 minutes of gelation time, with concentration of 10 mM using different solvents. Figure 47 shows the vial from the gelation test 5 before and after the inversion test.

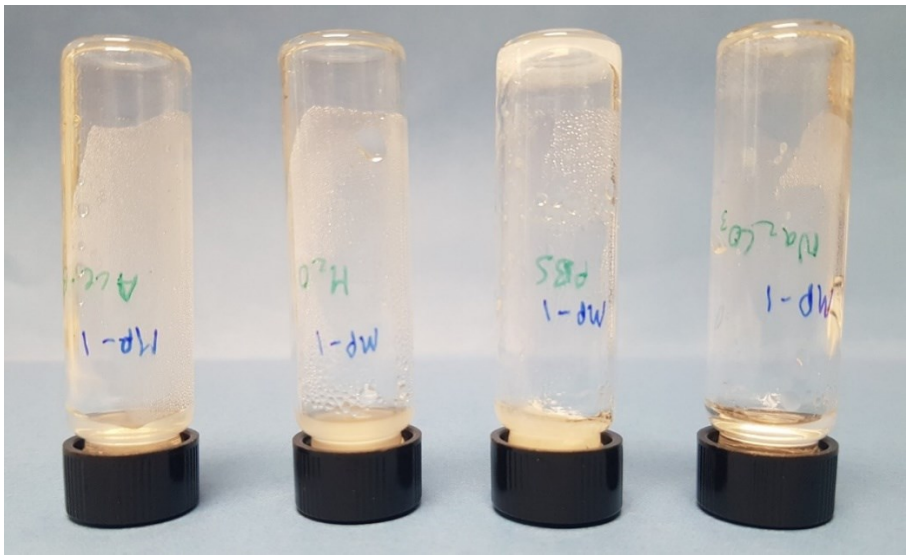

Figure 46. Gelation tests 1-4 with concentrations of 10 mM from left to right, with solvents Ace B, H_2O, PBS and Na_2CO_3 respectively.

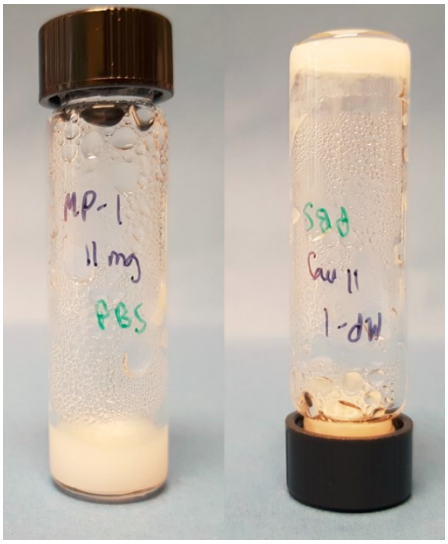

Figure 47. Gelation test 5 with concentration of 20 mM and PBS as solvent, before (left) and after (right) the inversion test.

During the 3D printing the pressure of the printer was difficult to control because of the type of the pressure controller. The gelator molecule used was from the second, prewashed, batch of **1** (which contained DIPEA). The gel was first printed onto untreated plastic surface: no desired pattern was created as the gel came out as a liquid. After printing it formed and stayed in a gel form. The second print was performed onto a treated plastic surface: same results were obtained as previously, but the formed gel was weaker. The third print was done onto a treated glass surface: the 'gel' expanded into a wide area immediately after printing and did not form a gel afterwards. Because the ink came out from the syringe as a clear liquid, it is possible that the

printing speed and pressure were too high. In addition, the used gel was most likely too weak to be used in 3D printing. Figure 48 shows the used printer.

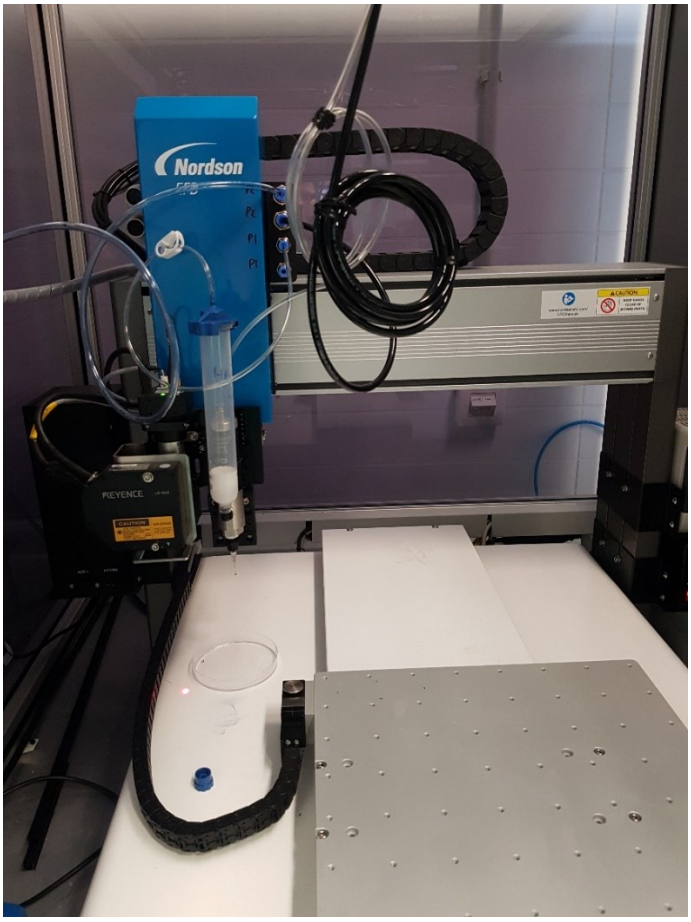

Figure 48. The used Nordson EFD printer.

In the rheological studies, three gel samples of molecule **1** were studied. One of the three samples was prepared from the first batch of **1**, and the two others from the second batch, which was washed once, but still contained DIPEA. The concentration of the gels was 20 mM, and the used solvent was PBS. Counted averages from the data of the three measurements were used for the graphs. All the axis values are presented in 10-base logarithmic scales for clarity.

In Figure 49 the elastic storage modulus *G'* and the elastic loss modulus *G''* as a function of applied stress is presented. Since the value of *G"* is higher than the value of *G'*, the substance behaves as a liquid.[123]

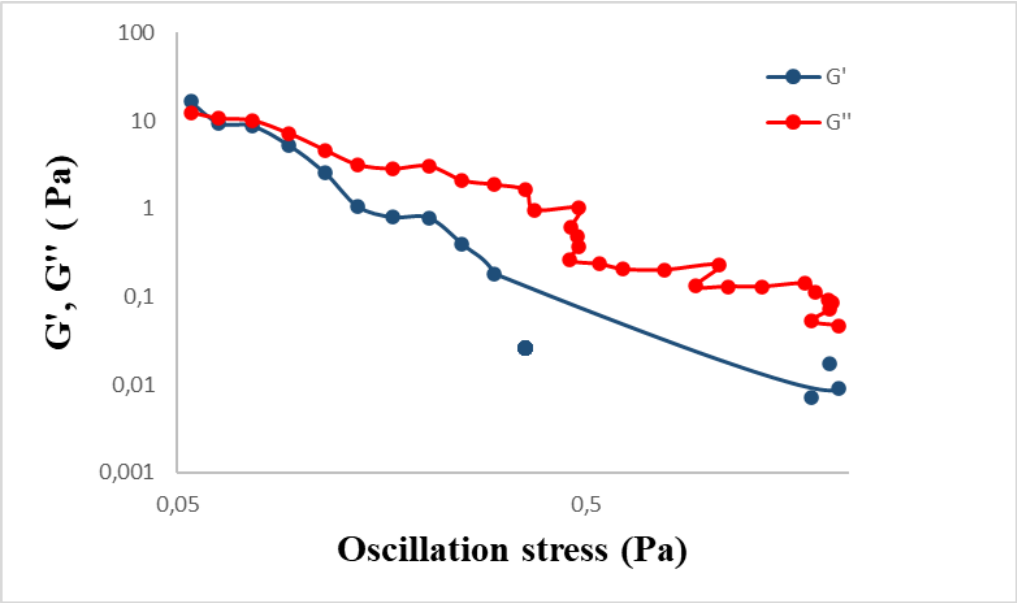

Figure 49. *G'* and *G''* as a function of applied stress. The elastic storage modulus *G'* is presented in blue, and the elastic loss modulus *G''* is presented in red. The axes values are presented in Pascals.

In Figure 50 is shown *G'* and *G''* as a function of frequency. For a substance to act like an elastic, *G'* should be higher than *G''*. This is clearly not the case in this experiment, which can be seen on the Figure.

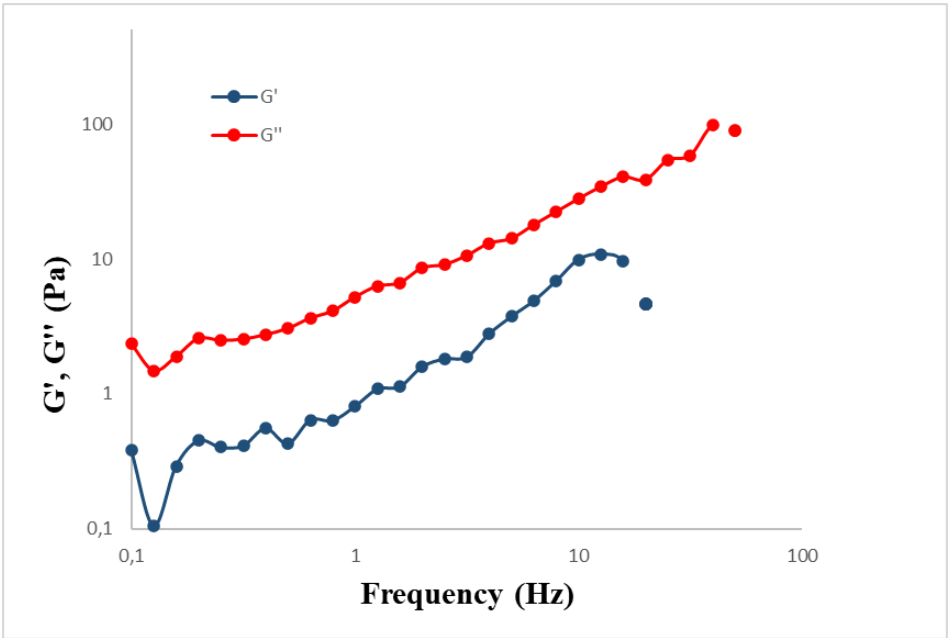

Figure 50. *G'* and *G''* as a function of frequency. The elastic storage modulus *G'* is presented in blue, and the elastic loss modulus *G''* is presented in red. The values on the axes are presented in Pascals and the frequency in Hertz.

The rheological studies show that the prepared hydrogel did not form even a weak gel, since the samples behaved more like a viscous liquid than an elastic solid.

11. Conclusions and future perspectives

The aim of this project was to find a suitable guanylation reaction for synthesizing dipeptide based hydrogelator, and to test 3D printing with the formed hydrogel. Overall, the synthesis was successful, and the desired molecule was obtained. Some of the yields were low and some troubles with the reaction steps were encountered. The intermediate products could have been dried straight for two days instead of one after synthesizing them to reduce the amount of unnecessary work. Due to time limitations the final product was not purified completely, and only few gelation tests were conducted. Since only a weak gel was formed, in the future the gelation properties of the molecule should be tested in different solvents using higher concentrations.

Printing supramolecular gels with the used 3D printer model seems to be a new area of research, due to the small number of published articles using the same printer model. This printing trial was one of the first printing experiments of this research group, because of which the tuning of the printing process was just starting. Other research groups using the same printer model have used stronger gels with additives as inks for successful printing.[124] The use of alginate, for example, with hydrogels for printing might lead to a better outcome, and a better control of the used pressure during printing would also be beneficial for preventing the separation of the liquid from the gel.

References

1. Yang, F.; Zhang, M.; Bhandari, B. and Liu, Y., Investigation on lemon juice gel as food material for 3D printing and optimization of printing parameters, *LWT*, **2018**, *87*, 67–76.

2. Torta, S. and Torta, J., *3D Printing : An Introduction*, Mercury Learning & Information, 2019.

3. Chia, H. N. and Wu, B. M., Recent advances in 3D printing of biomaterials, *J. Biol. Eng.*, **2015**, *9*, article no. 4.

4. Xu, W.; Jambhulkar, S.; Zhu, Y.; Ravichandran, D.; Kakarla, M.; Vernon, B.; Lott, D. G.; Cornella, J. L.; Shefi, O.; Miquelard-Garnier, G.; Yang, Y. and Song, K., 3D printing for polymer/particle-based processing: A review, *Composites. Part B*, **2021**, *223*, article no. 109102.

5. Godoi, F. C.; Prakash, S. and Bhandari, B. R., 3d printing technologies applied for food design: Status and prospects, *J. Food Eng.*, **2016**, *179*, 44–54.

6. Dragone, V.; Sans, V.; Rosnes, M. H.; Kitson, P. J. and Cronin, L., 3D-printed devices for continuous-flow organic chemistry, *Beilstein J. Org. Chem.*, **2013**, *9*, 951–959.

7. Nolan, M. C.; Fuentes Caparrós, A. M.; Dietrich, B.; Barrow, M.; Cross, E. R.; Bleuel, M.; King, S. M. and Adams, D. J., Optimising low molecular weight hydrogels for automated 3D printing, *Soft Matter*, **2017**, *13*, 8426–8432.

8. Nadgorny, M.; Xiao, Z. and Connal, L. A., 2D and 3D-printing of self-healing gels: design and extrusion of self-rolling objects, *Mol. Syst. Des. Eng.*, **2017**, *2*, 283–292.

9. Hockaday, L. A.; Kang, K. H.; Colangelo, N. W.; Cheung, P. Y. C.; Duan, B.; Malone, E.; Wu, J.; Girardi, L. N.; Bonassar, L. J.; Lipson, H.; Chu, C. C. and Butcher, J. T., Rapid 3D printing of anatomically accurate and mechanically heterogeneous aortic valve hydrogel scaffolds, *Biofabrication*, **2012**, *4*, article no. 035005.

10. Das, A. K. and Gavel, P. K., Low molecular weight self-assembling peptide-based materials for cell culture, antimicrobial, anti-inflammatory, wound healing, anticancer, drug delivery, bioimaging and 3D bioprinting applications, *Soft Matter*, **2020**, *16*, 10065–10095.

11. Rangel Euzcateguy, G.; Parajua-Sejil, C.; Marchal, P.; Chapron, D.; Averlant-Petit, M.; Stefan, L.; Pickaert, G. and Durand, A., Rheological investigation of supramolecular physical gels in water/dimethylsulfoxide mixtures by lysine derivatives, *Polym. Int.*, **2021**, *70*, 256–268.

12. Datta, S.; Barua, R.; Sarkar, R.; Barui, A.; Chowdhury, A. R. and Datta, P., Design and development of alginate: Poly-l-lysine scaffolds by 3D bio printing and studying their mechanical, structural and cell viability properties., *IOP Conf. Ser.: Mater. Sci. Eng.*, **2018**, *402*, article no. 012113.

13. Nelson, D. and Cox, M., *Lehninger Principles of Biochemistry*, 5th edition, W. H. Freeman and Company, New York, 2008.

14. Wang, L.; Gao, W.; Ng, S. and Pumera, M., Chiral Protein–Covalent Organic Framework 3D-Printed Structures as Chiral Biosensors, *Anal. Chem.*, **2021**, *93*, 5277–5283.

15. Morris, S. M., Arginine: beyond protein, *Am. J. Clin. Nutr.*, **2006**, *83*, 508S-512S.

16. Zheng, M.; Pan, M.; Zhang, W.; Lin, H.; Wu, S.; Lu, C.; Tang, S.; Liu, D. and Cai, J., Poly(α-l-lysine)-based nanomaterials for versatile biomedical applications: Current advances and perspectives, *Bioact. Mater.*, **2021**, *6*, 1878–1909.

17. Roy, S. and Banerjee, A., Amino acid based smart hydrogel: formation, characterization and fluorescence properties of silver nanoclusters within the hydrogel matrix, *Soft Matter*, **2011**, *7*, 5300-5308.

18. Rangel Euzcateguy, G.; Parajua-Sejil, C.; Marchal, P.; Chapron, D.; Averlant-Petit, M.-C.; Stefan, L.; Pickaert, G. and Durand, A., Rheological investigation of the influence of dextran on the self-assembly of lysine derivatives in water/dimethylsulfoxide mixtures, *Colloids Surf., A.*, **2021**, *625*, article no. 126908.

19. Wu, Z.; Cui, Q. and Yethiraj, A., Why Do Arginine and Lysine Organize Lipids Differently? Insights from Coarse-Grained and Atomistic Simulations, *J. Phys. Chem. B*, **2013**, *117*, 12145–12156.

20. Fokkens, M.; Schrader, T. and Klärner, F.-G., A Molecular Tweezer for Lysine and Arginine, *J. Am. Chem. Soc.*, **2005**, *127*, 14415–14421.

21. Perween, S.; Chandanshive, B.; Kotamarthi, H. C. and Khushalani, D., Single amino acid based self-assembled structure, *Soft Matter*, **2013**, *9*, 10141-10145.

22. Liu, G.; Li, X.; Sheng, J.; Li, P.-Z.; Ong, W. K.; Phua, S. Z. F.; Ågren, H.; Zhu, L. and Zhao, Y., Helicity Inversion of Supramolecular Hydrogels Induced by Achiral Substituents, *ACS Nano*, **2017**, *11*, 11880–11889.

23. Lehn, J.-M., Toward complex matter: Supramolecular chemistry and self-organization, *PNAS*, **2002**, *99*, 4763–4768.

24. Huang, F. and Anslyn, E. V., Introduction: Supramolecular Chemistry, *Chem. Rev.*, **2015**, *115*, 6999–7000.

25. Mezger, T. G., *The Rheology Handbook*, 2nd edition, Vincentz Network, Hannover, 2006.

26. Yu, G.; Yan, X.; Han, C. and Huang, F., Characterization of supramolecular gels, *Chem. Soc. Rev.*, **2013**, *42*, 6697-6722.

27. Steed, J. and Atwood, J., *Supramolecular Chemistry*, 2nd edition, Wiley, Chichester, 2009.

28. Smith, D. K., Molecular Gels - Nanostructured Soft Materials in Atwood, J. L. and Steed, J. W. (edit.), *Organic Nanostructures*, Wiley-VCH, Weinheim, Germany, 2008, 111–154.

29. Xiong, M.; Wang, C.; Zhang, G. and Zhang, D., CHAPTER 3. Molecular Gels

Responsive to Physical and Chemical Stimuli in *Functional molecular gels*, RSC, **2013**, 67–94.

30. Ferreira, L. J. and Camara, F. V., *Hydrogels: Synthesis, Characterization and Applications*, Nova Science Publishers, New York, 2012.

31. Vintiloiu, A. and Leroux, J. C., Organogels and their use in drug delivery - A review, *J. Controlled Release*, **2008**, 125, 179–192.

32. Shao, T.; Falcone, N. and Kraatz, H. B., Supramolecular Peptide Gels: Influencing Properties by Metal Ion Coordination and Their Wide-Ranging Applications, *ACS Omega*, **2020**, *5*, 1312–1317.

33. Kim, M. S.; Park, S. J.; Chun, H. J. and Kim, C.-H., Thermosensitive Hydrogels for Tissue Engineering, *Tissue Eng. Regener. Med.*, **2011**, *8*, 117–123.

34. Tao, M.; Xu, K.; He, S.; Li, H.; Zhang, L.; Luo, X. and Zhong, W., Zinc-ion-mediated self-assembly of forky peptides for prostate cancer-specific drug delivery, *Chem. Commun.*, **2018**, *54*, 4673–4676.

35. Basak, S.; Nandi, N.; Paul, S.; Hamley, I. W. and Banerjee, A., A tripeptide-based self-shrinking hydrogel for waste-water treatment: Removal of toxic organic dyes and lead (Pb^{2+}) ions, *Chem. Commun.*, **2017**, *53*, 5910–5913.

36. Babu, S. S.; Praveen, V. K. and Ajayaghosh, A., Functional π-Gelators and Their Applications, *Chem. Rev.*, **2014**, *114*, 1973–2129.

37. Zanna, N. and Tomasini, C., Peptide-Based Physical Gels Endowed with Thixotropic Behaviour, *Gels*, **2017**, *3*, article no. 39.

38. Singh, N.; Mohitk; Miravet, J. F.; Ulijn, R. V and Escuder, B., Peptide-Based Molecular Hydrogels as Supramolecular Protein Mimics, *Chem. Eur. J.* **2017**, *23*, 981-993.

39. Almohammed, S.; Alruwaili, M.; Reynaud, E. G.; Redmond, G.; Rice, J. H. and Rodriguez, B. J., 3D-Printed Peptide-Hydrogel Nanoparticle Composites for Surface-Enhanced Raman Spectroscopy Sensing, *ACS Appl. Nano Mater.*, **2019**, *2*, 5029–5034.

40. Hsu, W.-P.; Koo, K.-K. and Myerson, A. S., The Gel-Crystallization of l-Phenylalanine and Aspartame from Aqueous Solutions, *Chem. Eng. Commun.*, **2002**, *189*, 1079–1090.

41. Ramalhete, S. M.; Nartowski, K. P.; Sarathchandra, N.; Foster, J. S.; Round, A. N.; Angulo, J.; Lloyd, G. O. and Khimyak, Y. Z., Supramolecular Amino Acid Based Hydrogels: Probing the Contribution of Additive Molecules using NMR Spectroscopy, *Chem. - Eur. J.*, **2017**, *23*, 8014–8024.

42. Yan, X.; Zhu, P. and Li, J., Self-assembly and application of diphenylalanine-based nanostructures, *Chem. Soc. Rev.*, **2010**, *39*, 1877-1890.

43. Rubio-Magnieto, J.; Tena-Solsona, M.; Escuder, B. and Surin, M., Self-assembled hybrid hydrogels based on an amphipathic low molecular weight peptide derivative and a water-soluble poly(para-phenylene vinylene), *RSC Adv.*, **2017**, *7*, 9562–9566.

44. Qin, H.; Xu, P.; Zhou, C. and Wang, Y., Effects of l-Arginine on water holding capacity

and texture of heat-induced gel of salt-soluble proteins from breast muscle, *LWT - Food Sci. Technol.*, **2015**, *63*, 912–918.

45. Zhang, J.; Feng, X.; Patil, H.; Tiwari, R. V. and Repka, M. A., Coupling 3D printing with hot-melt extrusion to produce controlled-release tablets, *Int. J. Pharm.*, **2017**, *519*, 186–197.

46. Dumpa, N.; Butreddy, A.; Wang, H.; Komanduri, N.; Bandari, S. and Repka, M. A., 3D printing in personalized drug delivery: An overview of hot-melt extrusion-based fused deposition modeling, *Int. J. Pharm.*, **2021**, *600*, article no. 120501.

47. Lahtinen, E.; Precker, R. L. M.; Lahtinen, M.; Hey-Hawkins, E. and Haukka, M., Selective Laser Sintering of Metal-Organic Frameworks: Production of Highly Porous Filters by 3D Printing onto a Polymeric Matrix, *ChemPlusChem*, **2019**, *84*, 222–225.

48. Gordeev, E. G.; Degtyareva, E. S. and Ananikov, V. P., Analysis of 3D printing possibilities for the development of practical applications in synthetic organic chemistry, *Russ. Chem. Bull.*, **2016**, *65*, 1637–1643.

49. Sun, J.; Zhou, W.; Huang, D.; Fuh, J. Y. H. and Hong, G. S., An Overview of 3D Printing Technologies for Food Fabrication, *Food Bioprocess Technol.*, **2015**, *8*, 1605–1615.

50. Kamlow, M.-A.; Vadodaria, S.; Gholamipour-Shirazi, A.; Spyropoulos, F. and Mills, T., 3D printing of edible hydrogels containing thiamine and their comparison to cast gels, *Food Hydrocolloids*, **2021**, *116*, article no. 106550.

51. Lipton, J. I.; Cutler, M.; Nigl, F.; Cohen, D. and Lipson, H., Additive manufacturing for the food industry, *Trends Food Sci. Technol.*, **2015**, *43*, 114–123.

52. Lipton, J.; Arnold, D.; Nigl, F.; Lopez, N.; Cohen, D.; Noren, N. and Lipson, H., Multi-Material Food Printing with Complex Internal Structure Suitable for Conventional Post-Processing, *SFFS*, **2010**, 809–815.

53. Bertasa, M.; Dodero, A.; Alloisio, M.; Vicini, S.; Riedo, C.; Sansonetti, A.; Scalarone, D. and Castellano, M., Agar gel strength: A correlation study between chemical composition and rheological properties, *Eur. Polym. J.*, **2020**, *123*, article no. 109442.

54. Watase, M. and Arakawa, K., Rheological Properties of Hydrogels of Agar-agar. III. Stress Relaxation of Agarose Gels, *Bull. Chem. Soc. Jpn.*, **1968**, *41*, 1830–1834.

55. Gomes, L. R.; Simões, C. D. and Silva, C., Demystifying thickener classes food additives though molecular gastronomy, *Int. J. Gastron. Food Sci.*, **2020**, *22*, article no. 100262.

56. Wang, L.; Zhang, M.; Bhandari, B. and Yang, C., Investigation on fish surimi gel as promising food material for 3D printing, *J. Food Eng.*, **2018**, *220*, 101–108.

57. Wang, J. and Shaw, L. L., Rheological and extrusion behavior of dental porcelain slurries for rapid prototyping applications, *Mater. Sci. Eng. A*, **2005**, *397*, 314–321.

58. Shahbazi, M.; Jäger, H.; Ettelaie, R. and Chen, J., Construction of 3D printed reduced-fat meat analogue by emulsion gels. Part I: Flow behavior, thixotropic feature, and network structure of soy protein-based inks, *Food Hydrocolloids.*, **2021**, *120*, article no.

106967.

59. Rupp, H.; Döhler, D.; Hilgeroth, P.; Mahmood, N.; Beiner, M. and Binder, W. H., 3D Printing of Supramolecular Polymers: Impact of Nanoparticles and Phase Separation on Printability, *Macromol. Rapid Commun.*, **2019**, *40*, article no. 1900467.

60. Wang, J.; Liu, Y.; Zhang, X.; Rahman, S. E.; Su, S.; Wei, J.; Ning, F.; Hu, Z.; Martínez-Zaguilán, R.; Sennoune, S. R.; Cong, W.; Christopher, G.; Zhang, K. and Qiu, J., 3D printed agar/ calcium alginate hydrogels with high shape fidelity and tailorable mechanical properties, *Polymer.*, **2021**, *214*, article no. 123238.

61. Katime, I. and Mendizábal, E., Swelling Properties of New Hydrogels Based on the Dimethyl Amino Ethyl Acrylate Methyl Chloride Quaternary Salt with Acrylic Acid and 2-Methylene Butane-1,4-Dioic Acid Monomers in Aqueous Solutions, *Mater. Sci. Appl.*, **2010**, *01*, 162–167.

62. Jungst, T.; Smolan, W.; Schacht, K.; Scheibel, T. and Groll, J., Strategies and Molecular Design Criteria for 3D Printable Hydrogels, *Chem. Rev.*, **2016**, *116*, 1496–1539.

63. Zheng, S. Y.; Shen, Y.; Zhu, F.; Yin, J.; Qian, J.; Fu, J.; Wu, Z. L. and Zheng, Q., Programmed Deformations of 3D-Printed Tough Physical Hydrogels with High Response Speed and Large Output Force, *Adv. Funct. Mater.*, **2018**, *28*, article no. 1803366.

64. Jin, Y.; Shen, Y.; Yin, J.; Qian, J. and Huang, Y., Nanoclay-Based Self-Supporting Responsive Nanocomposite Hydrogels for Printing Applications, *ACS Appl. Mater. Interfaces*, **2018**, *10*, 10461–10470.

65. Sydney Gladman, A.; Matsumoto, E. A.; Nuzzo, R. G.; Mahadevan, L. and Lewis, J. A., Biomimetic 4D printing, *Nat. Mater.*, **2016**, *15*, 413–418.

66. Liu, S.; Shi, X.; Li, X.; Sun, Y.; Zhu, J.; Pei, Q.; Liang, J. and Chen, Y., A general gelation strategy for 1D nanowires: dynamically stable functional gels for 3D printing flexible electronics, *Nanoscale*, **2018**, *10*, 20096–20107.

67. Piras, C. C.; Kay, A. G.; Genever, P. G.; Fitremann, J. and Smith, D. K., Self-assembled gel tubes, filaments and 3D-printing with in situ metal nanoparticle formation and enhanced stem cell growth, *Chem. Sci.*, **2022**, *13*, 1972–1981.

68. Magdassi, S.; Shacham-Diamand, Y. and Kamyshny, A., *Nanomaterials for 2D and 3D Printing*, Wiley-VCH, Germany, 2017.

69. Peng, X.; Liu, T.; Zhang, Q.; Shang, C.; Bai, Q.-W. and Wang, H., Surface Patterning of Hydrogels for Programmable and Complex Shape Deformations by Ion Inkjet Printing, *Adv. Funct. Mater.*, **2017**, *27*, article no. 1701962.

70. Ding, Z.; Yuan, C.; Peng, X.; Wang, T.; Qi, H. J. and Dunn, M. L., Direct 4D printing via active composite materials, *Sci. Adv.*, **2017**, *3*, article no. 1602890.

71. Raviv, D.; Zhao, W.; McKnelly, C.; Papadopoulou, A.; Kadambi, A.; Shi, B.; Hirsch, S.; Dikovsky, D.; Zyracki, M.; Olguin, C.; Raskar, R. and Tibbits, S., Active Printed Materials for Complex Self-Evolving Deformations, *Sci. Rep.*, **2014**, *4*, 7422.

72. Liu, J.; Erol, O.; Pantula, A.; Liu, W.; Jiang, Z.; Kobayashi, K.; Chatterjee, D.; Hibino, N.; Romer, L. H.; Kang, S. H.; Nguyen, T. D. and Gracias, D. H., Dual-Gel 4D Printing of Bioinspired Tubes, *ACS Appl. Mater. Interfaces*, **2019**, *11*, 8492–8498.

73. Mahmoudi, M.; Wang, C.; Moreno, S.; Burlison, S. R.; Alatalo, D.; Hassanipour, F.; Smith, S. E.; Naraghi, M. and Minary - Jolandan, M., Three-Dimensional Printing of Ceramics through "Carving" a Gel and "Filling in" the Precursor Polymer, *ACS Appl. Mater. Interfaces*, **2020**, *12*, 31984–31991.

74. Xie, Z.-T.; Kang, D.-H. and Matsusaki, M., Resolution of 3D bioprinting inside bulk gel and granular gel baths, *Soft Matter*, **2021**, *17*, 8769–8785.

75. Shi, L.; Carstensen, H.; Hölzl, K.; Lunzer, M.; Li, H.; Hilborn, J.; Ovsianikov, A. and Ossipov, D. A., Dynamic Coordination Chemistry Enables Free Directional Printing of Biopolymer Hydrogel, *Chem. Mater.*, **2017**, *29*, 5816–5823.

76. Tan, Z.; Parisi, C.; Di Silvio, L.; Dini, D. and Forte, A. E., Cryogenic 3D Printing of Super Soft Hydrogels, *Sci. Rep.*, **2017**, *7*, article no. 16293.

77. Wang, C.; Zhao, Q. and Wang, M., Cryogenic 3D printing for producing hierarchical porous and rhBMP-2-loaded Ca-P/PLLA nanocomposite scaffolds for bone tissue engineering, *Biofabrication*, **2017**, *9*, article no. 025031.

78. Adamkiewicz, M. and Rubinsky, B., Cryogenic 3D printing for tissue engineering, *Cryobiology*, **2015**, *71*, 518–521.

79. Zhang, W.; Ullah, I.; Shi, L.; Zhang, Y.; Ou, H.; Zhou, J.; Ullah, M. W.; Zhang, X. and Li, W., Fabrication and characterization of porous polycaprolactone scaffold *via* extrusion-based cryogenic 3D printing for tissue engineering, *Mater. Des.*, **2019**, *180*, article no. 107946.

80. Chuan, Y. L. and Pandya, S. A. K., Fabrication of Non-Implant 3D Printed Skin, *MATEC Web Conf.*, **2018**, *152*, article no. 02016.

81. Mao, B.; Bentaleb, A.; Louerat, F.; Divoux, T. and Snabre, P., Heat-induced aging of agar solutions: Impact on the structural and mechanical properties of agar gels, *Food Hydrocolloids*, **2017**, *64*, 59–69.

82. Kollamaram, G.; Croker, D. M.; Walker, G. M.; Goyanes, A.; Basit, A. W. and Gaisford, S., Low temperature fused deposition modeling (FDM) 3D printing of thermolabile drugs, *Int. J. Pharm.*, **2018**, *545*, 144–152.

83. Wei, J.; Wang, J.; Su, S.; Wang, S.; Qiu, J.; Zhang, Z.; Christopher, G.; Ning, F. and Cong, W., 3D printing of an extremely tough hydrogel, *RSC Adv.*, **2015**, *5*, 81324–81329.

84. Firth, J.; Basit, A. W. and Gaisford, S., The Role of Semi-Solid Extrusion Printing in Clinical Practice, *AAPS*, **2018**, *31*, 133–151.

85. Johannesson, J.; Khan, J.; Hubert, M.; Teleki, A. and Bergström, C. A. S., 3D-printing of solid lipid tablets from emulsion gels, *Int. J. Pharm.*, **2021**, *597*, article no. 120304.

86. Wang, C.; Ye, X.; Zhao, Y.; Bai, L.; He, Z.; Tong, Q.; Xie, X.; Zhu, H.; Cai, D.; Zhou, Y.; Lu, B.; Wei, Y.; Mei, L.; Xie, D. and Wang, M., Cryogenic 3D printing of porous scaffolds for in situ delivery of 2D black phosphorus nanosheets, doxorubicin hydrochloride and osteogenic peptide for treating tumor resection-induced bone defects, *Biofabrication*, **2020**, *12*, article no. 035004.

87. Elbadawi, M.; McCoubrey, L. E.; Gavins, F. K. H.; Ong, J. J.; Goyanes, A.; Gaisford, S. and Basit, A. W., Disrupting 3D printing of medicines with machine learning, *Trends Pharml. Sci.*, **2021**, *42*, 745–757.

88. Piluso, S.; Skvortsov, G. A.; Altunbek, M.; Afghah, F.; Khani, N.; Koç, B. and Patterson, J., 3D bioprinting of molecularly engineered PEG-based hydrogels utilizing gelatin fragments, *Biofabrication*, **2021**, *13*, article no. 045008.

89. Abelseth, E.; Abelseth, L.; De la Vega, L.; Beyer, S. T.; Wadsworth, S. J. and Willerth, S. M., 3D Printing of Neural Tissues Derived from Human Induced Pluripotent Stem Cells Using a Fibrin-Based Bioink, *ACS Biomater. Sci. Eng.*, **2019**, *5*, 234–243.

90. Ong, C. S.; Yesantharao, P.; Huang, C. Y.; Mattson, G.; Boktor, J.; Fukunishi, T.; Zhang, H. and Hibino, N., 3D bioprinting using stem cells, *Pediatr. Res.*, **2018**, *83*, 223–231.

91. Datta, S.; Das, A.; Sasmal, P.; Bhutoria, S.; Roy Chowdhury, A. and Datta, P., Alginate-poly(amino acid) extrusion printed scaffolds for tissue engineering applications, *Int. J. Polym. Mater. Polym. Biomater.*, **2020**, *69*, 65–72.

92. Costantini, M.; Colosi, C.; Święszkowski, W. and Barbetta, A., Co-axial wet-spinning in 3D bioprinting: state of the art and future perspective of microfluidic integration, *Biofabrication*, **2019**, *11*, article no. 012001.

93. Jia, W.; Gungor-Ozkerim, P. S.; Zhang, Y. S.; Yue, K.; Zhu, K.; Liu, W.; Pi, Q.; Byambaa, B.; Dokmeci, M. R.; Shin, S. R. and Khademhosseini, A., Direct 3D bioprinting of perfusable vascular constructs using a blend bioink, *Biomaterials*, **2016**, *106*, 58–68.

94. Sareen, S.; Joseph, L. and Mathew, G., Improvement in solubility of poor water-soluble drugs by solid dispersion, *Int. J. Pharm. Investig.*, **2012**, *2*, 12-17.

95. Patil, H.; Tiwari, R. V. and Repka, M. A., Hot-Melt Extrusion: from Theory to Application in Pharmaceutical Formulation, *AAPS PharmSciTech*, **2016**, *17*, 20–42.

96. Arany, P.; Papp, I.; Zichar, M.; Regdon, G.; Béres, M.; Szalóki, M.; Kovács, R.; Fehér, P.; Ujhelyi, Z.; Vecsernyés, M. and Bácskay, I., Manufacturing and Examination of Vaginal Drug Delivery System by FDM 3D Printing, *Pharmaceutics*, **2021**, *13*, article no. 1714.

97. Tiboni, M.; Campana, R.; Frangipani, E. and Casettari, L., 3D printed clotrimazole intravaginal ring for the treatment of recurrent vaginal candidiasis, *Int. J. Pharm.*, **2021**, *596*, article no. 120290.

98. Parrilla, M.; Vanhooydonck, A.; Watts, R. and De Wael, K., Wearable wristband-based electrochemical sensor for the detection of phenylalanine in biofluids, *Biosens.*

Bioelectron., **2022**, *197*, article no. 113764.

99. Lu, Y.; Xiang, Z.; Li, N.; Huang, X. and Song, J., Photocurable epsilon-poly-L-lysine for digital light processing 3D printing, *Mater. Lett.*, **2022**, *318*, article no. 132169.

100. Helps, T.; Taghavi, M. and Rossiter, J., Thermoplastic electroactive gels for 3D-printable artificial muscles, *Smart Mater. Struct.*, **2019**, *28*, article no. 085001.

101. Mirdamadi, E.; Tashman, J. W.; Shiwarski, D. J.; Palchesko, R. N. and Feinberg, A. W., FRESH 3D Bioprinting a Full-Size Model of the Human Heart, *ACS Biomater. Sci. Eng.*, **2020**, *6*, 6453–6459.

102. Chalard, A.; Mauduit, M.; Souleille, S.; Joseph, P.; Malaquin, L. and Fitremann, J., 3D printing of a biocompatible low molecular weight supramolecular hydrogel by dimethylsulfoxide water solvent exchange, *Addit. Manuf.*, **2020**, *33*, article no. 101162.

103. Lozano, R.; Stevens, L.; Thompson, B. C.; Gilmore, K. J.; Gorkin, R.; Stewart, E. M.; in het Panhuis, M.; Romero-Ortega, M. and Wallace, G. G., 3D printing of layered brain-like structures using peptide modified gellan gum substrates, *Biomaterials*, **2015**, *67*, 264–273.

104. D'Souza, S. E.; Ginsberg, M. H. and Plow, E. F., Arginyl-glycyl-aspartic acid (RGD): a cell adhesion motif, *Trends Biochem. Sci.*, **1991**, *16*, 246–250.

105. Duffy, G. L.; Liang, H.; Williams, R. L.; Wellings, D. A. and Black, K., 3D reactive inkjet printing of poly-ε-lysine/gellan gum hydrogels for potential corneal constructs, *Mater. Sci. Eng. C*, **2021**, *131*, article no. 112476.

106. Shih, I.-L. and Shen, M.-H., Optimization of cell growth and poly(ε-lysine) production in batch and fed-batch cultures by *Streptomyces albulus* IFO 14147, *Process Biochem.*, **2006**, *41*, 1644–1649.

107. Liu, Y.; Hu, Q.; Dong, W.; Liu, S.; Zhang, H. and Gu, Y., Alginate/Gelatin-Based Hydrogel with Soy Protein/Peptide Powder for 3D Printing Tissue-Engineering Scaffolds to Promote Angiogenesis, *Macromol. Biosci.*, **2022**, *22*, article no. 2100413.

108. Lim, S. H.; Kathuria, H.; Amir, M. H. Bin; Zhang, X.; Duong, H. T. T.; Ho, P. C.-L. and Kang, L., High resolution photopolymer for 3D printing of personalised microneedle for transdermal delivery of anti-wrinkle small peptide, *J. Controlled Release*, **2021**, *329*, 907–918.

109. Li, S.; Xu, Y.; Yu, J. and Becker, M. L., Enhanced osteogenic activity of poly(ester urea) scaffolds using facile post-3D printing peptide functionalization strategies, *Biomaterials*, **2017**, *141*, 176–187.

110. Wang, C.; Ye, X.; Zhao, Y.; Bai, L.; He, Z.; Tong, Q.; Xie, X.; Zhu, H.; Cai, D.; Zhou, Y.; Lu, B.; Wei, Y.; Mei, L.; Xie, D. and Wang, M., Cryogenic 3D printing of porous scaffolds for in situ delivery of 2D black phosphorus nanosheets, doxorubicin hydrochloride and osteogenic peptide for treating tumor resection-induced bone defects, *Biofabrication*, **2020**, *12*, article no. 035004.

111. Zhang; Wang; Fu; Ye; Wang and Zhou, Fabrication and Application of Novel Porous

Scaffold in Situ-Loaded Graphene Oxide and Osteogenic Peptide by Cryogenic 3D Printing for Repairing Critical-Sized Bone Defect, *Molecules*, **2019**, *24*, article no. 1669.

112. Mendes, A. C.; Baran, E. T.; Reis, R. L. and Azevedo, H. S., Self-assembly in nature: using the principles of nature to create complex nanobiomaterials, *WIREs. Nanomed. Nanobiotechnol.*, **2013**, *5*, 582–612.

113. Jian, H.; Wang, M.; Dong, Q.; Li, J.; Wang, A.; Li, X.; Ren, P. and Bai, S., Dipeptide Self-Assembled Hydrogels with Tunable Mechanical Properties and Degradability for 3D Bioprinting, *ACS Appl. Mater. Interfaces*, **2019**, *11*, 46419–46426.

114. Alonso-Moreno, C.; Carrillo-Hermosilla, F.; Garcés, A.; Otero, A.; López-Solera, I.; Rodríguez, A. M. and Antiñolo, A., Simple, Versatile, and Efficient Catalysts for Guanylation of Amines, *Organometallics*, **2010**, *29*, 2789–2795.

115. Bakka, T. A. and Gautun, O. R., Simple generalized reaction conditions for the conversion of primary aliphatic amines to surfactant-like guanidine salts with 1 H - pyrazole carboxamidine hydrochloride, *Synth. Commun.*, **2017**, *47*, 169–172.

116. Loudet, A.; Han, J.; Barhoumi, R.; Pellois, J.-P.; Burghardt, R. C. and Burgess, K., Non-covalent delivery of proteins into mammalian cells, *Org. Biomol. Chem.*, **2008**, *6*, 4516-4522.

117. Gros, E.; Deshayes, S.; Morris, M. C.; Aldrian-Herrada, G.; Depollier, J.; Heitz, F. and Divita, G., A non-covalent peptide-based strategy for protein and peptide nucleic acid transduction, *Biochim. Biophys. Acta - Biomembr.*, **2006**, *1758*, 384–393.

118. Tsikas, D. and Wu, G., Homoarginine, arginine, and relatives: analysis, metabolism, transport, physiology, and pathology, *Amino Acids*, **2015**, *47*, 1697–1702.

119. Simpson, J. H., *Organic Structure Determination Using 2-D NMR Spectroscopy*, 2nd esition, Academic Press, San Diego, USA, 2012.

120. Glish, G. L. and Vachet, R. W., The basics of mass spectrometry in the twenty-first century, *Nat. Rev. Drug Discovery*, **2003**, *2*, 140–150.

121. Tena-Solsona, M., *Hydrogels based on short amphipathic peptides: self-assembly studies and applications*, Universitat Jaume I, Castelló de la Plana, 2015.

122. NMR Chemical Shifts of Impurities Charts, https://www.sigmaaldrich.com/ES/en/technical-documents/technical-article/analytical-chemistry/nuclear-magnetic-resonance/1h-nmr-and-13c-nmr-chemical-shifts-of-impurities-chart. (Accessed on July 2022).

123. Dawn, A. and Kumari, H., Low Molecular Weight Supramolecular Gels Under Shear: Rheology as the Tool for Elucidating Structure-Function Correlation, *Chem. Eur. J.*, **2018**, *24*, 762–776.

124. Schutyser, M. A. I.; Houlder, S.; de Wit, M.; Buijsse, C. A. P. and Alting, A. C., Fused deposition modelling of sodium caseinate dispersions, *J. Food Eng.*, **2018**, *220*, 49–55.

Appendices

1. ^{1}H, ^{1}H COSY NMR spectrum of **4**

2. ^{1}H, ^{1}H COSY NMR spectrum of **5**

3. ^{1}H, ^{1}H COSY NMR spectrum of **7**

4. Mass spectrum of $ZFKC_3$

5. ^{1}H, ^{1}H COSY NMR spectrum of $ZFKC_3$

6. ^{1}H, ^{1}H COSY NMR spectrum of first batch of **1**

7. Mass spectrum of first batch of **1**

8. ^{1}H, ^{1}H COSY NMR spectrum of second batch of **1**

9. Mass spectrum of the second batch of **1**

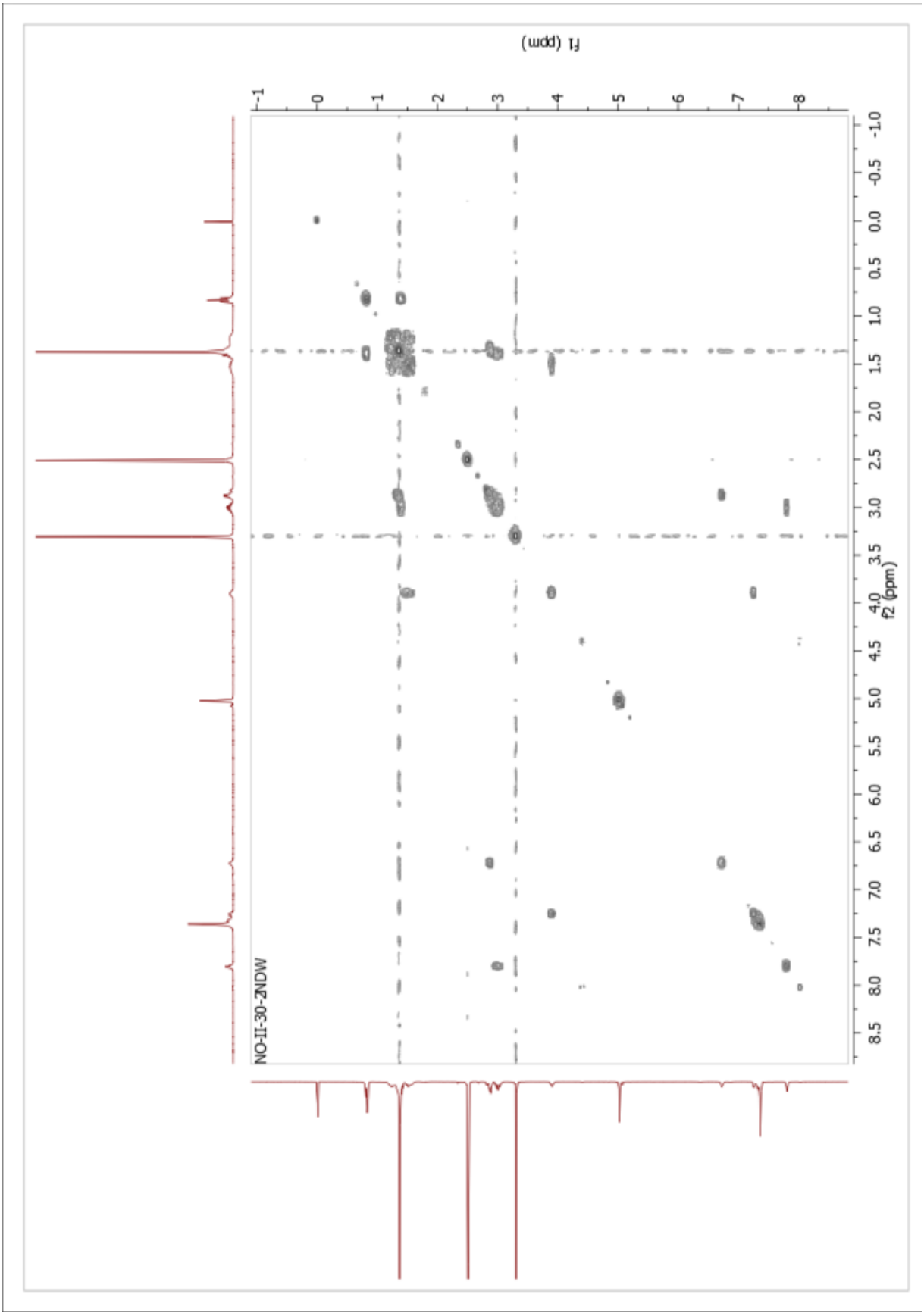
f1 (ppm)
f2 (ppm)
NO-II-30-2NDW

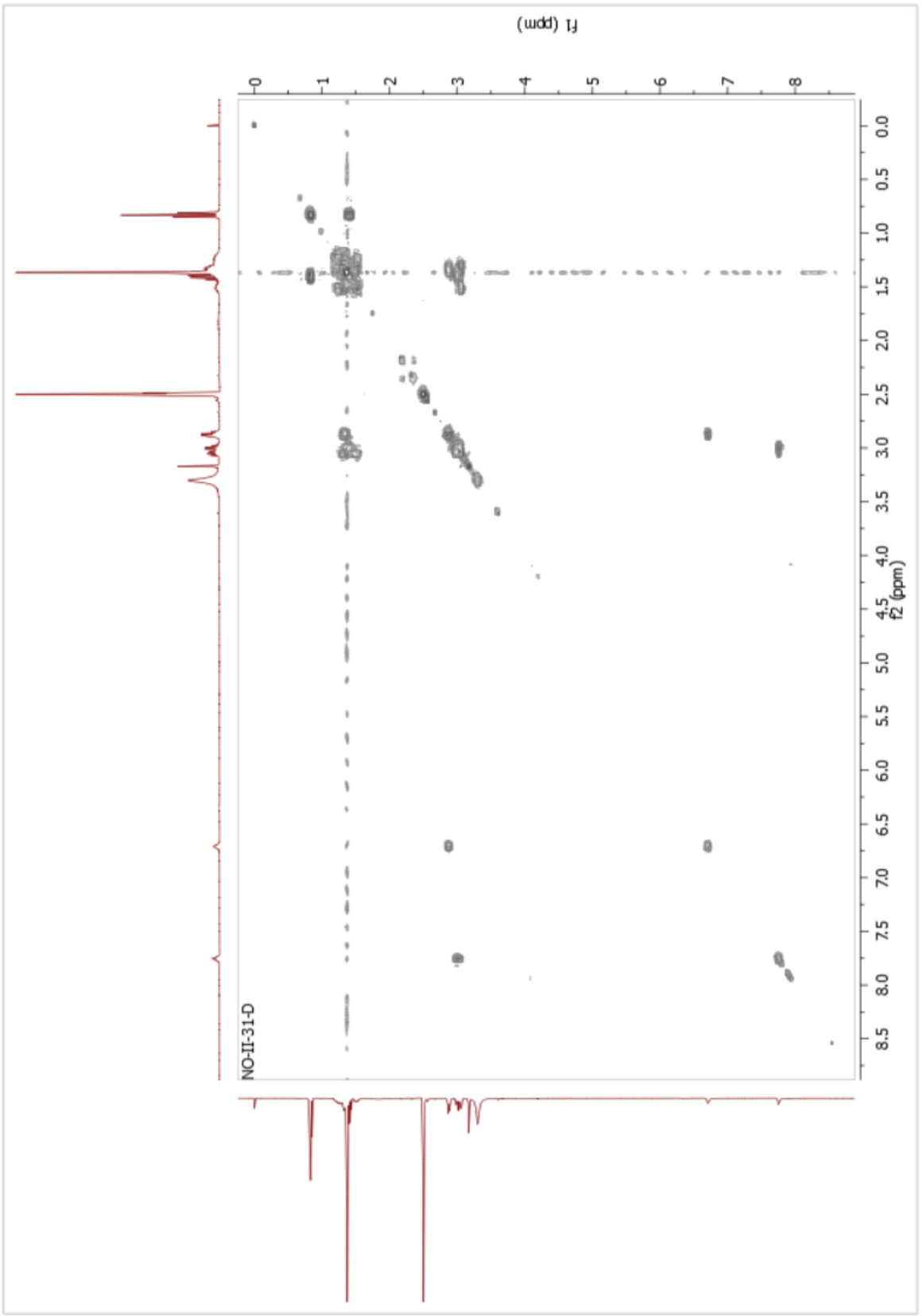
f1 (ppm)
f2 (ppm)
NO-II-31-D

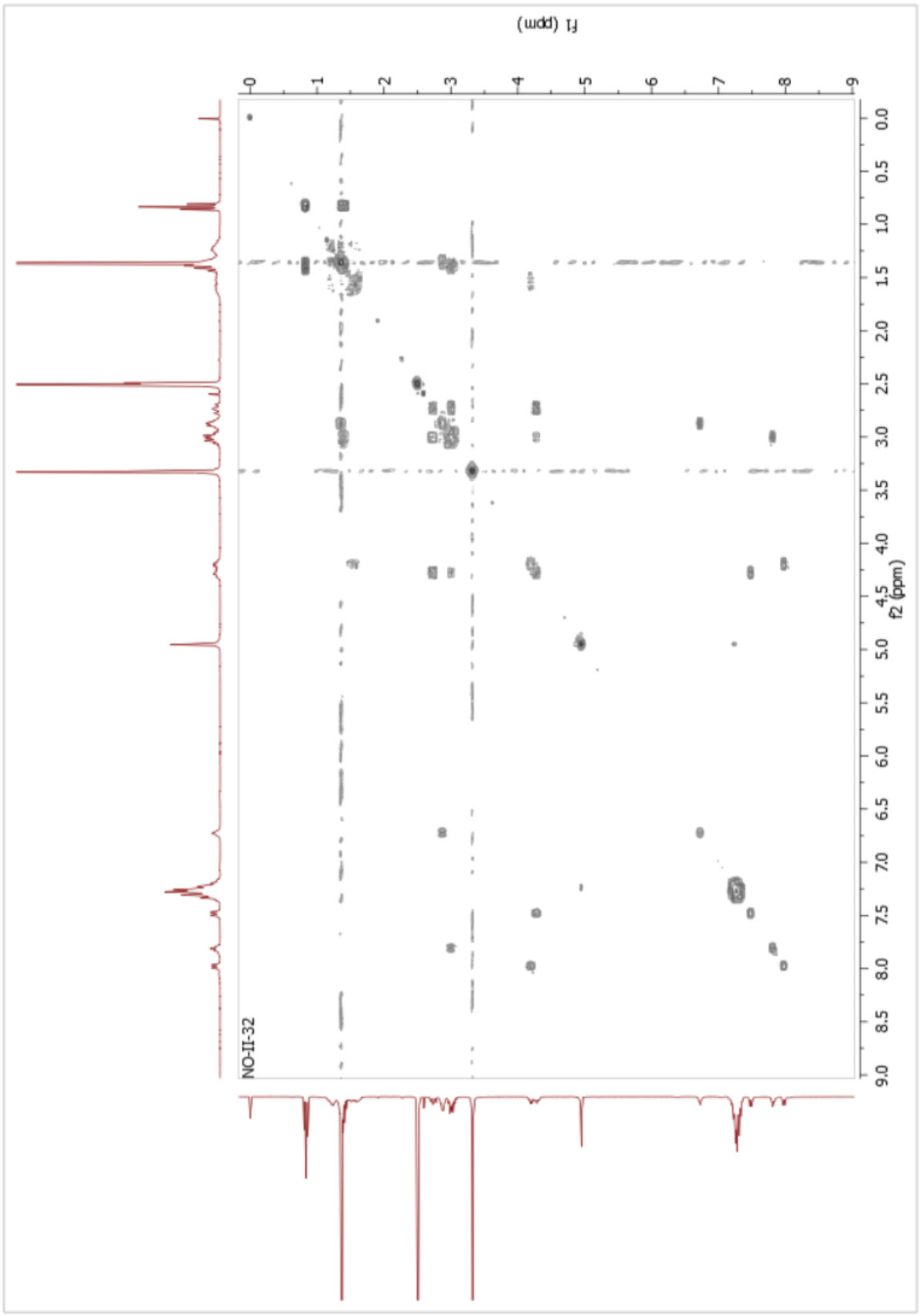
f1 (ppm)
f2 (ppm)
NO-II-32

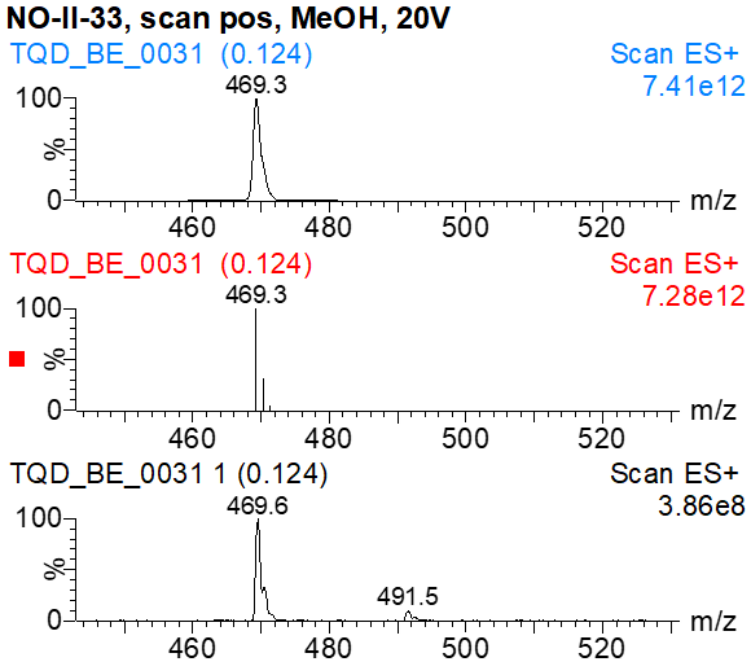
NO-II-33, scan pos, MeOH, 20V
TQD_BE_0031 (0.124)
Scan ES+
7.41e12
469.3
100
%
0
460
480
500
520
m/z
TQD_BE_0031 (0.124)
Scan ES+
7.28e12
469.3
TQD_BE_0031 1 (0.124)
Scan ES+
3.86e8
469.6
491.5

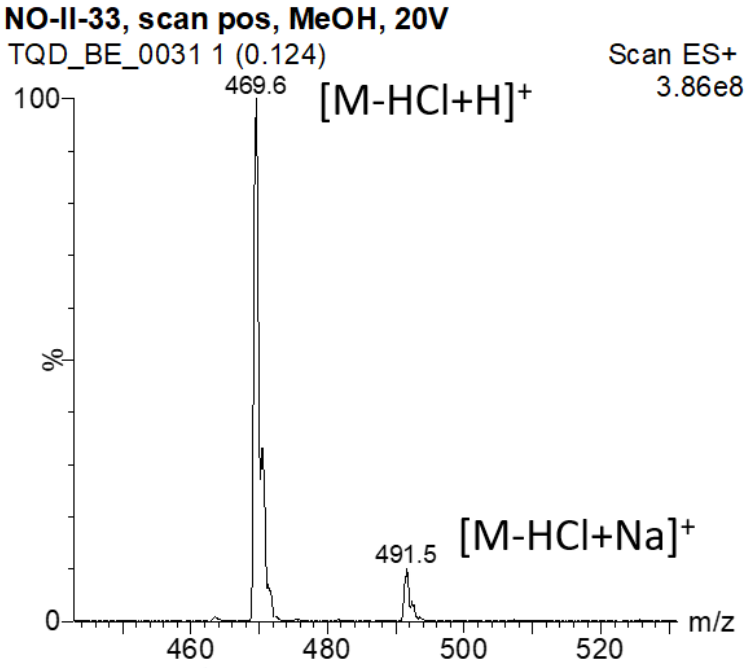
NO-II-33, scan pos, MeOH, 20V
TQD_BE_0031 1 (0.124)
Scan ES+
3.86e8
469.6
[M-HCl+H]+
491.5
[M-HCl+Na]+
100
%
0
460
480
500
520
m/z

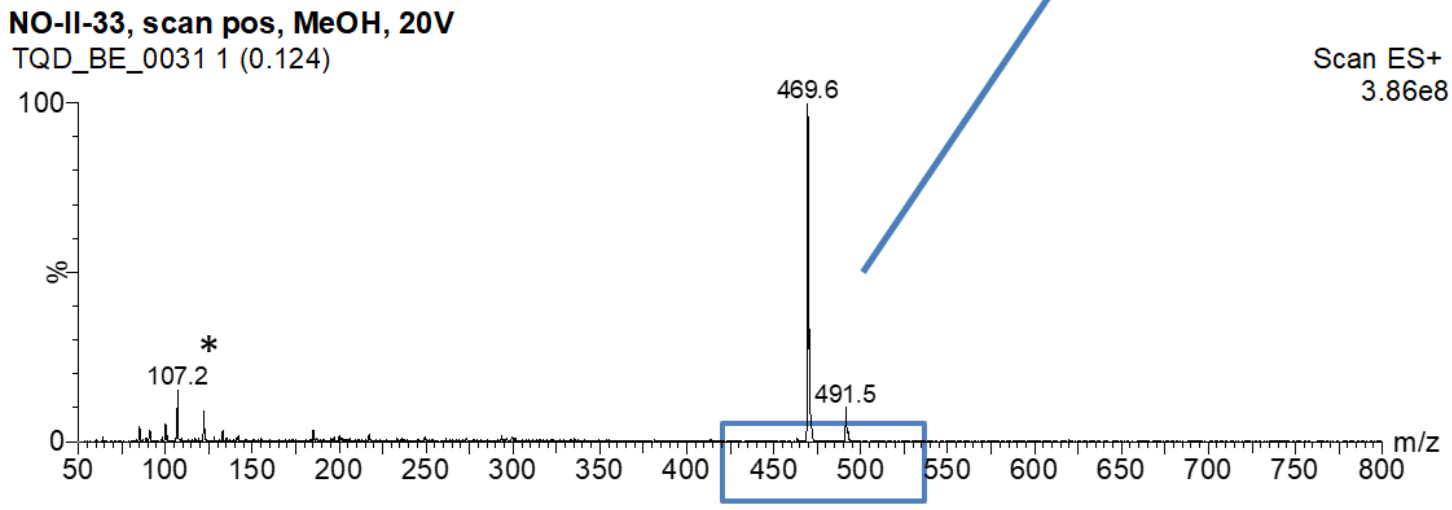
NO-II-33, scan pos, MeOH, 20V
TQD_BE_0031 1 (0.124)
Scan ES+
3.86e8
469.6
491.5
107.2
*
100
%
0
50
100
150
200
250
300
350
400
450
500
550
600
650
700
750
800
m/z

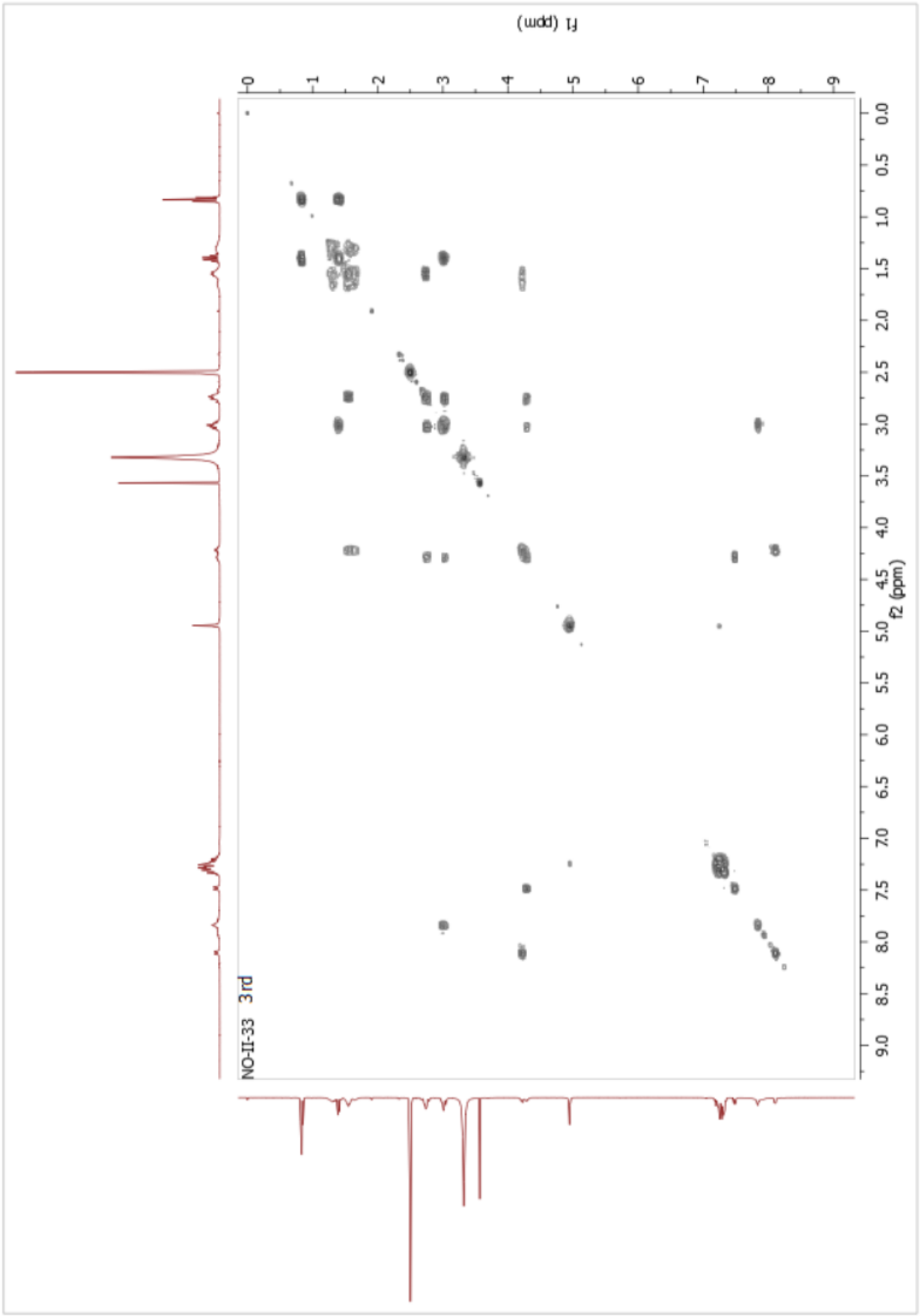
f1 (ppm)
f2 (ppm)
NO-II-33 3rd

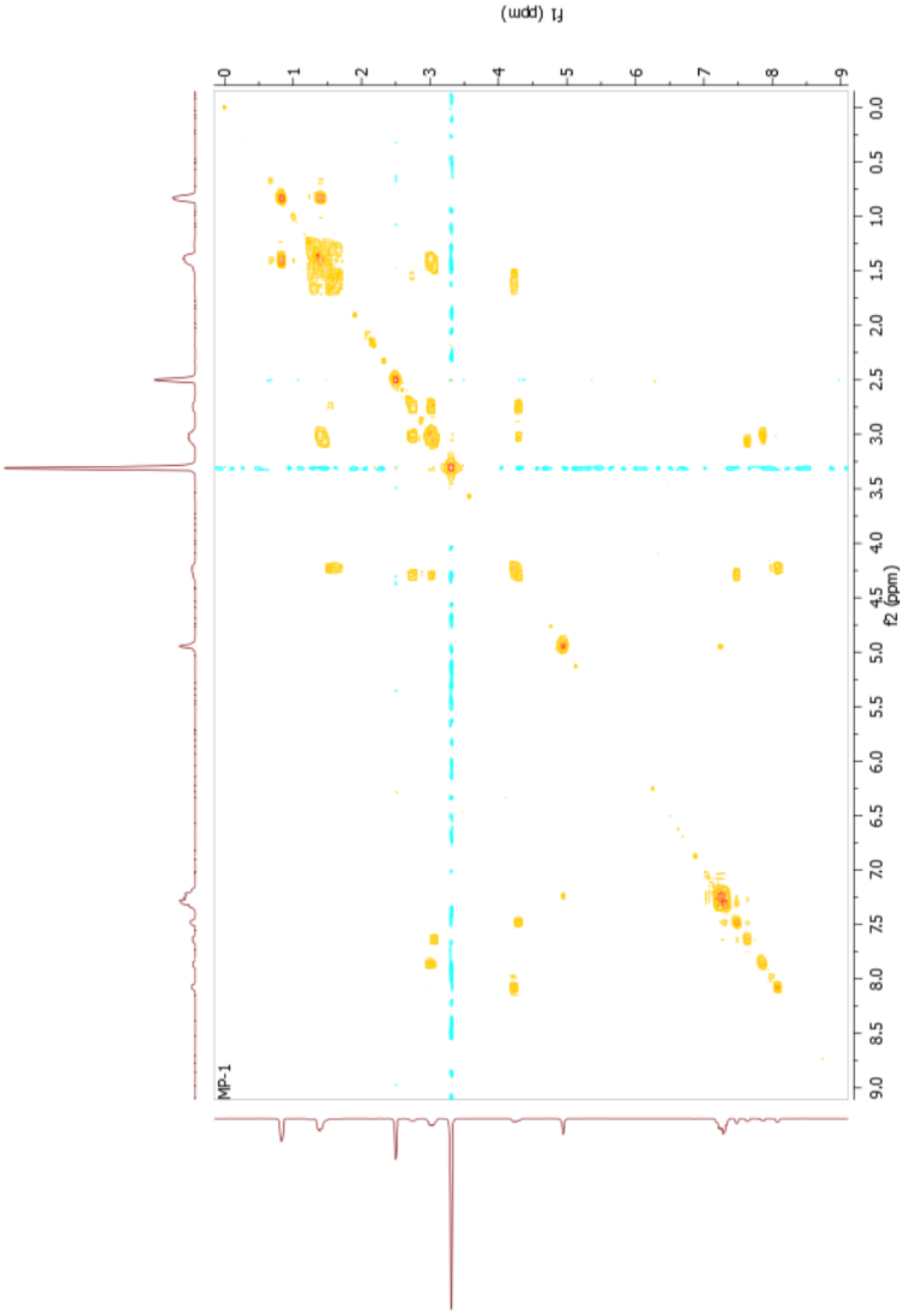
f1 (ppm)
f2 (ppm)
MP-1

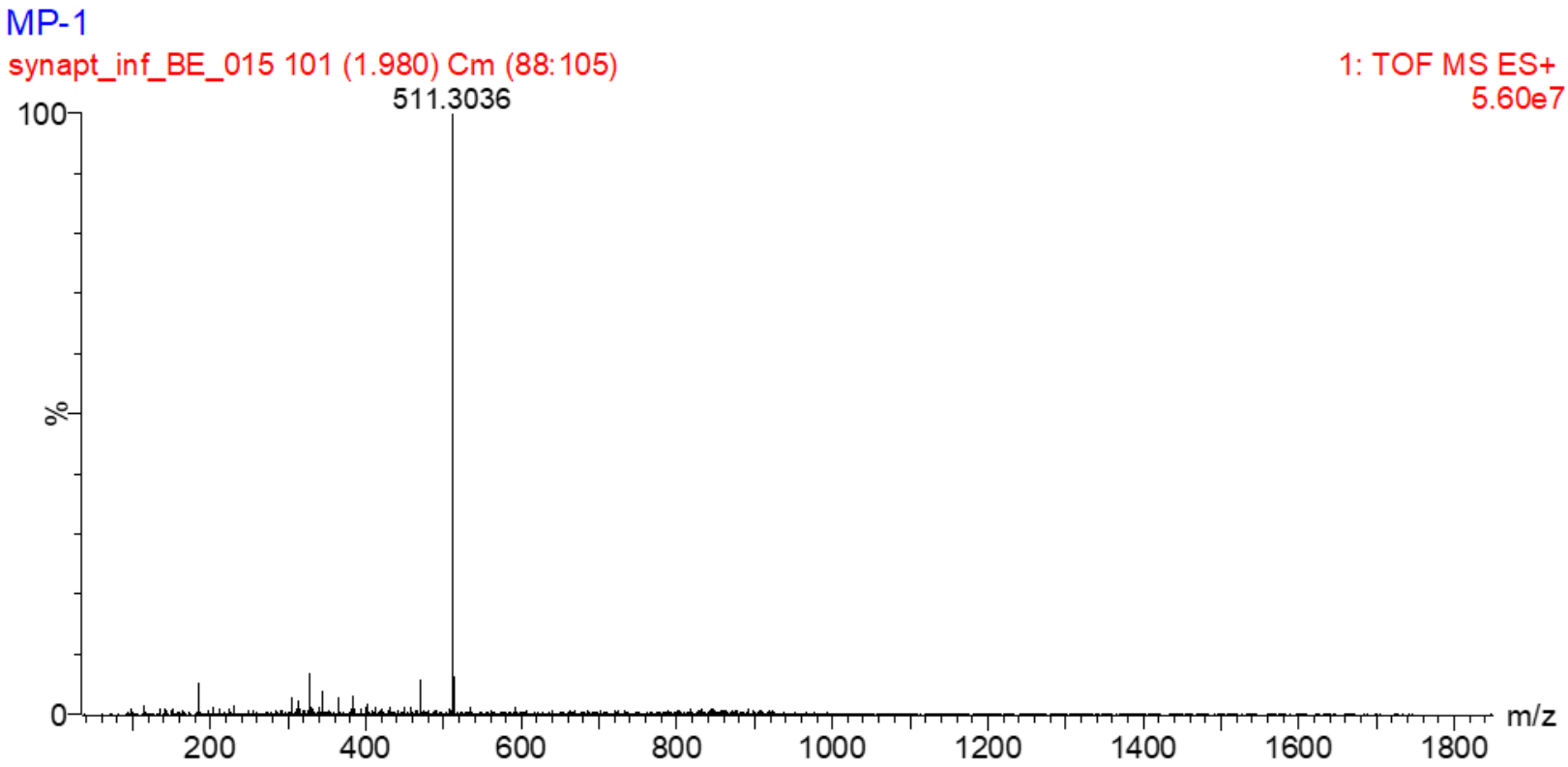

[M+H]+=511.3036

[M+H]+=511.3033 (0.6 ppm)

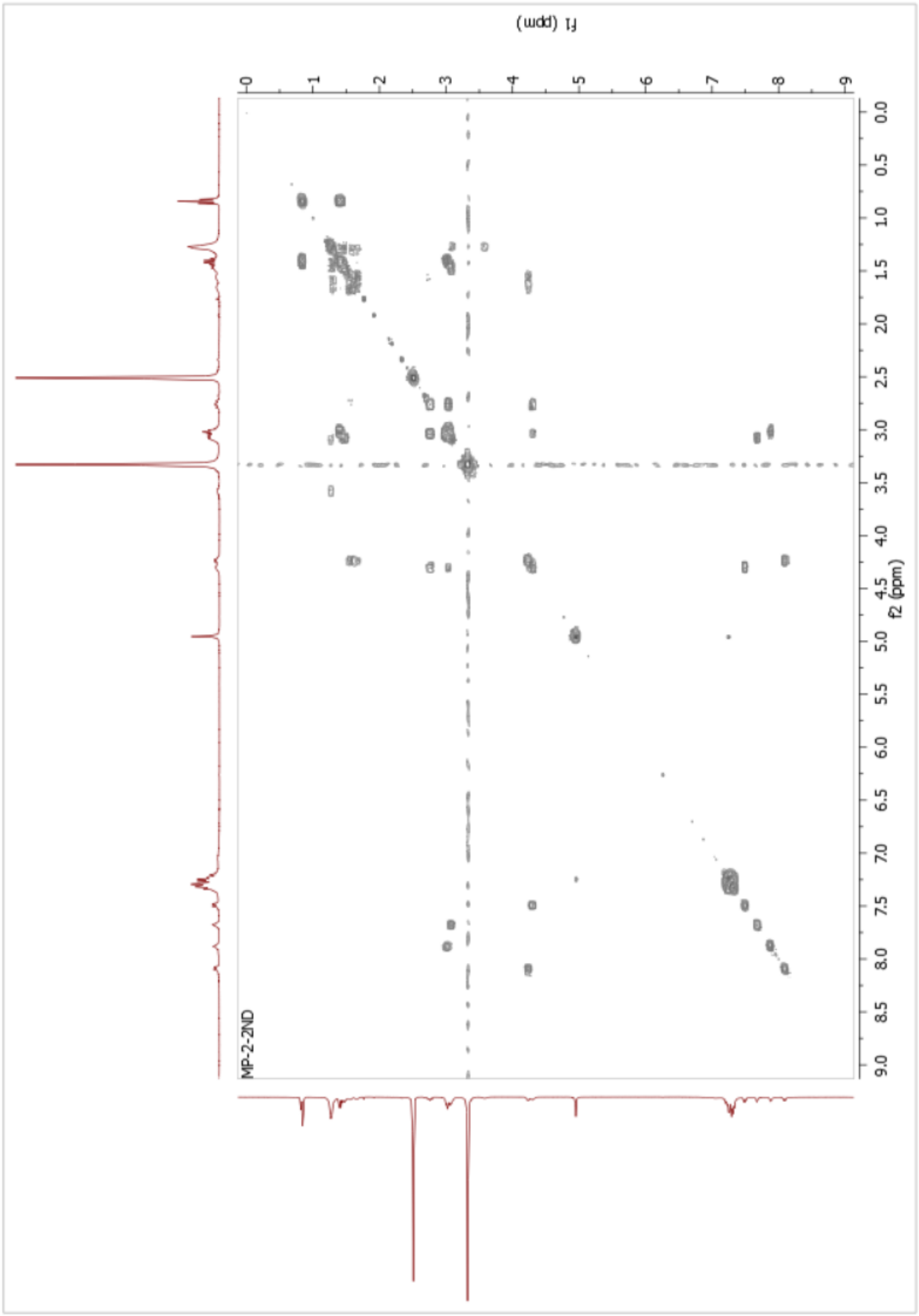
f1 (ppm)
f2 (ppm)
MP-2-2ND

[M+H]=511.3033

[M+H]=511.3042 (1.8 ppm)